

Deciphering the Nature of *Virgil*: An Obscured AGN Lurking Within an Apparently Normal Lyman- α Emitter During Cosmic Reionization

PIERLUIGI RINALDI,¹ PABLO G. PÉREZ-GONZÁLEZ,² GEORGE H. RIEKE,¹ JIANWEI LYU,¹ FRANCESCO D'EUGENIO,^{3,4}
ZIHAO WU,⁵ STEFANO CARNIANI,⁶ TOBIAS J. LOOSER,^{3,4} IRENE SHIVAEI,² LEINDERT A. BOOGAARD,⁷
TANIO DIAZ-SANTOS,^{8,9} LUIS COLINA,² GÖRAN ÖSTLIN,¹⁰ STACEY ALBERTS,¹ JAVIER ÁLVAREZ-MÁRQUEZ,²
MARIANNA ANNUZIATELLA,¹¹ MANUEL ARAVENA,¹² RACHANA BHATAWDEKAR,¹³ ANDREW J. BUNKER,¹⁴
KARINA I. CAPUTI,^{15,16} STÉPHANE CHARLOT,¹⁷ ALEJANDRO CRESPO GÓMEZ,¹⁸ MIRKO CURTI,¹⁹ ANDREAS ECKART,²⁰
STEVEN GILLMAN,^{16,21} KEVIN HAINLINE,¹ NIMISHA KUMARI,²² JENS HJORTH,²³ EDOARDO IANI,²⁴ HANAE INAMI,²⁵
ZHIYUAN JI,¹ BENJAMIN D. JOHNSON,⁵ GARETH C. JONES,^{3,4} ÁLVARO LABIANO,²⁶ ROBERTO MAIOLINO,^{3,4,27}
JENS MELINDER,¹⁰ THIBAUD MOUTARD,^{13,28} FLORIAN PEISSKER,²⁰ MARCIA RIEKE,¹ BRANT ROBERTSON,²⁹ JAN SCHOLTZ,^{3,4}
SANDRO TACHELLA,^{3,4} PAUL P. VAN DER WERF,⁷ FABIAN WALTER,³⁰ CHRISTINA C. WILLIAMS,³¹ CHRIS WILLOTT,³²
JORIS WITSTOK,^{16,33} HANNAH ÜBLER,³⁴ AND YONGDA ZHU¹

¹Steward Observatory, University of Arizona, 933 North Cherry Avenue, Tucson, AZ 85721, USA

²Centro de Astrobiología (CAB), CSIC-INTA, Cra. de Ajalvir Km. 4, 28850- Torrejón de Ardoz, Madrid, Spain

³Kavli Institute for Cosmology, University of Cambridge, Madingley Road, Cambridge, CB3 0HA, UK

⁴Cavendish Laboratory, University of Cambridge, 19 JJ Thomson Avenue, Cambridge, CB3 0HE, UK

⁵Center for Astrophysics | Harvard & Smithsonian, 60 Garden St., Cambridge MA 02138 USA

⁶Scuola Normale Superiore, Piazza dei Cavalieri 7, I-56126 Pisa, Italy

⁷Leiden Observatory, Leiden University, PO Box 9513, NL-2300 RA Leiden, The Netherlands

⁸Institute of Astrophysics, Foundation for Research and Technology-Hellas (FORTH), Heraklion, 70013, Greece

⁹School of Sciences, European University Cyprus, Diogenes street, Engomi, 1516 Nicosia, Cyprus

¹⁰Department of Astronomy, Stockholm University, Oscar Klein Centre, AlbaNova University Centre, 106 91 Stockholm, Sweden

¹¹Centro de Astrobiología (CAB), CSIC-INTA, Cra. de Ajalvir Km. 4, 28850- Torrejón de Ardoz, Madrid, Spain

¹²Instituto de Estudios Astrofísicos, Facultad de Ingeniería y Ciencias, Universidad Diego Portales, Av. Ejército 441, Santiago 8370191, Chile

¹³European Space Agency (ESA), European Space Astronomy Centre (ESAC), Camino Bajo del Castillo s/n, 28692 Villanueva de la Cañada, Madrid, Spain

¹⁴Department of Physics, University of Oxford, Denys Wilkinson Building, Keble Road, Oxford OX1 3RH, UK

¹⁵Kapteyn Astronomical Institute, University of Groningen, P.O. Box 800, 9700AV Groningen, The Netherlands

¹⁶Cosmic Dawn Center (DAWN), Copenhagen, Denmark

¹⁷Sorbonne Université, CNRS, UMR 7095, Institut d'Astrophysique de Paris, 98 bis bd Arago, 75014 Paris, France

¹⁸Space Telescope Science Institute (STScI), 3700 San Martin Drive, Baltimore, MD 21218, USA

¹⁹European Southern Observatory, Karl-Schwarzschild-Strasse 2, 85748 Garching, Germany

²⁰Physikalisches Institut der Universität zu Köln, Zùlpicher Str. 77, 50937 Köln, Germany

²¹DTU Space, Technical University of Denmark, Elektrovej, Building 328, 2800, Kgs. Lyngby, Denmark

²²AURA for European Space Agency, Space Telescope Science Institute, 3700 San Martin Drive, Baltimore, MD, 21210

²³DARK, Niels Bohr Institute, University of Copenhagen, Jagtvej 155A, 2200 Copenhagen, Denmark

²⁴Institute of Science and Technology Austria (ISTA), Am Campus 1, 3400 Klosterneuburg, Austria

²⁵Hiroshima Astrophysical Science Center, Hiroshima University, 1-3-1 Kagamiyama, Higashi-Hiroshima, Hiroshima 739-8526, Japan

²⁶Telespazio UK for the European Space Agency, ESAC, Camino Bajo del Castillo s/n, 28692 Villanueva de la Cañada, Spain

²⁷Department of Physics and Astronomy, University College London, Gower Street, London WC1E 6BT, UK

²⁸Aix Marseille Univ, CNRS, CNES, LAM, Marseille, France

²⁹Department of Astronomy and Astrophysics, University of California, Santa Cruz, 1156 High Street, Santa Cruz, CA 95064, USA

³⁰Max Planck Institut für Astronomie, Königstuhl 17, D-69117, Heidelberg, Germany

³¹NSF National Optical-Infrared Astronomy Research Laboratory, 950 North Cherry Avenue, Tucson, AZ 85719, USA

³²NRC Herzberg, 5071 West Saanich Rd, Victoria, BC V9E 2E7, Canada

³³Niels Bohr Institute, University of Copenhagen, Jagtvej 128, DK-2200, Copenhagen, Denmark

³⁴Max-Planck-Institut für extraterrestrische Physik (MPE), Gießenbachstraße 1, 85748 Garching, Germany

Submitted to ApJ

ABSTRACT

We present a comprehensive analysis of the MIRI Extremely Red Object *Virgil*, a Lyman- α emitter at $z_{\text{spec}} = 6.6379 \pm 0.0035$ with the photometric properties of a Little Red Dot. Leveraging new JWST/MIRI imaging from the MIDIS and PAHSPECS programs, we confirm *Virgil*'s extraordinary nature among galaxies in JADES/GOODS-South, exhibiting a strikingly red NIRCам-to-MIRI color ($F444W - F1500W = 2.84 \pm 0.04$ mag). Deep NIRSpec/PRISM spectroscopy from the OASIS program offers key insights into the host galaxy, revealing properties of an average star-forming galaxy during Cosmic Reionization, such as a subsolar metallicity, low-to-moderate dust content, and a relatively high ionization parameter and electron temperature. By estimating the star formation rate of *Virgil* from UV and H α , we find evidence that the galaxy is either entering or fading out of a bursty episode. Although line-ratio diagnostics employed at high- z would classify *Virgil* as an Active Galactic Nucleus (AGN), this classification becomes ambiguous once redshift evolution is considered. Nonetheless, *Virgil* occupies the same parameter space as recently confirmed AGNs at similar redshifts. The new deep MIRI data at 15 μm reinforce the AGN nature of *Virgil*, as inferred from multiple spectral energy distribution (SED) fitting codes. *Virgil*'s rising infrared SED and UV excess resemble those of Dust-Obscured Galaxies (DOGs) studied with *Spitzer* at Cosmic Noon, particularly blue-excess HotDOGs. Our results highlight the need for a multi-wavelength approach incorporating MIRI to uncover such extreme sources at $z \gtrsim 6$ and to shed light on the interplay between galaxy evolution and early black hole growth during Cosmic Reionization.

Keywords: Active galactic nuclei(16); High-redshift galaxies (734); Galaxy evolution (594); Near infrared astronomy (1093); AGN host galaxies (2017); Galaxy formation (595); Photoionization (2060); Spectral energy distribution (2129); Infrared astronomy (786); Galaxies (573); Infrared photometry (792)

1. INTRODUCTION

Infrared (IR) astronomy has advanced dramatically in recent decades. The Infrared Astronomical Satellite (IRAS; Neugebauer et al. 1984) and the Infrared Space Observatory (ISO; Helou & Kessler 1995) provided the first all-sky IR surveys, laying the foundation for extragalactic studies. These efforts paved the way for the *Spitzer* Space Telescope (Gehrz et al. 2007)—*the last of the Great Observatories*¹—and later, the *Herschel* Space Observatory (Pilbratt et al. 2010). While *Herschel* extended coverage into the far-IR, *Spitzer* remained unmatched in mid-IR sensitivity and resolution throughout the pre-*JWST* era (Gardner et al. 2023).

With the Infrared Array Camera (IRAC; Fazio et al. 2004) and the Multiband Imaging Photometer (MIPS; Rieke et al. 2004), *Spitzer* allowed us to advance our understanding of galaxy evolution. It enabled robust estimates of stellar mass (M_*), age, and star formation rate (SFR) in high-redshift galaxies (e.g., Papovich et al. 2006; Yan et al. 2006; Bradač 2020), uncovered massive systems at $z > 6$, and observed some of the most distant sources known at the time—e.g., GN-z11 (Oesch

et al. 2014, 2016) and MACS0647-JD (Lam et al. 2019; Strait et al. 2020). It also revealed strong nebular emission through photometric excesses (e.g., Huang et al. 2016), Balmer breaks, and early dust content (Papovich et al. 2006). In parallel, it advanced studies of active galactic nuclei (AGNs; Lacy & Sajina 2020) and clarified the role of luminous and ultraluminous infrared galaxies (LIRGs/ULIRGs) in driving feedback between starbursts, black holes, and the interstellar medium (ISM; Armus et al. 2020). Many of these phenomena—such as early dust and strong emission lines—are now confirmed by *JWST* photometry and spectroscopy (Rinaldi et al. 2023; Boyett et al. 2024; Kuruvanthodi et al. 2024; Langeroodi et al. 2024).

In particular, *Spitzer* played a key role in advancing the study of Extremely Red Objects (EROs; Elston et al. 1988, 1989)—sources with very red mid-IR to optical colors—triggering extensive investigations into their nature (e.g., Wilson et al. 2004; Yan et al. 2004; Stern et al. 2006; Wilson et al. 2007). Initially believed to be $z \approx 10$ sources (e.g., Mobasher et al. 2005), EROs were later found to include Submillimeter Galaxies (SMGs; Blain et al. 2002) and Dust-Obscured Galaxies (DOGs; Dey et al. 2008). DOGs—categorized as power-law or “bump” types (with a SED flattening at long wave-

¹ As described in Rieke (2006).

lengths) —likely trace a transition from dusty star formation to AGN activity during gas-rich mergers, with their red colors driven by heavy obscuration and mid-IR re-emission. Additionally, EROs were found to overlap with high-redshift galaxies (Bouwens et al. 2011) selected via the Lyman break technique (Steidel et al. 1996), highlighting their heterogeneous nature.

Despite its breakthroughs, *Spitzer* was limited by its spatial resolution. This limitation has now been overcome by JWST, which combines unparalleled sensitivity, angular resolution, and wavelength coverage with both the Near-Infrared Camera (NIRCam, 0.7–4.8 μm ; Rieke et al. 2023a) and the Mid-Infrared Instrument (MIRI, 5.6–25.5² μm ; Wright et al. 2023). The launch of JWST marks a significant leap forward compared to its predecessors, including the *Hubble* Space Telescope (HST), heralding a *golden era* of IR extragalactic astronomy.

Since its launch, JWST has pushed the boundaries of the redshift frontier, with groundbreaking discoveries at very high redshift, such as GS-z12-0, GS-z13-0, GS-z14-0, and GS-z14-1 (Curtis-Lake et al. 2023; Carniani et al. 2024a; Bunker et al. 2024) from the JWST Advanced Deep Extragalactic Survey (JADES; Bunker et al. 2020; Eisenstein et al. 2023a; Rieke et al. 2023b) team, as well as other very high- z sources identified by independent teams (e.g., Arrabal Haro et al. 2023; Wang et al. 2023). These observations have offered unprecedented insights into the very early Universe, with the Near Infrared Spectrograph’s Micro-Shutter Assembly (NIRSpec/MSA; Ferruit et al. 2022; Jakobsen et al. 2022) playing a crucial role in spectroscopically confirming galaxies at $z > 10$.

With JWST, the ERO “industry” is back in the spotlight, unveiling even more compact and red sources (Labbé et al. 2023), now known as “Little Red Dots” (LRDs; Matthee et al. 2024). The study of these sources and their nature has triggered a huge amount of literature in a very short time (e.g., Furtak et al. 2023; Killi et al. 2023; Kokorev et al. 2023; Übler et al. 2023; Akins et al. 2024; Barro et al. 2024; Greene et al. 2024; Kocovski et al. 2024; Kokorev et al. 2024; Hainline et al. 2024a; Pérez-González et al. 2024a; Rinaldi et al. 2024a; Williams et al. 2024).

Recent studies highlighted MIRI’s critical role in uncovering EROs, revealing “exotic” objects undetectable even in the deepest NIRCam surveys, such as JADES (Eisenstein et al. 2023a; Rieke et al. 2023b), or showing unexpected spectral energy distribution (SED) upturns in objects that NIRCam would typically classify as star-

forming galaxies (SFGs). In this context, the MIRI Deep Imaging Survey (MIDIS; Östlin et al. 2024) has been fundamental in identifying the first MIRI Extremely Red Objects (MEROs): *Cerberus* (Pérez-González et al. 2024b) and *Virgil* (Iani et al. 2024a).

While the nature of *Cerberus*—a source uniquely detected at 10 μm —remains entirely unknown because it is so faint, *Virgil* offers a great opportunity for detailed investigation thanks to its detection across multiple facilities, including HST, JWST (NIRCam and MIRI), and VLT/MUSE (Bacon et al. 2023). As reported in Iani et al. (2024a), *Virgil* is identified as a Lyman- α emitter (LAE) at $z_{\text{spec}} = 6.6312 \pm 0.0019$ (from VLT/MUSE) located in GOODS-South (GOODS-S; Dickinson et al. 2003; Giavalisco et al. 2004). It exhibits very red colors between NIRCam and MIRI bands ($F444W - F1000W > 2 \text{ mag}$; Iani et al. 2024a), thus revealing that the MIRI photometric information is crucial at $z \gtrsim 6$ to identify it and similar objects, as the strong upturn happens entirely outside the wavelength range of NIRCam.

Iani et al. (2024a) concluded that *Virgil* could be either a dusty starburst—similar to what has been proposed for GN20 (e.g., Colina et al. 2023)—or a SFG hosting a dust-obscured AGN. Recent JWST/NIRSpec observations of GN20 reveal complex kinematics, extended H α emission, and signatures of AGN-driven feedback (Übler et al. 2024a). However, unlike GN20, *Virgil* is both much less massive and more compact, making its extreme red colors and potential AGN activity even more remarkable. In this case, no AGN counterparts were identified in any of the existing multi-wavelength catalogs of GOODS-S (Ranalli et al. 2013; Luo et al. 2017; Lyu et al. 2022; Gillman et al. 2025), including the most recent AGN catalog from Lyu et al. (2024) with MIRI data, which is based on the Systematic Mid-infrared Instrument Legacy Extragalactic Survey (SMILES; Alberts et al. 2024; Rieke et al. 2024). In the latter case, this could be due to the limited depth of the SMILES observations, which are not deep enough to clearly detect ($> 3\sigma$) this object in the MIRI bands above 7.7 μm .

Moreover, Iani et al. (2024a) demonstrated that *Virgil*’s SED closely resembles that of a typical LRD (see their Figure 10). Although *Virgil* does not meet all photometric color criteria for LRDs (e.g., Kokorev et al. 2024), it satisfies the compactness criterion in the F444W band, possibly making it one of the first LRDs where the host galaxy is well-detected. Interestingly, Iani et al. (2024a) highlight the peculiar ultraviolet (UV) morphology of *Virgil*, consistent with the findings of Rinaldi et al. (2024a), where nearly 30% of the photometrically selected LRDs exhibit a complex

² Here we refer to the MIRI imager. However, the MIRI Medium Resolution Spectroscopy (MRS) extends up to $\approx 27 \mu\text{m}$.

UV morphology, suggesting that interactions may play a significant role in triggering AGNs in LRDs.

In this paper, we take a step forward by performing a detailed analysis of *Virgil*, leveraging the very recent data collected by the MIDIS (PID: 6511, PI: Östlin), PAHSPECS (PID: 5279, PIs: Shivaiei, Díaz-Santos, and Boogaard), and OASIS (PID: 5997, PIs: Looser & D’Eugenio) teams. These include exceptionally deep MIRI imaging at 5.6, 7.7, 10, and 15 μm , and deep NIRSpec/PRISM data. The deep NIRSpec/PRISM data enable the most comprehensive analysis of a LRD to date, providing critical insights into *Virgil*’s physical properties at UV and optical wavelengths, while the new MIRI data at 15 μm further confirm its extreme nature, suggesting a strong similarity to other EROs previously studied in the *Spitzer* era.

This paper is structured as follows. In Section 2, we describe the dataset used in this study, including HST and JWST observations, with particular focus on the MIRI data reduction. Section 3 presents a detailed analysis of the spectral properties of *Virgil*, based on NIRSpec data obtained by the OASIS team. Sections 4 and 5 present updated photometry and SED fitting, incorporating the newly acquired MIRI data from the MIDIS and PAHSPECS teams. In Section 6, we discuss the nature of *Virgil*, and in Section 7, we summarize our main conclusions.

Throughout this paper, we consider a cosmology with $H_0 = 70 \text{ km s}^{-1} \text{ Mpc}^{-1}$, $\Omega_M = 0.3$, and $\Omega_\Lambda = 0.7$. All magnitudes are total and refer to the AB system (Oke & Gunn 1983). A Kroupa (2001) initial mass function (IMF) is assumed (0.1–100 M_\odot). Moreover, in Table 1, we report the line ratios that will be adopted throughout this work.

2. DATASET

In this work, we used data from HST and JWST, which are available in GOODS-S. In particular, we will briefly describe the data reduction for the MIDIS data and the NIRSpec/PRISM data collected by OASIS.

2.1. HST

Regarding the HST data, we used the ACS/WFC and WFC3/IR data from the Hubble Legacy Field (HLF) observations that cover GOODS-S. The HLF provides deep imaging in 9 HST bands covering a wide range of wavelengths (0.4–1.6 μm), from the optical (ACS/WFC F435W, F606W, F775W, F814W, and F850LP filters) to the near-infrared (WFC3/IR F105W, F125W, F140W and F160W filters). We refer the reader to Whitaker et al. (2019) for a more detailed description of this dataset.

Index	Definition
R3	$\log_{10} \left(\frac{[\text{O III}]\lambda 5007}{\text{H}\beta} \right)$
O32	$\log_{10} \left(\frac{[\text{O III}]\lambda\lambda 4959, 5007}{[\text{O II}]\lambda\lambda 3727, 3729} \right)$
R23	$\log_{10} \left(\frac{[\text{O III}]\lambda\lambda 4959, 5007 + [\text{O II}]\lambda\lambda 3727, 3729}{\text{H}\beta} \right)$
Ne3O2	$\log_{10} \left(\frac{[\text{Ne III}]\lambda 3869}{[\text{O II}]\lambda\lambda 3727, 3729} \right)$
Ne3O2Hd	$\log_{10} \left(\frac{[\text{Ne III}]\lambda 3869 + [\text{O II}]\lambda\lambda 3727, 3729}{\text{H}\delta} \right)$
O3Hg	$\log_{10} \left(\frac{[\text{O III}]\lambda 4363}{\text{H}\gamma} \right)$
O33	$\log_{10} \left(\frac{[\text{O III}]\lambda 5007}{[\text{O III}]\lambda 4363} \right)$

Table 1. Definitions of line ratios adopted in this work. We use the O32 definition from Calabrò et al. (2024a), that has a fixed offset of $\log_{10}(1.3)$ between our values and the more common definition of O32 ($\equiv [\text{O III}]\lambda 5007/[\text{O II}]\lambda\lambda 3727, 3729$).

2.2. NIRC*am*

We made use of NIRC*am* data from JADES Data Release 2 (JADES DR2 – PIDs: 1180, 1210; PIs.: D. Eisenstein, N. Luetzendorf; Eisenstein et al. 2023a,b), which includes observations from the JWST Extragalactic Medium-band Survey (JEMS – PID: 1963; PIs: C. C. Williams, S. Tacchella, M. Maseda; Williams et al. 2023) and the First Reionization Epoch Spectroscopically Complete Observations (FRESCO – PID: 1895; PI: P. Oesch; Oesch et al. 2023).

The JADES/NIRC*am* data allowed us to cover a wide range in wavelengths ($\approx 1 - 5 \mu\text{m}$) with the following bands: F090W, F115W, F150W, F182M, F200W, F210M, F277W, F335M, F356W, F430M, F444W, F460M, F480M. The estimated 5σ depth from 30.5 to 30.9 mag (depths are calculated using 0.2''-diameter circular apertures assuming point-source morphologies; see Hainline et al. 2024b for details).

2.3. MIRI

We utilized MIRI data from the MIDIS (PID: 6511, PI: Östlin), PAHSPECS (PID: 5279, PIs: Shivaiei, Díaz-Santos, and Boogaard), and SMILES (PID: 1207, PI: Rieke) programs, which allowed us to cover a wide range of wavelengths (5.6 – 25.5 μm). Specifically, MIDIS provides observations at 5.6, 7.7, and 10 μm , PAHSPECS enables photometry at 15 μm , and SMILES samples 12.8, 18, 21, and 25.5 μm . For SMILES, we relied on publicly available images released by the SMILES team. In contrast, we independently reduced the MIDIS data, while the PAHSPECS team provided a $5'' \times 5''$ cutout centered on *Virgil*. Details on the MIRI/F1500W data reduction will be presented in Shivaiei et al. (in prep.),

based on the procedures described in Pérez-González et al. (2024a) and Östlin et al. (2024).

To process the MIDIS data, we employed our custom MIRI pipeline (already calibrated in Rinaldi et al. 2023; Jani et al. 2024b and further improved), built on the latest `mwst` pipeline (1.17.1) with `pmmap_1321`. We used the default `stage 1` and `stage 2` steps of the `mwst` pipeline to produce calibrated data (`*_cal.fits`). Additionally, we implemented custom steps for creating a master background, performing a super-background subtraction and homogenization, and alignment to a common world coordinate system (WCS) based on the JADES DR2 catalog (Eisenstein et al. 2023a).

Our custom pipeline relies on a multi-tiered approach. First, it combines the `*_cal.fits` files into an initial mosaic using a custom drizzle algorithm based on the official package provided by STScI³. This initial mosaic serves as the baseline for creating a source mask to exclude sources in the individual `*_cal.fits` files. To construct this mask, our pipeline uses SOURCE EXTRACTOR (Bertin & Arnouts 1996). A preliminary `master.background` is then built by reprojecting this preliminary source mask onto each exposure, stacking all exposures into a 3D array, and computing the `biweight location` along the z-axis. This method minimizes the influence of outliers and provides a robust estimate of the 2D background (i.e., `master.background`).

For each exposure, our pipeline iteratively estimates a scale factor (`A`) to optimize the subtraction of the `master.background`. The scale factor is recalculated at each iteration using clipped data to ensure convergence and minimize residuals between the corrected and original images. Once the `master.background` is subtracted, the pipeline filters each exposure along rows and columns to remove residual patterns while masking out the sources. This procedure is similar to the standard approach used to mitigate wisp effects in NIRCam data, as described by Bagley et al. (2024).

Then, the pipeline drizzles together all the single exposures to produce a new mosaic, from which it creates a `master.source.mask`. At this level, the pipeline makes use of both SOURCEEXTRACTOR and NOISECHISEL (Akhlaghi & Ichikawa 2017) to create the `master.source.mask`: SOURCEEXTRACTOR effectively identifies compact sources. In contrast NOISECHISEL detects faint sources and extended regions around bright objects. The `master.source.mask` is then reprojected onto each single exposure to improve the `master.background` and super-background subtraction

and homogenization, following a methodology similar to the one outlined in Bagley et al. (2024).

After this step, the exposures are filtered again in rows and columns and aligned to the JADES DR2 reference catalog using a modified version of the `tweakreg.step` within the `mwst` pipeline.

The final steps include running the `outlier.step` and `resampling.step`, producing the final mosaic. This final mosaic is then used to refine the `master.source.mask` and iterate the entire procedure for further optimization. Similar methodologies have already been widely used when reducing MIRI data (e.g., Alberts et al. 2024; Pérez-González et al. 2024a; Östlin et al. 2024).

Finally, we estimated the 5σ depth in our reduced MIRI images, which is 28.6, 28.3, 27.1, and 24.9 mag at, respectively, 5.6, 7.7, 10, and 15 μm ($r = 0.3''$). The 5σ depth for the SMILES images at 12.8, 18, 21, and 25.5 μm is 24.4, 23.3, 22.8, and 20.8 mag (Alberts et al. 2024; $r = 0.4 - 0.7''$). Depths are estimated using circular apertures assuming point-source morphologies.

2.4. NIRSpec/PRISM

The OASIS program consists of two ultra-deep NIRSpec/MSA pointings, each with a total exposure time of 28 hours, using the PRISM/CLEAR configuration to obtain low-resolution ($R \approx 30-300$) spectroscopy over the 0.6 – 5.3 μm range. The observations are executed in multiple visits, with each pointing incorporating three nodding positions within the MSA to improve background subtraction, and multiple dithered observations to mitigate detector artifacts. The MSA configuration is designed to target a sample of 223 galaxies at $5 < z < 8$. The NIRSpec observations are performed using the NRSRAID6 readout pattern with three groups per integration and a total of six integrations per exposure.

To reduce the NIRSpec/PRISM data, we made use of the pipeline developed by the ESA NIRSpec Science Operations Team (SOT) and the Guaranteed Time Observations (GTO) NIRSpec teams, with optimizations aimed at improving background subtraction, rectification, 1D extraction, and spectral combination. While broadly consistent with the STScI pipeline used for generating archive products, these enhancements ensure more accurate spectral calibration, particularly for compact sources affected by spatial offsets within the slit. A wavelength correction is applied to mitigate this bias, which arises when sources are not perfectly centered along the dispersion axis. For a more detailed description of the NIRSpec data reduction, we refer the reader to Bunker et al. (2024) and D'Eugenio et al. (2024).

³ <https://github.com/spacetelescope/drizzle>.

A more detailed description of this dataset will be presented in Looser & D’Eugenio et al. (in prep.).

3. ON THE NATURE OF VIRGIL: INSIGHTS FROM NIRSPEC/PRISM

In this section, we delve into the nature of *Virgil* based on NIRSpec/PRISM data. Due to the extended nature of Virgil in the NIRSpec wavelength range, we corrected the flux following the method outlined in Carniani et al. (2024b). We applied a first-order polynomial ($\alpha_1 + \alpha_0\lambda$) to model the wavelength-dependent slit losses and calibrated the flux to match the NIRCам photometry. That is, we focus on the rest-frame UV and optical spectral regions. All the line fluxes and properties estimated in this section are summarized in Table 2.

3.1. Redshift assessment of *Virgil*

We used MSAEXP (Brammer 2023; Heintz et al. 2025) to estimate the spectroscopic redshift. MSAEXP fits the data using a combination of Gaussian continuum splines and emission line templates. We set `nsplines = 11` as an input parameter and searched for the minimum reduced χ^2 value within the redshift range $z = 6 - 7$, based on the prior spectroscopic estimate from VLT/MUSE (Bacon et al. 2023). As shown in the 2D spectrum (Figure 1), a faint Ly α feature—possibly blended with NV λ 1240—is visible, consistent with the detection reported by Bacon et al. (2023). The line appears spatially offset, suggesting it may originate from a distinct kinematic component, potentially explaining the slight redshift discrepancy with the MUSE measurement. Several other emission lines are detected, yielding an unambiguous redshift of $z_{\text{spec}} = 6.6379 \pm 0.0035$, which is slightly higher than the VLT/MUSE estimate⁴ but still consistent to the second decimal place.

3.2. *Virgil’s physical properties from its UV/optical spectrum*

3.2.1. Balmer Decrement and Dust Content

We estimated the color excess, $E(B - V)_{\text{gas}}$, by analyzing the Balmer decrement between H β and H α . We measured an observed Balmer decrement of 3.70 ± 0.19 . However, since we cannot resolve [N II] $\lambda\lambda$ 6548, 6583 individually, we applied the correction from Anders & Fritze-v. Alvensleben (2003) for low-metallicity objects ($10 - 20\% Z_{\odot}$; see next section), where the corrected H α flux is $\approx 91\%$ of the observed (H α + [N II] $\lambda\lambda$ 6548, 6583). After this correction, the Balmer decrement is

⁴ The redshift from VLT/MUSE is based on a single line identification.

Table 2. Emission Line Fluxes and Derived Properties for *Virgil*

Line	Value	Error
N IV] λ 1487	47.3	19.0
C IV] λ 1549	28.3	18.7
C III] λ 1906	48.4	16.4
[O II] $\lambda\lambda$ 3727,3729	67.4	5.4
[Ne III] λ 3867	34.6	5.5
He I λ 3889	20.9	5.5
[Ne II] λ 3968	22.9	4.5
H δ λ 4102	20.5	4.2
H γ λ 4340	32.4	4.9
[O III] λ 4363	16.5	4.7
H β λ 4861	92.5	4.1
[O III] λ 4959	206.0	5.2
[O III] λ 5007	587.9	5.2
He I λ 5877	15.5	4.2
H α λ 6563*	304.9	6.6
H α (narrow) λ 6563	219.9	12.5
H α (broad) λ 6563	168.8	17.9
Galaxy Properties		
FWHM (broad H α) [km/s]	1750	575
$E(B - V)_{\text{gas}}$ [mag]	0.24	0.07
$E(B - V)_{\text{stars}}$ [mag]	0.10	0.03
A_V (H α /H β) [mag]	0.65	0.18
12+log(O/H)**	7.78	0.18
$T_e(O^+)$ [K]	14800	600
$T_e(O^{2+})$ [K]	18300	3200
log ₁₀ (\mathcal{U})**	-2.03	0.08
n_e *** [cm ⁻³]	< 500	–
EW ₀ (H α) [Å]	422	20
EW ₀ ([O III] $\lambda\lambda$ 4959.5007) [Å]	1514	18
SFR(H α) [M_{\odot} yr ⁻¹]	6.10	0.93
SFR(UV) [M_{\odot} yr ⁻¹]	2.96	1.02
$\Sigma_{\text{SFR}(H\alpha)}$ [M_{\odot} yr ⁻¹ kpc ⁻²]	5.25	0.80
\mathcal{B}	0.32	0.16
M_{UV} [mag]	-18.70	0.17
β	-1.76	0.18
$f_{\text{esc}, LyC}$	0.02	0.01
ξ_{ion} [log ₁₀ (Hz erg ⁻¹)]	24.91	0.18
z_{spec}	6.6379	0.0035

NOTE—Observed fluxes and errors (not corrected for dust) are given in units of 10^{-20} erg s⁻¹ cm⁻². We also show the H α fluxes for the narrow and broad components obtained by MSAEXP. Derived galaxy properties with associated uncertainties are provided. * refers to H α corrected for the contribution from [N II] $\lambda\lambda$ 6548, 6583. ** refers to the estimated median quantities, while *** refers to upper limits (2σ).

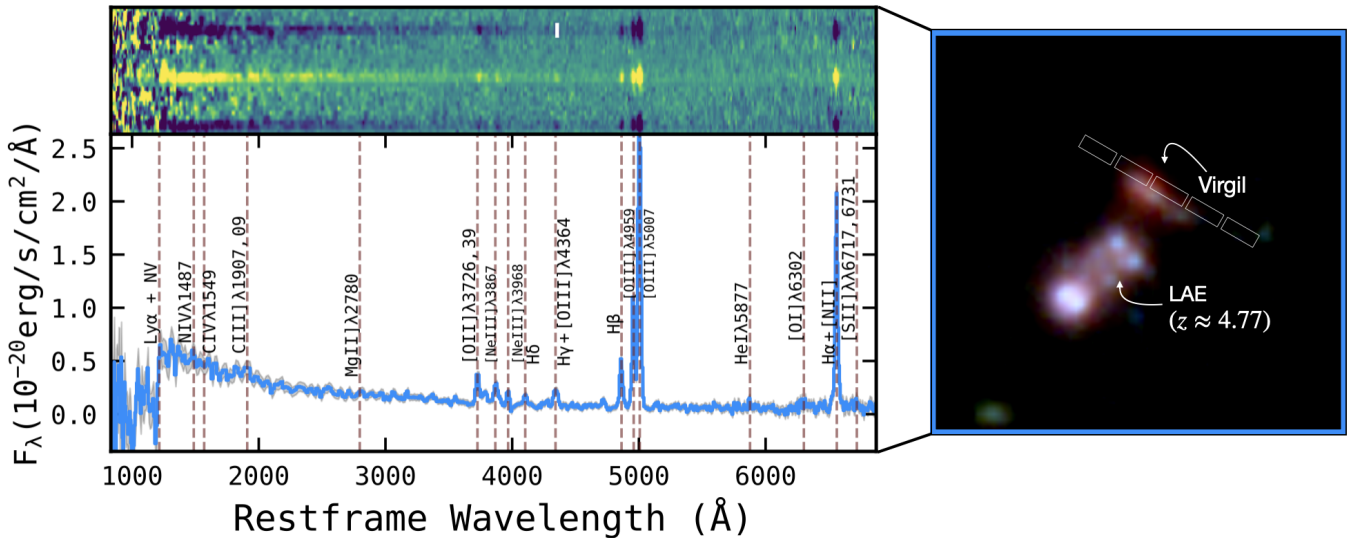


Figure 1. **Left panel:** 2D MSA/PRISM spectrum produced by MSAEXP. We optimally scaled the trace to highlight all of the significant line detections. We show the data in azure, while the uncertainty is highlighted in gray. Assuming the best-fit MSAEXP $z_{\text{spec}} = 6.6379 \pm 0.0035$, we show the positions of the emission lines as dashed vertical lines. **Right panel:** JWST/NIRCam RGB image ($2.5'' \times 2.5''$) along with the slit positions showed in white. We highlight *Virgil* and the foreground LAE at $z \approx 4.77$ already studied in Matthee et al. (2022) with VLT/MUSE data.

3.30 ± 0.16 . Assuming Case B recombination (Osterbrock & Ferland 2006), and adopting an electron temperature of 1.8×10^4 K (as derived in the next section) and an electron density of 10^2 cm^{-3} , we use PYNEB (Luridiana et al. 2015) to compute an intrinsic $\text{H}\alpha/\text{H}\beta$ ratio of 2.76. The measured ratio corresponds to $E(B - V)_{\text{gas}} = 0.24 \pm 0.07$ mag, assuming the Small Magellanic Cloud (SMC) reddening law (Gordon et al. 2003), which has been shown to reproduce well the dust attenuation in high-redshift galaxies (e.g., Reddy et al. 2018) and reddened quasars (e.g., Hopkins et al. 2004). This value leads to an attenuation of $A_V = 0.65 \pm 0.18$ mag, adopting $R_V = 2.74 \pm 0.13$ (Gordon et al. 2003). It further implies $E(B - V)_{\text{stars}} = 0.10 \pm 0.03$ mag⁵.

To further assess the dust attenuation, we also compared the Balmer decrement for $\text{H}\beta$ with respect to $\text{H}\gamma$ and $\text{H}\delta$ (expected theoretical ratios of 0.474 and 0.263, respectively, under Case B recombination; Osterbrock & Ferland 2006). The resulting $E(B - V)_{\text{gas}}$ values were consistent with a low level or zero attenuation.

If *Virgil* instead hosted a Type 1 AGN (see Section 3.4), the broad component of $\text{H}\alpha$ must be excluded when computing the Balmer decrement. In this case, considering only the narrow component of $\text{H}\alpha$ and treating the detected broad $\text{H}\beta$ as a narrow line due to its low significance, we would obtain a lower Balmer decrement

⁵ Assuming the differential dust attenuation, we adopt $E(B - V)_{\text{stars}} = 0.44 \times E(B - V)_{\text{gas}}$ (Koyama et al. 2019; Shivaeei et al. 2020).

of 2.38 ± 0.18 , consistent with a dust-free scenario. Alternatively, in this scenario, the Balmer decrement may be intrinsically lower, as observed in some $z \approx 4 - 7$ galaxies with density-bounded regions or in low-mass extreme emitters (Sandles et al. 2024; McClymont et al. 2024; Scarlata et al. 2024).

3.2.2. Gas-Phase Metallicity and Ionization State

Both MSAEXP and our internal routine successfully deblended $\text{H}\gamma$ and $[\text{O III}]\lambda 4363$. Additionally, we detect the $[\text{O II}]\lambda\lambda 3727, 3729$ doublet. These lines, along with $[\text{O III}]\lambda\lambda 4959, 5007$, enabled us to estimate the electron temperatures (T_e) of O^+ and O^{2+} and the gas-phase metallicity (e.g., Izotov et al. 2006; Curti et al. 2024; Sanders et al. 2024). For this purpose, we employed a non-parametric approach based on Langeroodi & Hjorth (2024a), utilizing the GENESIS-METALLICITY tool⁶, which is built on PYNEB (Luridiana et al. 2015). We derived $T_e(\text{O}^+) = (1.48 \pm 0.06) \times 10^4$ K and $T_e(\text{O}^{2+}) = (1.83 \pm 0.32) \times 10^4$ K (adopting the direct method). We highlight that $T_e(\text{O}^{2+})$ is higher than typical values observed in galactic H II regions, but is consistent with the temperatures measured in the most metal-poor galaxies (e.g., Skillman et al. 2013).

Furthermore, the GENESIS-METALLICITY tool offers the option to estimate gas-phase metallicity using either the direct (T_e) method or strong-line calibrations,

⁶ The tool is available at https://github.com/langeroodi/genesis_metallicity/tree/main.

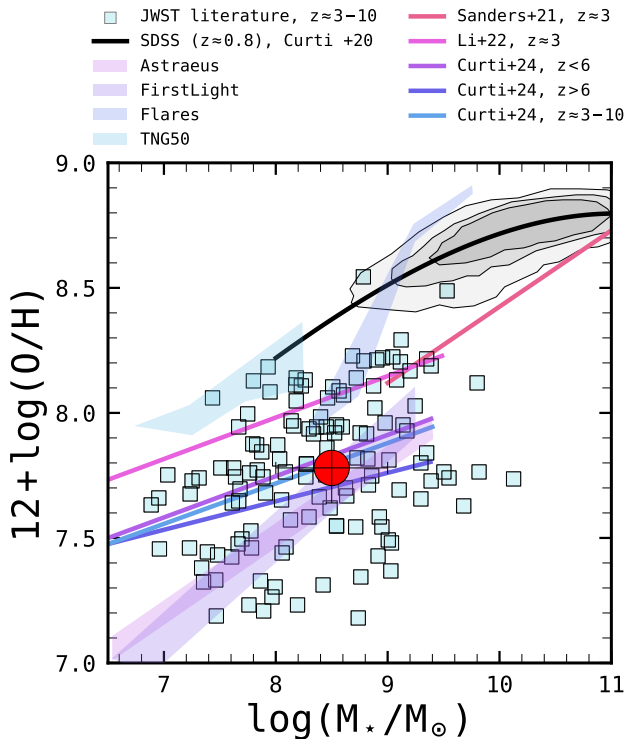


Figure 2. The stellar mass-gas-phase metallicity relation. *Virgil* is shown as a red filled circle. The stellar mass is taken from Iani et al. (2024a) (median value), with an error bar reflecting the uncertainty in the estimate, consistent with the results obtained in this paper (see Section 5). Filled squares represent recent JWST measurements at $z \approx 3$ –10, including galaxies from the JADES field (Curti et al. 2024), the CEERS field (Nakajima et al. 2023), and the SMACS J0723.3-7327 sample (Curti et al. 2023). For comparison, we show MZR determinations at lower redshifts from Curti et al. (2020) (Sloan Digital Sky Survey; SDSS) and Sanders et al. (2021) (MOSDEF at $z \approx 2$ –3). Additionally, we include the best-fit of the low-mass end of the MZR at $z \approx 3$ from Li et al. (2023), based on JWST/NIRISS slitless spectroscopy. Finally, we also show theoretical predictions at high redshift from ASTRAEUS (Ucci et al. 2023), FIRSTLIGHT (Langan et al. 2020), the First Light and Reionisation Epoch Simulations (FLARES; Lovell et al. 2021), and TNG50 simulations (Nelson et al. 2019).

depending on the available line fluxes. Both approaches yielded consistently low metallicities for *Virgil*, with $12 + \log(\text{O}/\text{H}) = 7.70 \pm 0.14$ for the direct method, and $12 + \log(\text{O}/\text{H}) = 7.91 \pm 0.04$ for the strong-line method. Based on the commonly accepted solar oxygen abundance ($12 + \log(\text{O}/\text{H}) = 8.69$; Asplund et al. 2009), this gives us $Z/Z_{\odot} \approx 0.11 - 0.18$.

In the recent literature, other emission lines have been proposed to trace the gas-phase metallicity (mostly from UV), such as C IV] $\lambda 1548$ and C III] $\lambda 1907$ (see Mingozi et al. 2022). Based on their Equation 7, which exploits

the equivalent width (EW) of C III] $\lambda 1907, 09$, we estimated that $12 + \log(\text{O}/\text{H}) = 7.78 \pm 0.21$ (in agreement with our previous measurements). As shown in the mass-metallicity relation (MZR; Figure 2), *Virgil* is in good agreement with the relation recently reported by Curti et al. (2024) for galaxies at $z \gtrsim 6$ by leveraging the JADES sample as well as the recent literature from JWST.

We further investigate the ionization state of *Virgil*'s gas by examining the ionization parameter, $\log_{10}(\mathcal{U})$, a key ISM property that reflects the intensity and hardness of the ionizing radiation, gas density, and the geometry of gas relative to ionizing sources. The O32 index, a well-established tracer of $\log_{10}(\mathcal{U})$, yields a value of -2.03 ± 0.08 based on the empirical calibration from Papovich et al. (2022) (their Equation 4), which was derived from galaxies at $1.1 < z < 2.3$ in the CLEAR survey (Simons et al. 2023). Notably, this value is consistent with the estimate from UV-based tracers identified by Mingozi et al. (2022), who calibrated $\log(\text{C III]}/\text{O III])$, $\log(\text{C IV}]/\text{C III])$, $\log(\text{EW}(\text{O III}))$, and $\log(\text{EW}(\text{C IV}))$ against O32. Applying their Equations 8 and 10, we find an average $\log_{10}(\mathcal{U}) = -1.99 \pm 0.15$, confirming a high level of ionization in agreement with the O32-based result. Alternatively, using the relation between $\log_{10}(\mathcal{U})$ and the Ne3O2 index from Witstok et al. (2021) (their Equation 3), we derive $\log_{10}(\mathcal{U}) = -2.33 \pm 0.07$. While slightly lower than the previous estimates, this value remains indicative of a highly ionized ISM, which is in line with the average galaxy population during EoR.

We were also able to fit the [S II] $\lambda\lambda 6717, 6731$ doublet, although with a low SNR ($\approx 2\sigma$). Following the theoretical framework of Kewley et al. (2019), we estimated an upper limit on the electron density, $n_e \approx 500 \text{ cm}^{-3}$, considering its weak dependence on T_e (Zhang 2024). However, the low spectral resolution of NIRSpect/PRISM⁷ prevents deblending the [O II] $\lambda\lambda 3727, 3729$ doublet, limiting further constraints on n_e . Recently, Topping et al. (2025) analyzed deep JWST/NIRSpect spectra of SFGs at $z \approx 1.4 - 10$ as part of the AURORA survey (Shapley et al. 2024), focusing on the [S II] $\lambda\lambda 6717, 6731$ doublet (detected up to $z \approx 6.8$), its evolution over cosmic time, and its correlation with various parameters (e.g., line ratios, star formation rate). Notably, our upper limit aligns with the average n_e expected at $z \approx 6.5$, and it is consistent with the estimate obtained using their relation with the star formation rate (SFR; their Equation 2) and Ne3O2 (their Equation 3).

⁷ $R \approx 30$ –420, depending on the observed wavelength.

As a final note, we report the detection of the N IV]λ1487 emission line, while N III]λ1750 is detected at a significance well below 2σ . Additionally, MSAEXP identifies a possible N Vλ1240 feature, although it may be blended with Lyα due to the low resolution of NIRSpec/PRISM. The presence of N IV]λ1487 has been proposed as a signature of low-luminosity quasars (Glikman et al. 2007; Bunker et al. 2023; Cameron et al. 2023). However, we note that NIRSpec spectra often exhibit spurious oscillations in this wavelength range, and higher-resolution, deeper observations will be necessary to confirm the reality of these lines. For this reason, we do not discuss this further.

3.2.3. UV-β slope, Burstiness, and Ionizing Photon Production Efficiency

We modified the official MSAEXP code to enable estimation of the UV β slope (in the rest-frame wavelength range $\lambda \approx 1500 - 2500 \text{ \AA}$) by fitting a linear relation ($\log_{10}(f_\lambda) = \beta \log_{10}\lambda + q$) using non-linear least squares optimization via `curve_fit` (SCIPY). We also employed a Monte Carlo approach, performing 1000 linear fits to spectral realizations with randomly perturbed fluxes and adopting the median and standard deviation of the resulting β values. We retrieved $\beta = -1.76 \pm 0.18$.

To investigate the potential role of *Virgil* during EoR, we estimated its ionizing photon production efficiency, ξ_{ion} . Following the method outlined in Rinaldi et al. (2024b), we first derived the Lyman continuum escape fraction ($f_{\text{esc, LyC}}$) from the observed UV β slope using the prescription of Chisholm et al. (2022). We then computed ξ_{ion} based on its dependence on $(1 - f_{\text{esc, LyC}})^{-1}$ (Equation 2 in Rinaldi et al. 2024b). We find $f_{\text{esc, LyC}} = 0.02 \pm 0.01^8$ and $\log_{10}(\xi_{\text{ion}}/\text{Hz erg}^{-1}) = 24.91 \pm 0.18$. The latter is below the canonical value (25.2 ± 0.1 ; Robertson et al. 2013), but still in agreement with the average high- z population at $z \approx 6 - 7$ (Matthee et al. 2017; Rinaldi et al. 2024b; Simmonds et al. 2024a). This result is not a surprise, as the rest-frame equivalent width (EW_0) for Hα is about $422 \pm 20 \text{ \AA}$, and very high ξ_{ion} is often associated with very strong line emitters (i.e., large $\text{EW}_0(\text{H}\alpha)$; see Figure 5 from Rinaldi et al. 2024b).

Following the work presented in Atek et al. (2022) and Navarro-Carrera et al. (2024), high- z galaxies are expected to grow through bursty episodes of star formation, driven by large temporal fluctuations in their

SFR—a trend recently suggested also by Langeroodi & Hjorth (2024b).

The NIRSpec/PRISM spectrum enabled us to estimate the star formation rate (SFR)⁹ directly from emission lines, specifically Hα, using the calibration from Kennicutt & Evans (2012) based on a Kroupa IMF. In particular, we adopt:

$$\log_{10} \left(\frac{\text{SFR}}{M_\odot \text{ yr}^{-1}} \right) = \log_{10} (L_{\text{H}\alpha} / (\text{erg s}^{-1})) - 41.64, \quad (1)$$

where the coefficient 41.64 corresponds to the calibration at sub-solar metallicity (10–20% Z_\odot ; Theios et al. 2019).

We find that $\log_{10}(\text{SFR}(\text{H}\alpha)/(M_\odot \text{ yr}^{-1})) = 0.79 \pm 0.07$. Based on the estimate from Iani et al. (2024a) for the effective radius ($r_{\text{eff}} \approx 0.43 \text{ pkpc}$), we retrieve $\Sigma_{\text{SFR}(\text{H}\alpha)} = \text{SFR}(\text{H}\alpha)/2\pi r_{\text{eff}}^2 = 5.25 \pm 0.80 M_\odot \text{ yr}^{-1} \text{ kpc}^{-2}$, which is in line with recent results from Calabrò et al. (2024b) at $z \approx 6.5$.

The detection of Hα allowed us to estimate another key parameter: the burstiness, defined as $\mathcal{B} = \log_{10}(\text{SFR}(\text{H}\alpha)/\text{SFR}(\text{UV}))$ (Atek et al. 2022). We derived SFR(UV) at 1500 Å using the calibration from Kennicutt & Evans (2012), adapted for sub-solar metallicity following Theios et al. (2019), obtaining $\log_{10}(\text{SFR}(\text{UV})/M_\odot \text{ yr}^{-1}) = 0.47 \pm 0.15$. This yields a burstiness parameter of $\mathcal{B} = 0.32 \pm 0.16$, indicating that the source is currently forming stars at a rate more than two times higher than its recent past average.

The timescales of Hα and UV emission provide further insights. Following the discussion presented in Faisst et al. (2019), Iani et al. (2024b), and Navarro-Carrera et al. (2024)¹⁰, after a star formation episode, Hα is initially enhanced due to newly formed O and B stars, while the UV luminosity is still rising. This results in $\text{SFR}(\text{H}\alpha)/\text{SFR}(\text{UV}) > 1$, which has been suggested as a signature of a bursty star formation phase (Atek et al. 2022). As massive stars rapidly evolve and die, Hα emission declines, while longer-lived UV-emitting stars sustain the UV luminosity, leading to $\text{SFR}(\text{H}\alpha)/\text{SFR}(\text{UV}) < 1$. As these UV-bright stars also fade, the ratio eventually returns to unity.

Our findings suggest that *Virgil* likely experienced a previous burst of star formation well before the most recent one (i.e., the one currently producing Hα), which

⁹ Both SFR(Hα) and SFR(UV) are corrected for dust attenuation.

¹⁰ See Figure 12 in Faisst et al. 2019 based on different SFHs, Figure 15 in Iani et al. (2024b) based on STARBURST99, and Figure 7 in Navarro-Carrera et al. 2024 based on FIRSTLIGHT simulations.

⁸ Although the systematic uncertainty reported by Chisholm et al. (2022) is on the order of 0.05, the lower bound of our estimate makes $f_{\text{esc, LyC}}$ consistent with 0%. Nonetheless, the resulting ξ_{ion} would not differ significantly from the reported value.

explains its SFR(UV) and likely placed its \mathcal{B} below unity. We now measure $\mathcal{B} = 0.32 \pm 0.16$, indicating that the source is either entering a new bursty phase or fading out of one. Notably, this is consistent with its position in the SFR– M_* plane (Rinaldi et al. 2022, 2024c), where it overlaps with the separation line for the starburst cloud proposed by Caputi et al. (2017, 2021). This suggests we may be observing *Virgil* at a transitional stage in its star formation history.

3.3. The ISM Conditions of *Virgil*: Excitation vs. Ionization

Since the NIRSPEC/PRISM spectrum provides access to [O II] $\lambda\lambda 3727, 3729$, [Ne III] $\lambda 3869$, H δ , H β , and [O III] $\lambda\lambda 4959, 5007$ at $z \approx 6.64$, we investigated the interstellar medium (ISM) conditions of *Virgil* by leveraging the following line ratios: O32, R23, Ne3O2, and Ne3O2Hd. To fully explore the complexity of the ISM in this source, we closely followed the methodology described in Calabrò et al. (2023) and Calabrò et al. (2024a), running PYCLOUDY (v0.9.15) with CLOUDY version 17.01 (Ferland et al. 2017). We adopted their setup (see Calabrò et al. 2024a, Section 2.3) to generate line predictions for direct comparison with our results.

Briefly, we modeled SFGs with a spherically symmetric, radiation-bounded shell of gas surrounding a population of young (O- and B-type) stars, adopting the incident radiation field from BPASS stellar population models (with an IMF extending up to $100 M_*$ and a continuous star formation in the past 30 Myr; Eldridge et al. 2017). Following Calabrò et al. (2024a), we considered the metallicity range from 0.05 to 1 times solar (i.e., 0.05, 0.1, 0.15, 0.2, 0.3, 0.4, 0.5, 0.7, 1), with the solar reference consistent with Asplund et al. (2009). In all cases, we derived predictions for four different ionization parameters $\log_{10}(\mathcal{U}) = -3, -2.5, -2, \text{ and } -1.5$ and for three gas density values ($10^2, 10^3, \text{ and } 10^4 \text{ cm}^{-3}$).

Given the low metallicity we inferred for this object, we decided to follow the approach adopted in Calabrò et al. (2024a) also for the dust depletion, where the metals are depleted in the beginning of our CLOUDY calculations, and we considered that this depletion is metallicity dependent, as discussed in Calabrò et al. (2023) (see their Table 2).

Finally, we explored the density-bounded scenario for the nebula by varying the stopping criterion in CLOUDY from a Lyman continuum (LyC) optical depth = 10 (fully ionization bounded case) to 0.1 (fully density-bounded case). This would correspond to an escape fraction of ionizing photons going from 0% to 100%. A density-bounded scenario typically enhances the flux of high-ionization species relative to

low-ionization species. That is, this would increase the O32 and Ne3O2 indices, mimicking the effect of a high ionization parameter. However, as previously found, *Virgil* has a very low $f_{esc, \text{LyC}}$ ($\approx 2\%$), so the increase in O32 and Ne3O2 would be very minimal (< 0.05 dex), thus not impacting our conclusions. We refer the reader to Calabrò et al. (2023) and Calabrò et al. (2024a) for a more detailed description of the models adopted in this work.

As reported by Calabrò et al. (2024a), the ionization of the ISM increases with redshift, as seen in the R23–O32 diagram (Figure 3, left panel) from the local Universe (SDSS) to high redshifts (see redshift bins from $z \approx 4$ to $z \approx 12$ in Calabrò et al. 2024a). For comparison, we include recent high-redshift ($z \approx 4 - 12$) NIRSPEC results from Cameron et al. (2023); Mascia et al. (2023); Nakajima et al. (2023); Boyett et al. (2024); Calabrò et al. (2024a,b); Roberts-Borsani et al. (2024), along with the low-redshift sample from the Sloan Digital Sky Survey (SDSS; York et al. 2000; Kauffmann et al. 2003). Additionally, we include metal-poor and high-ionization systems selected in the local Universe to approximate the properties of high-redshift galaxies (Bian et al. 2018).

Virgil lies in the upper region of this diagram, but it is not as extreme as, for instance, GHZ2 at $z \approx 12$, analyzed by Calabrò et al. (2024a) and first reported by Zavala et al. (2025). Overall, its behavior aligns with other high- z galaxies observed during the Epoch of Reionization (EoR). Comparing its position with photoionization models for SFGs, *Virgil* overlaps with a wide range of models, from high-ionization systems ($\log_{10}(\mathcal{U}) = -1.5$) with nearly solar metallicity to lower-ionization ($\log_{10}(\mathcal{U}) = -2.5$) metal-poor environments, spanning a variety of electron densities ($10^2 - 10^4 \text{ cm}^{-3}$). This degeneracy complicates its interpretation. However, independent measurements (see Section 3.2.2) suggest $\log_{10}(\mathcal{U}) \approx -2$ and a metal-poor composition ($\approx 10 - 20\% Z_{\odot}$), help to constrain its nature. Taken together, these results suggest that *Virgil* shares properties with the average SFG population during EoR.

We also investigated the Ne3O2Hd–Ne3O2 diagram (Figure 3, right panel). As with R23–O32, we include SDSS galaxies from the local Universe and high- z analogs from Bian et al. (2018). *Virgil* falls within the region occupied by other high- z galaxies (e.g., Heintz et al. 2025) and lies along the evolutionary sequence reported by Calabrò et al. (2024b) at $z \approx 4 - 12$. Compared to R23–O32, this diagram exhibits less degeneracy with photoionization models. However, model predictions in this case would suggest a lower $\log_{10}(\mathcal{U})$ for metal-poor solutions, but still within the range inferred for this object when using different tracers.

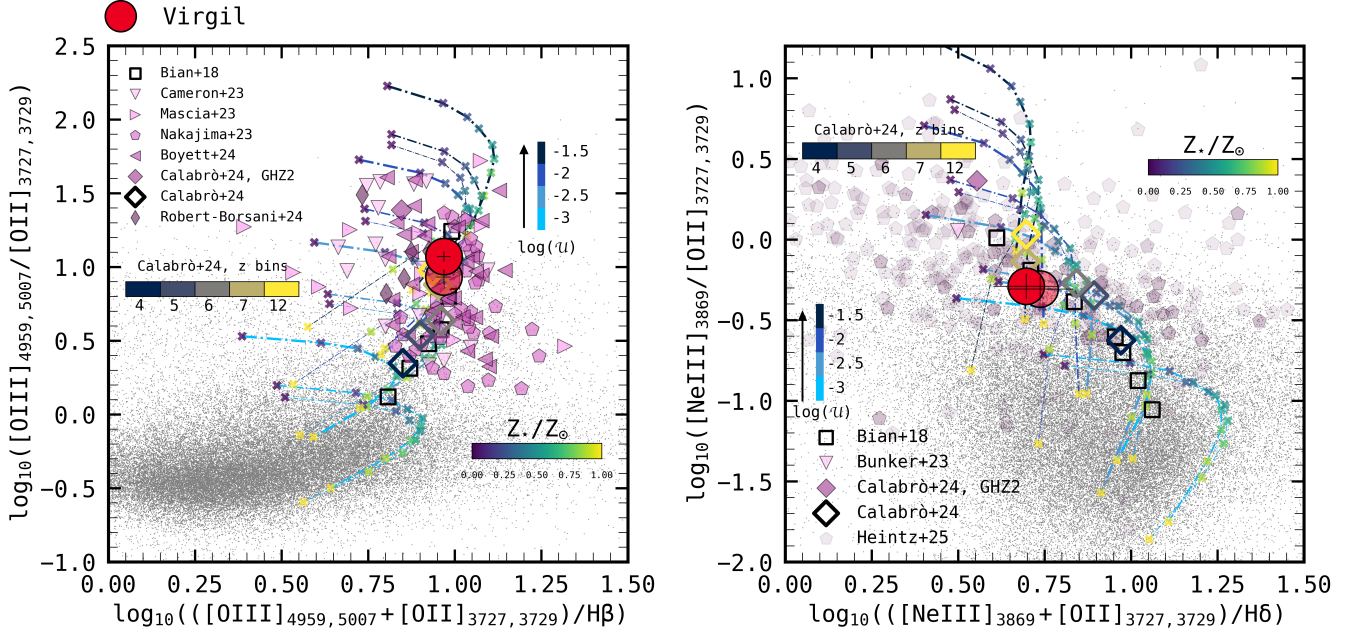


Figure 3. Left Panel: O32–R23. Right Panel: Ne3O2Hd–Ne3O2. *Virgil* is shown as a red filled circle, with higher opacity representing the case without dust correction and lower opacity indicating the dust-corrected one. In both panels, we show the photoionization models from CLOUDY with the following setup: n_e (10^2 , 10^3 , and 10^4 cm^{-3} ; increasing thickness), $\log_{10}(\mathcal{U})$ (-3, -2.5, -2, -1.5; different shades of blue), and different metallicities (0.05 to solar; color-coded in viridis using “x” symbols). For comparison, we show low- z SF galaxies from SDSS (York et al. 2000; Kauffmann et al. 2003) and local high- z analogues from Bian et al. (2018). To put our results in context, we also show recent observations at high- z from Bunker et al. (2023); Cameron et al. (2023); Mascia et al. (2023); Nakajima et al. (2023); Boyett et al. (2024); Calabrò et al. (2024a,b); Roberts-Borsani et al. (2024); Heintz et al. (2025) at $z \approx 4 - 12$.

Without the prior assumption that *Virgil* may host an AGN, as proposed in Iani et al. (2024a), these two diagrams, together with the previously derived physical properties, indicate that *Virgil* has a hard ionizing radiation field and ionization properties consistent with the average SFG population observed during EoR. However, its exceptionally high equivalent width for $[\text{O III}]\lambda\lambda 4959, 5007$ (1514 ± 18 Å), combined with its low metallicity ($10 - 20\% Z_{\odot}$) and relatively low M_{\star} ($\log_{10}(M_{\star}/M_{\odot}) \approx 8.5$ from Iani et al. 2024a), suggest that *Virgil* is a relatively low- M_{\star} extreme line emitter, consistent with the sample studied by Boyett et al. (2024), which spans similar redshifts.

Interestingly, following the discussion in Rhoads et al. (2023) and the spectral properties analyzed so far, *Virgil* could resemble a typical Green Pea (GP; Cardamone et al. 2009; Jaskot & Oey 2013; Henry et al. 2015; Izotov et al. 2016; Brunner et al. 2020, among others) or a Blueberry (BB; e.g., Cameron et al. 2023; Langeroodi et al. 2023), which are often referred to as the best nearby analogs to high-redshift galaxies.

3.4. Does the spectrum indicate that *Virgil* is an AGN?

Iani et al. (2024a) modeled *Virgil* across all available photometric bands (from HST and JWST), performing

SED fitting using multiple codes, and concluded that it contains an AGN. We will re-examine this approach with improved data in Section 4. To investigate this possibility further, we exploit NIRSpect/PRISM data to search for spectral signatures indicative of an AGN.

3.4.1. Searching for Broadening in the Balmer Lines

In Iani et al. (2024a), we found that *Virgil*'s SED resembles that of a LRD, which often exhibits broad Balmer lines (e.g., Furtak et al. 2023; Kokorev et al. 2023; Matthee et al. 2024; Rinaldi et al. 2024a). Using MSAEXP, we modeled the NIRSpect/PRISM data with and without a broad component for the Balmer lines ($\text{H}\alpha$ and $\text{H}\beta$), closely examining the residuals. Figure 4 presents the results in two panels. To take into account the effects of the line-spread function, we additionally convolve our model with a Gaussian of variable resolution (Isobe et al. 2023; de Graaff et al. 2024). On the left, we show the fit to the $\text{H}\alpha$ + $[\text{NII}]$ complex without a broad- $\text{H}\alpha$ component, while on the right, we show the fit with the broad- $\text{H}\alpha$ component. In the latter case, the broad component is detected at the level of approximately 20σ and exhibits a full width at half maximum (FWHM) of 1750 ± 575 km/s.

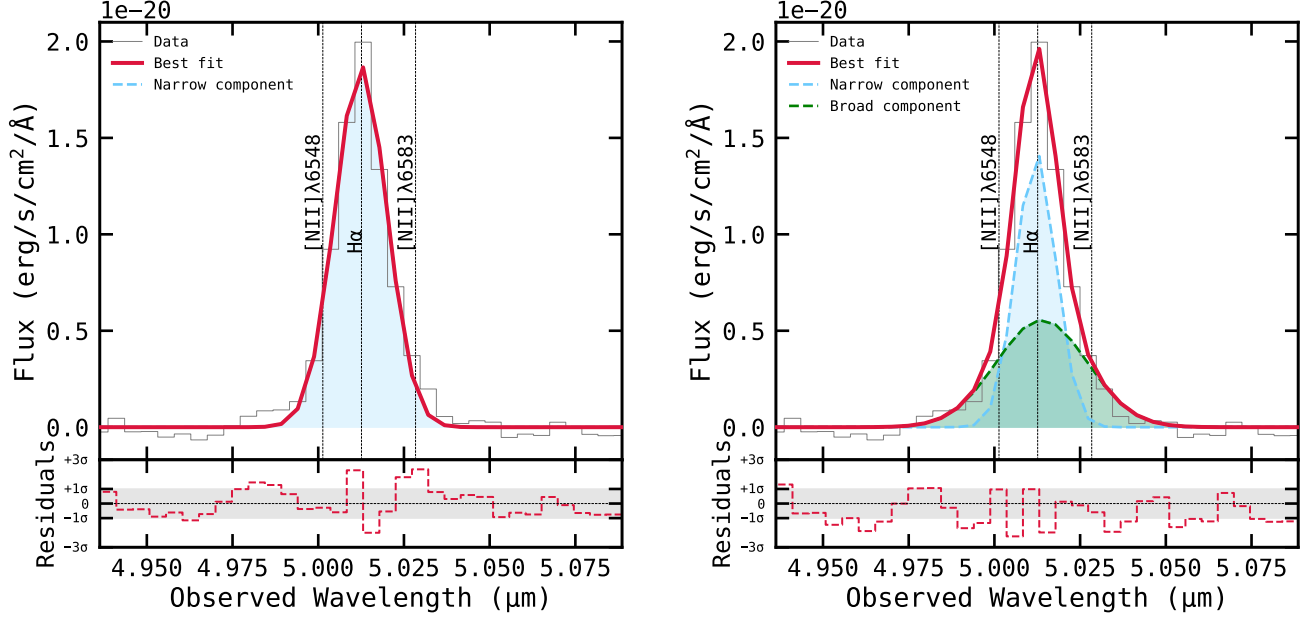


Figure 4. **Left panel:** Fit of the H α + [NII] complex without including a broad component. **Right panel:** Fit of the H α + [NII] complex with adding a broad component. In this case, the FWHM is 1750 ± 575 km s⁻¹. The residuals appear to behave better when a broad component is included, although the BIC shows only a marginal improvement with the added complexity.

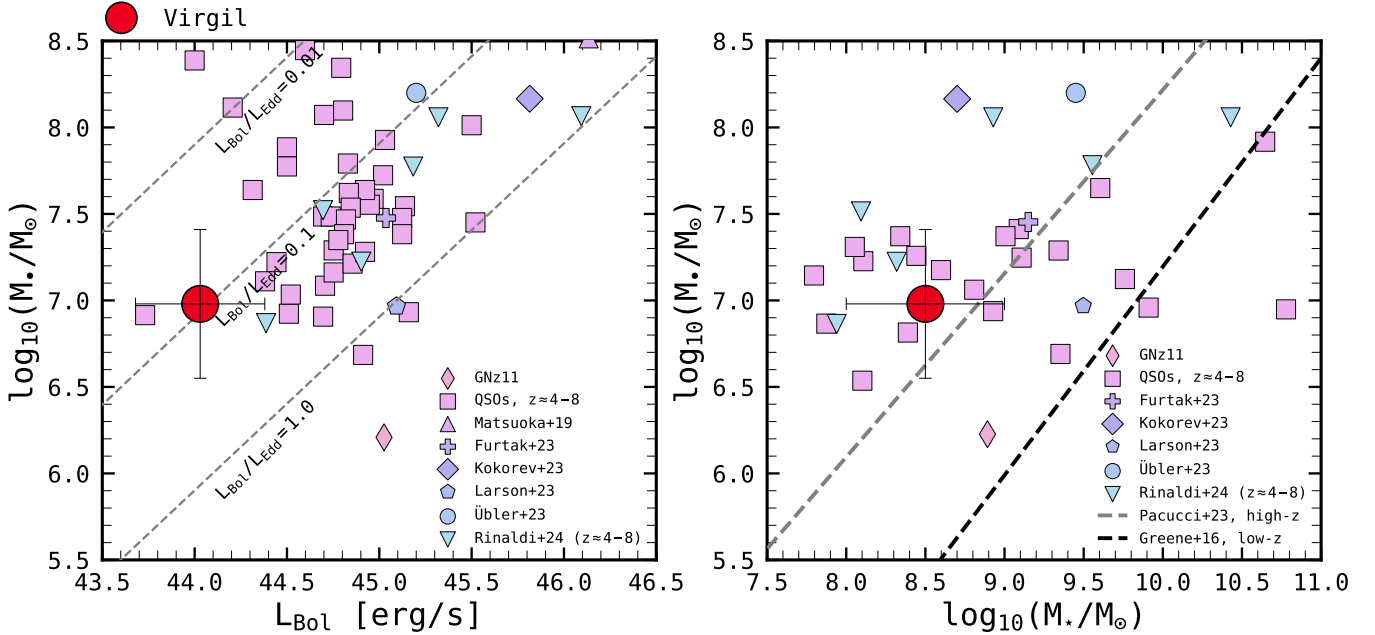


Figure 5. **Left panel:** The derived M_{\bullet} as a function of L_{Bol} , assuming *Virgil* has a broad component in H α . We also show other recent findings from the literature (with some of them selected as LRDs, Rinaldi et al. 2024a): Matsuoka et al. (2019); Furtak et al. (2023); Harikane et al. (2023); Kocevski et al. (2023); Kokorev et al. (2023); Larson et al. (2023); Übler et al. (2023); Maiolino et al. (2024). The dashed lines represent bolometric luminosities corresponding to Eddington ratios of $L_{\text{Bol}}/L_{\text{Edd}} = 0.01, 0.1, \text{ and } 1.0$. **Right panel:** The derived M_{\bullet} as a function of M_{\star} (stellar mass for *Virgil* comes from Iani et al. 2024a and its error bar reflects the overall uncertainty in fitting this object). For comparison, we show the bold black dashed line indicating the best fit to $z \approx 0$ AGN samples (Greene et al. 2016). The trend at higher redshifts is based on the recent analysis presented in Pacucci et al. (2023).

To assess the quality of these fits, we computed the Bayesian Information Criterion (BIC; Liddle 2007) for both scenarios. The model, including the broad component, achieved the lowest BIC, indicating the best balance between goodness-of-fit and model complexity. However, the ΔBIC is not large enough to definitively conclude that *Virgil* is a Type-1 AGN ($\Delta\text{BIC} < 2$). We also observe a tentative detection of a broad component in $\text{H}\beta$, but its significance falls below 2σ , leaving its presence uncertain. We want to highlight that these results may be affected by the source’s position within the slit (Figure 1, right panel): the slit only partially covers the galaxy, with the red knot located near the edge—or possibly even in the gap between shutters—potentially limiting our sensitivity to broad-line emission.

Nonetheless, under the assumption that *Virgil* exhibits $\text{H}\alpha$ with a broad component, we estimated the central black hole mass (M_\bullet). Assuming the gas in the broad line region (BLR) is virialized, M_\bullet was derived from the spectral properties of the $\text{H}\alpha$ BLR region using the calibration proposed by Reines et al. (2013):

$$\log_{10}\left(\frac{M_{\text{BH}}}{M_\odot}\right) = \alpha + \log_{10}(\epsilon) + \beta \log_{10}\left(\frac{L_{\text{H}\alpha, \text{broad}}}{1 \times 10^{42} \text{ erg/s}}\right) + \gamma \log_{10}\left(\frac{\text{FWHM}_{\text{broad}}}{1 \times 10^3 \text{ km/s}}\right), \quad (2)$$

where $\alpha = 6.57$, $\beta = 0.47$, and $\gamma = 2.06$, and ϵ is the scaling factor which depends on the structure, kinematics, and orientation of the BLR. Different studies report ϵ ranging from 0.75 to 1.4 (e.g., Reines et al. 2013). Following Reines & Volonteri (2015), for our M_\bullet , we adopted $\epsilon = 1.075 \pm 0.325$. We retrieved $\log_{10}(M_\bullet/M_\odot) = 6.98 \pm 0.35$, which is in agreement with the estimate provided by Iani et al. (2024a) (based on photometry). We estimated the bolometric luminosity (L_{bol}) by using Equation 6 in Stern & Laor (2012), finding that $\log_{10}(L_{\text{bol}}/(\text{erg s}^{-1})) = 44.03 \pm 0.43$. We also adopted Equation 1 from Netzer (2009) from which we derive $\log_{10}(L_{\text{bol}}/(\text{erg s}^{-1})) = 45.17 \pm 0.02$, which likely represents an upper limit. Also in this case, these estimates are in agreement with Iani et al. (2024a). In Figure 5 we show our measurements of M_\bullet for *Virgil* in the context of the recent literature.

Based on the derived M_\bullet from the $\text{H}\alpha$ BLR, we also derived the Eddington luminosity. We found that $\log_{10}(L_{\text{Edd}}/(\text{erg s}^{-1})) = 4\pi G M_\bullet m_p c / \sigma_T = 45.07 \pm 0.35$, where G is the gravitational constant, m_p the proton mass, c the speed of light, and σ_T the Thomson scattering cross-section. Finally, we estimated the Eddington ratio as $\lambda_{\text{Edd}} = L_{\text{bol}}/L_{\text{Edd}}$. Depending on the choice of L_{bol} , the Eddington ratio (λ_{Edd}) ranges from ≈ 0.1 to 1.23, consistent with the typical values found for LRDs

Table 3. Black Hole Properties

Property	Value
FWHM* [km/s]	1750 ± 575
$\log_{10}(M_\bullet/M_\odot)$	6.98 ± 0.35
$\log_{10}(L_{\text{Bol}}/(\text{erg s}^{-1}))^{**}$	$44.03 \pm 0.43 - 45.17 \pm 0.02$
$\log_{10}(L_{\text{Edd}}/(\text{erg s}^{-1}))$	45.07 ± 0.35
λ_{Edd}	$0.1 - 1.23$

NOTE—These measurements rely on the assumption that the broadening of $\text{H}\alpha$ is real. Nonetheless, these values are in agreement with previous estimates from photometry presented in Iani et al. (2024a). * refers to the broad component of $\text{H}\alpha$. ** refers to the two values estimated by using both Stern & Laor (2012) and Netzer (2009) formulas.

(e.g., Noboriguchi et al. 2023). We show our results in Figure 5 and summarize these measurements in Table 3.

3.4.2. Searching for AGN Signatures with Line Ratio Diagnostics

Disentangling SFGs from AGNs at high redshift is particularly challenging. Classical diagnostics, such as the Baldwin, Phillips & Terlevich (BPT; Baldwin et al. 1981) diagram, were calibrated for low-redshift galaxies and strongly depend on metallicity, making them less reliable in the early Universe. At high redshift, galaxies are typically more metal-poor (e.g., Topping et al. 2024), with younger stellar populations and higher ionization parameters. These conditions shift SFGs toward the AGN locus in BPT-like diagrams, while AGN Narrow Line Regions (NLRs) often overlap with the SFG sequence. As a result, traditional line-ratio diagnostics become increasingly ambiguous, as also predicted by theoretical models (Nakajima & Maiolino 2022).

Although we are not able to resolve $[\text{N II}]\lambda 6548$ from $\text{H}\alpha$ and both $[\text{O I}]\lambda 6302$ and the $[\text{S II}]\lambda\lambda 6717, 6731$ doublet have $\text{SNR} \lesssim 2$, it is important to stress that classical BPT-like diagrams may not reliably determine whether *Virgil* hosts an AGN. Even when these lines are available, recent studies have shown that AGNs can occupy the same region as SFGs in BPT diagrams. For example, the $z \approx 5.55$ galaxy GS.3073 shows clear AGN signatures through broad $\text{H}\alpha$ and $\text{H}\beta$ emission, yet it lies within the SFG region in the BPT diagram (Übler et al. 2023). Like *Virgil*, GS.3073 is extremely metal-poor ($12 + \log(\text{O}/\text{H}) = 8.02$), underscoring how low metallicity can blur the distinction between star formation- and AGN-dominated galaxies at high redshift. Similar conclusions have been reported by Scholtz et al. (2023)

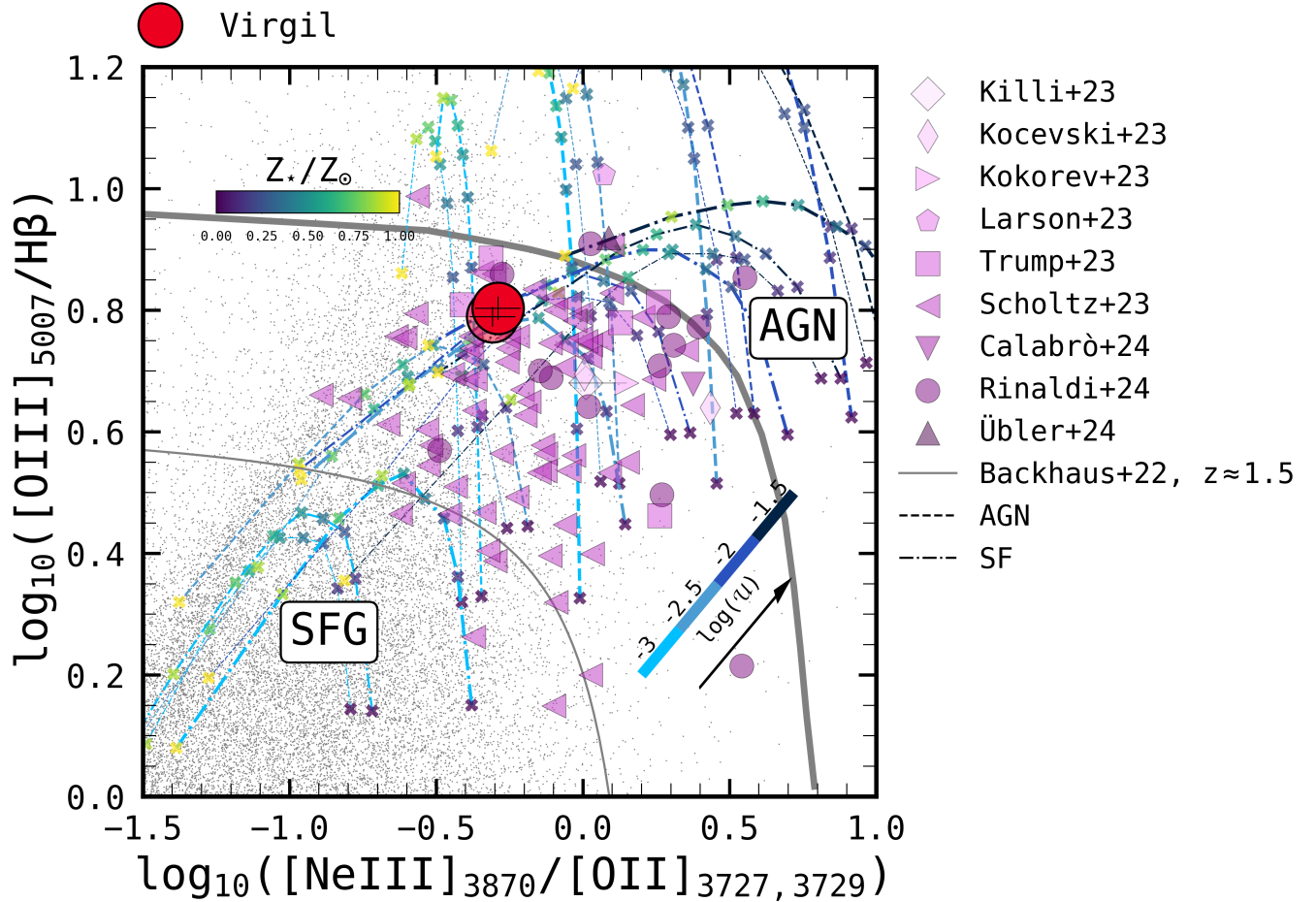


Figure 6. The “OHNO” diagram, displaying the following ratios: $[\text{OIII}]\lambda 5007/\text{H}\beta$ vs. $[\text{NeIII}]\lambda 3870/[\text{OII}]\lambda 3727, 3728$. *Virgil* is shown as a red filled circle, with higher opacity representing the case without dust correction and lower opacity indicating the dust-corrected one. We also show the recent literature at $z \gtrsim 4$ from Killi et al. (2023); Kocevski et al. (2023); Kokorev et al. (2023); Larson et al. (2023); Trump et al. (2023); Übler et al. (2024b); Calabrò et al. (2024a); Rinaldi et al. (2024a). In particular, sources from Rinaldi et al. (2024a) have been photometrically selected as LRDs, with some of them clearly showing broad components in their Balmer lines from NIRSpec data. For comparison, we also show SDSS (SFGs and AGNs) at low- z ($z \approx 0$) from York et al. (2000); Kauffmann et al. (2003). The separation line comes from Backhaus et al. (2022) at $z \approx 1.5$. We also show an extrapolation at $z \approx 6.5$ (increased thickness), based on Backhaus et al. (2024). For comparison, theoretical predictions (for both SFGs and AGNs; dashdot and dashed respectively) are shown with the following settings: n_e (10^2 , 10^3 , and 10^4 cm^{-3} ; increasing thickness), $\log_{10}(U)$ (-3, -2.5, -2, -1.5; different shades of blue), and different metallicities (0.05 to solar; color-coded in viridis using “x” symbols).

and Kocevski et al. (2023), in agreement with photoionization models from Nakajima & Maiolino (2022), which predict significant overlap between low-metallicity SFGs and AGNs in classical diagnostics.

Since the launch of JWST, the limitations of classical diagnostics have led to renewed efforts to develop alternative line-ratio diagrams optimized for high-redshift galaxies (e.g., Hirschmann et al. 2023; Mazzolari et al. 2024; Shapley et al. 2024; Backhaus et al. 2025). In the following, we employ a set of diagnostic diagrams that have been extensively used to distinguish AGNs from SFGs at high redshifts.

The “OHNO” diagram—One widely used high-redshift diagnostic is the “OHNO” diagram (Trouille et al. 2011; Zeimann et al. 2015; Backhaus et al. 2022, 2023; Cleri et al. 2023; Trump et al. 2023; Feuillet et al. 2024), which is based on Ne3O2 and R3 and has proven to be a robust ionization diagnostic for high-redshift galaxies. Ne3O2 is particularly useful as it involves emission lines with similar ionization energies and closely spaced wavelengths, minimizing dust attenuation effects. As with the R23–O32 and Ne3O2H δ –Ne3O2 diagrams, we also included photoionization models, following the configuration adopted by Calabrò et al. (2024a). For AGN models, we adopted the default CLOUDY

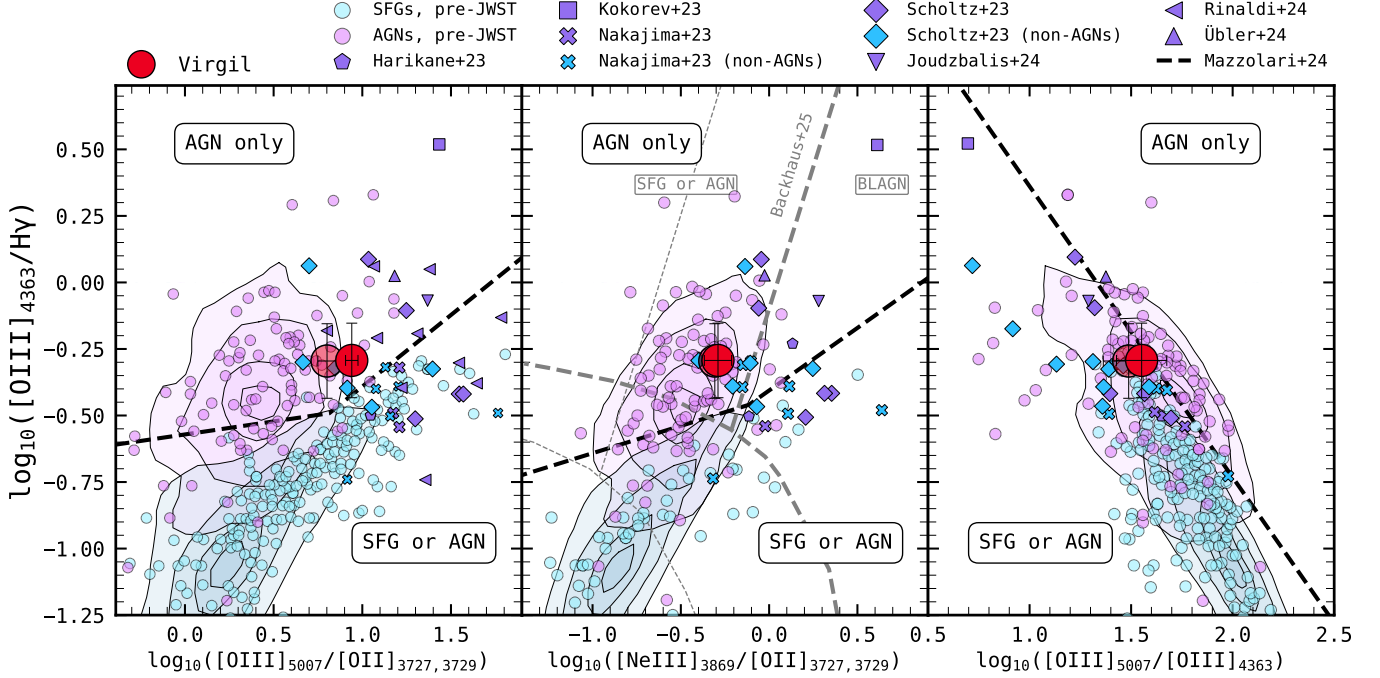


Figure 7. **Left Panel:** O32 vs. O3Hg. **Middle Panel:** Ne3O2 vs. O3Hg. **Right Panel:** O33 vs. O3Hg. *Virgil* is shown as a red filled circle, with higher opacity representing the case without dust correction and lower opacity indicating the dust-corrected one. The dashed black lines indicate the separation criteria proposed by Mazzolari et al. (2024) to distinguish AGNs from SFGs. The contour areas correspond to the SDSS sample in the local Universe (Abazajian et al. 2009) for comparison. Filled circles represent pre-JWST literature data for SFGs and AGNs (mostly at low redshift; Seyfert 1943; Izotov et al. 2006; Berg et al. 2012; Amorín et al. 2015; Perna et al. 2017; Yang et al. 2017a,b; Izotov et al. 2018; Dors et al. 2020; Armah et al. 2021; Pustilnik et al. 2021). For comparison with recent JWST-based studies, we include results from Harikane et al. (2023); Nakajima et al. (2023); Scholtz et al. (2023); Übler et al. (2024b); Juodžbalis et al. (2024); Rinaldi et al. (2024a) (with some of them having both SFGs and AGNs). In particular, the sample from Rinaldi et al. (2024a) consists of photometrically selected LRDs in GOODS-S, some exhibiting clear broadening in the Balmer lines. The gray dashed line in the middle panel represents the separation criterion at $z \gtrsim 4$ recently proposed by Backhaus et al. (2025) to distinguish BLAGNs from non-BLAGNs.

prescription, assuming a multi-component power-law continuum with a “blue bump” temperature of 10^6 K and spectral energy indices of $\alpha_{UV} = -0.5$, $\alpha_X = -1.35$, and $\alpha_{OX} = -1.4$ (Groves et al. 2004) for the UV, X-ray, and optical-to-X-ray ranges, respectively. We used the same grid of metallicities (0.05 to 1 solar) as for the models for SFGs. We refer the reader to Calabrò et al. (2023) and Calabrò et al. (2024a) for a more detailed discussion of these models.

It is worth noting that the OHNO diagram may be affected by its dependence on metallicity (Tripodi et al. 2024), where metal-poor objects, such as *Virgil*, can appear as outliers (Scholtz et al. 2023).

In Figure 6, we show the “OHNO” diagram with *Virgil* as well as the recent literature on other high- z sources (Killi et al. 2023; Kocevski et al. 2023; Kokorev et al. 2023; Larson et al. 2023; Trump et al. 2023; Scholtz et al. 2023; Übler et al. 2024b; Calabrò et al. 2024a; Rinaldi et al. 2024a; with some of them identified as Type 1 and Type 2 AGNs) and, for comparison, the sample of SFGs

and AGNs at $z \approx 0$ from York et al. (2000); Kauffmann et al. (2003).

Virgil exhibits moderately high Ne3O2 and R3 ratios¹¹ and it lies well above the separation line proposed by Backhaus et al. (2022) at $z \approx 1.5$. Thus, it is consistent with AGN model predictions at subsolar metallicities ($Z_{\text{gas}}/Z_{\odot} \lesssim 0.2$), moderate ionization parameters ($\log_{10}(U) \approx -3$), and $n_e \approx 10^3 - 10^4 \text{ cm}^{-3}$. However, *Virgil* is also consistent with SF models, overlapping with the parameter space expected for H II regions with high n_e ($\approx 10^3 - 10^4 \text{ cm}^{-3}$), high ionization parameter ($\log_{10}(U) \approx -2$), and wide range of metallicities.

Interestingly, *Virgil* occupies a region of the parameter space consistently populated by LRDs (some of which exhibit clear broadening in their Balmer lines; Rinaldi et al. 2024a), as well as other recently discovered AGNs (including Type 2; e.g., Kocevski et al. 2023; Koko-

¹¹ We show our measurements before and after applying dust corrections.

rev et al. 2023; Larson et al. 2023; Scholtz et al. 2023; Übler et al. 2024b). However, as shown in Calabrò et al. (2024a) and supported by CLOUDY model predictions, this region of parameter space is also consistently populated by SFGs with a different set of properties.

We then utilized the recent results of Backhaus et al. (2022, 2025) to extrapolate the separation line up to $z \approx 6.5$ (thick gray line), relying on the proposed redshift evolution of R3 and N3O2. In this scenario, *Virgil*, along with sources from Killi et al. (2023), Scholtz et al. (2023), Trump et al. (2023), as well as LRDs from Rinaldi et al. (2024a), and the BL AGN from Kokorev et al. (2024), would fall below the extrapolated separation line, placing *Virgil* within the SFG region—or at least blurring the net distinction that would otherwise arise using the relation at $z \approx 1.5$.

We emphasize that this is only a test to explore the implications of shifting the separation line to higher redshifts, based on the evolutionary trends proposed by Backhaus et al. (2022, 2025), and should not be interpreted as a definitive redefinition. Nonetheless, applying diagnostic diagrams calibrated at lower redshifts complicates the classification of *Virgil* and could provide misleading results in general.

Considering the degeneracies revealed by CLOUDY models in the region of the parameter space occupied by *Virgil* and the possible redshift evolution of R3 and Ne3O2, both the SFG and AGN scenarios (or a mixed nature) remain plausible for this source.

The [O III] λ 4363 diagrams—Mazzolari et al. (2024) proposed new separation lines for three diagnostic diagrams based on [O III] λ 4363, which has been linked to AGN activity (Brinchmann 2023) with higher ISM temperatures driven by AGN ionizing radiation (Übler et al. 2024b):

1. O32 vs. O3Hg
2. Ne3O2 vs. O3Hg
3. O33 vs. O3Hg

From a theoretical point of view, enhanced [O III] λ 4363 emission could hint at the presence of an AGN, as the ionizing photons produced by an AGN are typically more energetic than those from star formation, thus leading to significantly more efficient gas heating. Notably, it has been proposed that strong [O III] λ 4363-emitting regions may coincide with high-ionization nuclear emission-line regions (HINERs; Binette 1985), and that an enhanced [O III] λ 4363/[O III] λ 5007 ratio ($R_{[OIII]}$) would imply a strong connection with AGN activity. For *Virgil* we find that $R_{[OIII]} = 0.032 \pm 0.01$,

which is similar to what has been observed in other Seyfert 2s: ESO 138-G01, Mrk 1210, and NGC 4507, for which Binette et al. (2024) concluded that a high-density NLR component is likely present. In particular, the combination of such high $R_{[OIII]}$ and relatively high R3 would imply that their plasma is much hotter ($\approx 18000 - 20000$ K), possibly as a result of fast shocks (e.g., Binette et al. 1985). Following this line, Nagao et al. (2001) found, for a sample of low- z objects, that a high $R_{[OIII]}$ ratio correlates with objects exhibiting hotter MIR colors.

Below, we briefly overview each diagnostic diagram (already presented in Mazzolari et al. 2024).

We want to highlight that dust reddening can significantly affect the line ratios, particularly for the O32–O3Hg diagram, due to the wavelength separation between the adopted lines. This effect can cause AGNs to shift toward the SFG+AGN locus when there is substantial reddening. Nonetheless, the inverse scenario does not hold, as SFGs would not populate the AGN locus under any circumstances. The Ne3O2–O3Hg diagram, instead, is very similar to the “OHNO” diagram, but it is more stable as the separation between SFG and AGN is mainly based on a different gas temperature.

For O32–O3Hg, Mazzolari et al. (2024) showed that high- z sources are generally distributed toward the upper region of the diagram compared to local samples (SDSS, contour area). Moreover, they point out that a non-negligible fraction of high- z sources not classified as AGNs falls within the region occupied by local AGNs. In contrast, some high- z AGNs overlap with the area covered by their local analogs. Following the discussion in Mazzolari et al. (2024) and their photoionization models, SFGs should occupy a well-constrained region of the O32–O3Hg diagram, with their upper boundary closely matching the distribution of SDSS SFGs and local analogs. In contrast, AGNs are expected to populate both the SFG region and the area occupied by local AGN samples. They show that SFG models do not extend into the AGN-dominated region. However, AGN models can reach the SFG region for some local and high- z AGNs. They also conclude that these trends remain unchanged even when considering the entire grid of SFG models from Feltre et al. (2016), reinforcing the idea that AGN-driven photoionization can produce significantly higher [O III] λ 4363/ $H\gamma$ ratios than ionization from hot stars. This is likely due to the higher-energy ionizing photons in AGNs, which heat the gas more efficiently at a given ionization parameter.

As with the O32–O3Hg diagram, normal SFGs and local analogs primarily occupy the lower region of the Ne3O2–O3Hg parameter space, while AGNs are now

distributed across a broader area, including the upper-left region, which is not reached by any of the SFG models that [Mazzolari et al. \(2024\)](#) tested or by observed SFG samples. Notably, they also find that sources classified as AGNs in the O32–O3Hg diagram remain above the SFG distribution in this diagnostic. Likewise, sources not explicitly identified as AGNs but found within the AGN region of the first diagnostic continue to occupy the same region in the Ne3O2–O3Hg diagram.

The third diagnostic compares O33 and O3Hg. The overlap between local SFGs and AGNs is significantly larger than in the previous diagnostics. However, a distinct region characterized by high $[\text{O III}]\lambda 4363/\text{H}\gamma$ and high $[\text{O III}]\lambda 5007/[\text{O III}]\lambda 4363$ remains populated exclusively by local AGNs. As noted by [Mazzolari et al. \(2024\)](#), very few high- z galaxies fall within the AGN-only region, with most shifting toward lower $[\text{O III}]\lambda 5007/[\text{O III}]\lambda 4363$ values. They also show that current photoionization models do not cover this region.

According to [Mazzolari et al. \(2024\)](#), the distribution of SFG models closely follows that of local galaxies, particularly at the boundary with the AGN-only region. In contrast, AGN models extend across both the SFG and AGN regions. They also noted that when considering the full parameter grid of [Feltre et al. \(2016\)](#), SFG and AGN models would overlap entirely.

In the case of *Virgil*¹², we find that it consistently lies above or on the separation lines proposed by [Mazzolari et al. \(2024\)](#) (Figure 7), overlapping with AGNs and LRDs identified in recent studies based on JWST (e.g., [Kokorev et al. 2023](#); [Nakajima et al. 2023](#); [Scholtz et al. 2023](#); [Übler et al. 2023](#); [Juodžbalis et al. 2024](#); [Rinaldi et al. 2024a](#)).

Nonetheless, one should note that $[\text{O III}]\lambda 4363$ could be contaminated by $[\text{Fe II}]\lambda 4360$. However, [Curti et al. \(2017\)](#) showed that such contamination primarily occurs in galaxies with an enriched ISM, whereas *Virgil* is metal-poor. Additionally, [Mazzolari et al. \(2024\)](#), by using CLOUDY models over a wide range of metallicities ($-2 \leq \log(Z/Z_{\odot}) \leq 0.5$) and ionization parameters ($-4 \leq \log_{10}(\mathcal{U}) \leq -1$), found that the $[\text{Fe II}]\lambda 4288/[\text{Fe II}]\lambda 4360$ ratio is roughly constant (≈ 1.25). Therefore, they searched for $[\text{Fe II}]\lambda 4288$ in their sample populating the “AGN-only” region and found no evidence of its presence, concluding that any possible contamination from $[\text{Fe II}]\lambda 4360$ can be considered negligible.

¹² For *Virgil*, $[\text{O III}]\lambda 4363$ and $\text{H}\gamma$ were successfully deblended, with both lines detected at $\text{SNR} > 5$.

As with the “OHNO” diagram, we also explored the potential redshift evolution of key line ratio diagnostics. Specifically, we examined the Ne3O2 versus O3Hg plane (Figure 7, middle panel), based on the empirical evolution recently proposed by [Backhaus et al. \(2025\)](#). We display their separation lines at $z \approx 0$ and $z \approx 6.5$ (gray lines, with increased thickness). Under this redshift evolution, *Virgil* would fall in the SFG/AGN region, suggesting a mixed nature.

We want to highlight that [Backhaus et al. \(2025\)](#), based on photoionization models, found that only AGN-dominated sources populate the region above the separation line proposed by [Mazzolari et al. \(2024\)](#) in this diagram. Indeed, taken at face value, these line ratio diagnostics would clearly place *Virgil* in the AGN regime along with other claimed AGNs at similar redshifts. A similar argument can be made for the O32 and O33 diagnostics shown in the other two panels.

Altogether, this again underscores the complexity of distinguishing AGNs from SFGs at high redshift—especially when accounting for redshift evolution—as illustrated by *Virgil*’s position in a region indicative of a mixed nature.

Being in the “AGN” zone in the adopted diagnostic diagrams is a *condicio sine qua non* for being an AGN, as shown in Figures 6 and 7, although some galaxies in these regions have substantial star formation. If interpreted with no redshift correction, the two sets of diagnostic diagrams analyzed in this section would indicate that *Virgil* may host an AGN: (1) its position in the “OHNO” diagram aligns with regions typically occupied by AGNs and LRDs; while (2) in the $[\text{O III}]\lambda 4363$ -based diagrams from [Mazzolari et al. \(2024\)](#), *Virgil* occupies a region predominantly populated by recently discovered AGNs at high- z . However, this classification strongly depends on the assumption that the criteria to separate SFGs and AGNs remain unchanged with redshift. If the redshift evolution of the relevant line ratios is considered—particularly in light of recent findings (e.g., [Backhaus et al. 2025](#))—the classification of *Virgil* becomes more ambiguous, potentially suggesting a mixed nature or even a galaxy dominated by star formation.

In summary, we have conducted a detailed analysis of *Virgil* based on its emission-line spectrum. At first glance, *Virgil* appears to be a typical galaxy for its redshift, with low-to-moderate attenuation in its emission lines and low but representative metallicity. While its emission-line ratios could suggest AGN activity, this classification becomes ambiguous when accounting for the redshift evolution of diagnostic diagrams. Had it not been identified through its pronounced spectral steepening in the MIRI bands ([Iani et al. 2024a](#)), *Virgil* could

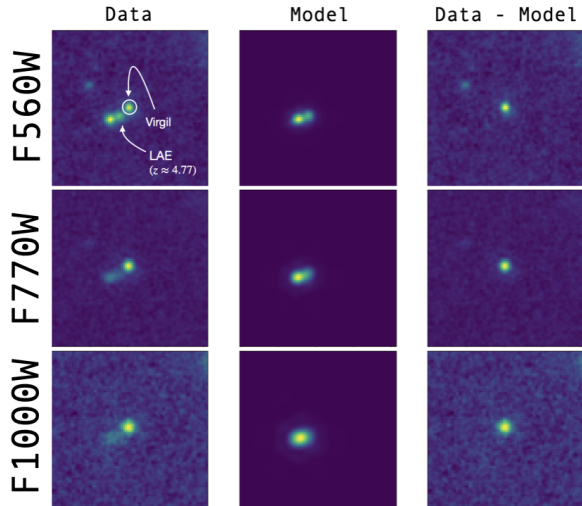


Figure 8. Illustrative example of the modeling and subtraction procedure applied to the foreground LAE at $z \approx 4.77$ located near *Virgil*. Each row corresponds to a different MIRI filter: F560W (top), F770W (middle), and F1000W (bottom). The three columns show, from left to right, the original data, the best-fit model of the LAE, and the residual after model subtraction (**data-model**). No modeling was applied to *Virgil*, which is visible in all panels and highlighted in the F560W stamp. Note that the displayed scales are optimized independently for each panel for visual clarity and are not uniform across filters.

easily be misclassified as an ordinary high- z SFG, sharing many properties with the bulk of the galaxy population during the EoR.

4. PHOTOMETRY AND SPECTRAL ENERGY DISTRIBUTION OF VIRGIL

The nature of *Virgil* remains ambiguous when relying solely on data below $5 \mu\text{m}$, even when rest-frame optical emission lines are considered, but changes significantly with the addition of longer wavelength observations. We leveraged these observations to perform updated photometry and SED fitting since deeper MIRI data are now available at 7.7 , 10 , and $15 \mu\text{m}$ from the MIDIS and PAHSPECS teams. We build on the SED fitting presented in Iani et al. (2024a), now incorporating the latest MIRI data. As the derived physical properties remain essentially unchanged, we refer the reader to Iani et al. (2024a) for a detailed description of the modeling and results. Here, we focus on a more interpretative discussion in light of the spectral analysis presented in this work.

4.1. Forward Modeling and Photometry of *Virgil*

We performed a set of customized photometric measurements using the PHOTUTILS package (Bradley et al. 2022). Object centroids were computed using the “win-

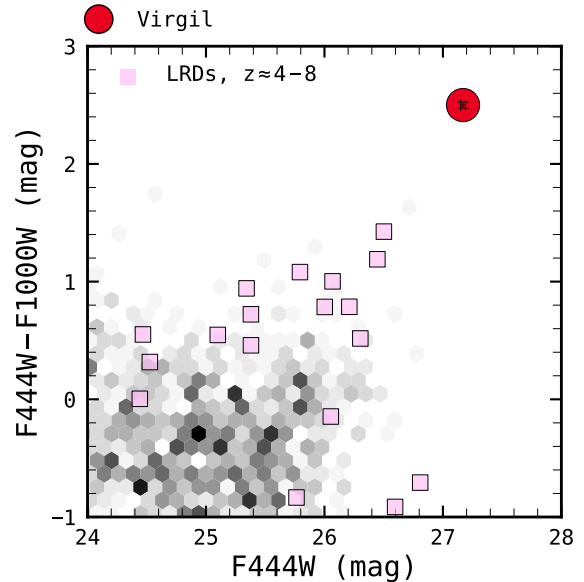


Figure 9. The color-magnitude diagram shows F444W along x-axis and F444W–F1000W along y-axis, including *Virgil*, data from SMILES and JADES (hexagons), and a sample of LRDs in GOODS-S at $z \approx 4-8$ previously reported by Kokorev et al. (2024), Pérez-González et al. (2024b), and Rinaldi et al. (2024a) with MIRI detection in the SMILES catalog in GOODS-S.

dowed positions” method implemented in Source Extractor (Bertin & Arnouts 1996). Depending on the filter, we employed a combination of Kron apertures (Kron 1980) with a Kron parameter of 2.5 and circular apertures. This approach was crucial as *Virgil* appears elongated, particularly at shorter wavelengths (NIRCam short channel), as noted in Iani et al. (2024a). In Figure 9, we show *Virgil*’s color F444W–F1000W (2.50 ± 0.02 mag) with respect to the SMILES sample in GOODS-S as well as a sample of LRDs at $z \approx 4-8$ already reported in Kokorev et al. (2024), Pérez-González et al. (2024b), and Rinaldi et al. (2024a). Interestingly, at $15 \mu\text{m}$, *Virgil* shows F444W–F1500W = 2.87 ± 0.04 mag, which highlights how extreme this source is at the MIRI wavelengths. An overview of *Virgil*’s appearance is presented in Figure 10.

For circular aperture photometry, we adopted filter-dependent radii, with apertures as large as $0.4-0.5''$ in the MIRI bands. In each case, we measured the background in a close region around *Virgil* and calculated the noise using nonadjacent pixels (5 pixels apart) to take into account noise correlation, as explained in Pérez-González et al. (2023). We corrected the photometry to total flux using aperture corrections from JADES (for HST and NIRCam) and SMILES (for MIRI). We validated our new measurements by comparing them with

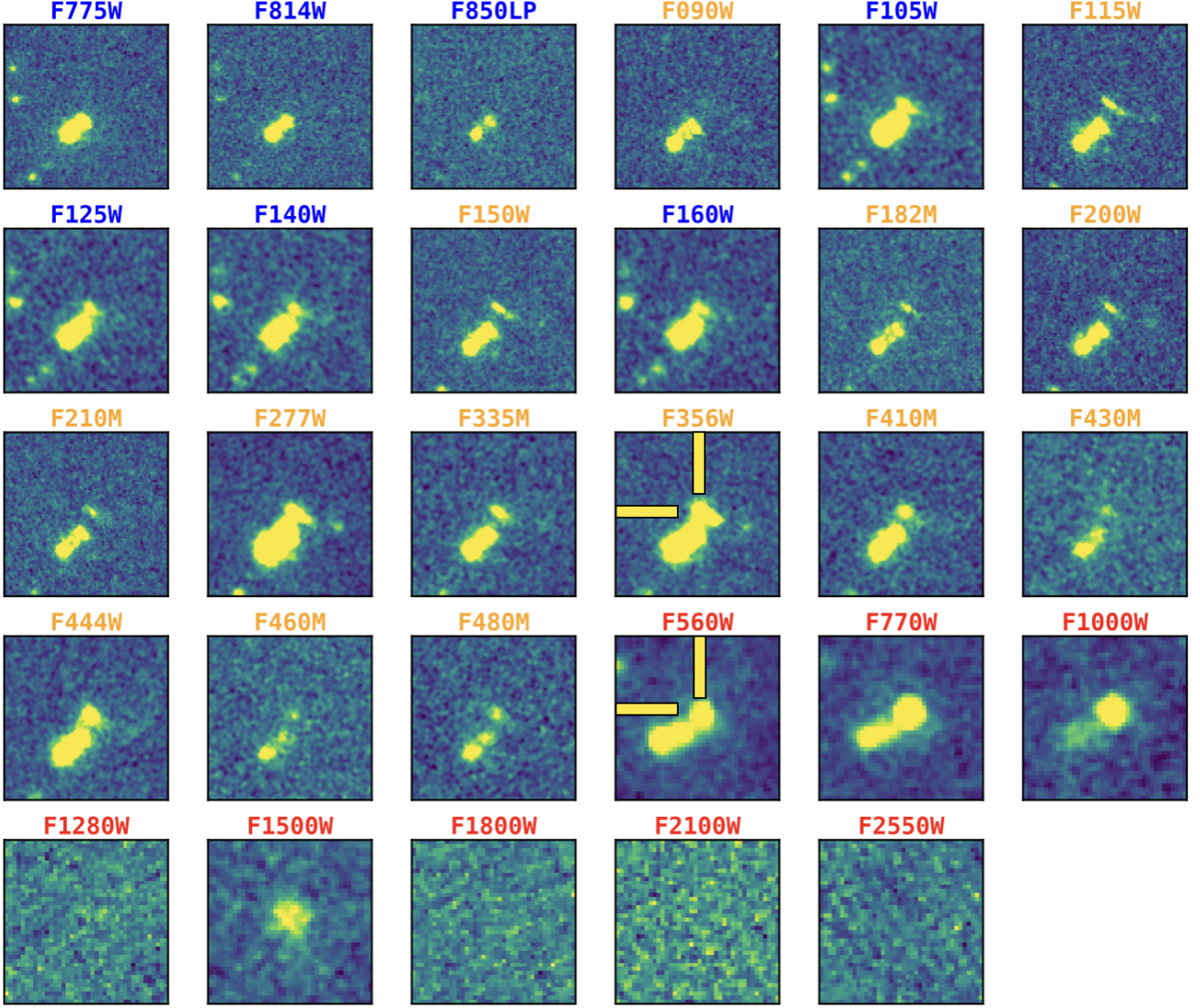


Figure 10. Cutouts ($2.5'' \times 2.5''$) centered on *Virgil*, showing imaging from HST (from F775W only), NIRCcam, and MIRI, each displayed at their native pixel scales (30 mas for HST and NIRCcam, 60 mas for MIRI), and color-coded in blue, orange, and red, respectively. *Virgil* is highlighted in F356W and F560W. Its elongated morphology, featuring two distinct knots, is clearly visible in the NIRCcam bands thanks to their superior resolution. F560W, F770W, and F1000W are from MIDIS; F1500W is from PAHSPECS, while the remaining MIRI bands are from SMILES. Each postage stamp is displayed using its intensity scale centered around the median pixel value to enhance visual contrast across filters.

those reported in Iani et al. (2024a), finding good agreement.

We used FORCEPHO to model and subtract the nearby LAE ($z_{\text{spec}} \approx 4.77$) to avoid light contamination during the photometric measurements. The LAE and *Virgil* were modeled using Sérsic (1968) profiles, with one Sérsic profile representing the extended flux of the LAE and four additional compact Sérsic profiles modeling its stellar clumps. We observed that *Virgil* consists of two knots, one of which likely drives the strong upturn in the SED at MIRI wavelengths, leading us to model these knots separately with two Sérsic profiles. We utilized FORCEPHO to sample all model parameters using

NIRCcam and HST images, employing the Hamiltonian Monte Carlo Markov Chain method. Each galaxy was then forward-modeled in the MIRI images by fitting the flux of each component using non-negative least squares regression, incorporating effective point-spread-function (ePSF) models provided by Libralato et al. (2024). Figure 8 presents the LAE-subtracted image using the best-estimated model, with minimal residuals at the LAE’s location, demonstrating the quality of our modeling. Although we obtained a model flux of *Virgil* during the process, we do not adopt it as fiducial, as the complex morphology of *Virgil* is not well represented by two Sérsic profiles. Nevertheless, we find good agreement be-

tween the model flux and the photometry results from the LAE-subtracted images.

4.2. *Virgil* is a Little Red Dot

First, we examined the photometric criteria for LRDs. Iani et al. (2024a) demonstrated that *Virgil* satisfies most of the commonly used color criteria for LRDs, except for a relatively blue F277W–F444W (Kokorev et al. 2024; Rinaldi et al. 2024a), which explains why it was not selected in recent LRD studies in GOODS-S (Kokorev et al. 2024; Pérez-González et al. 2024a; Rinaldi et al. 2024a). To further characterize *Virgil*, we adopted the methodology of Kocevski et al. (2024) and estimated the continuum slope ($f_\lambda = \lambda^\beta$) between two continuum bands to identify a V-shaped SED. Specifically, following Lin et al. (2024), we applied the criteria $\beta_{UV} < -0.37$ and $\beta_{opt} > 0$, where $\beta = -0.4((m_1 - m_2)/\log_{10}(\lambda_1/\lambda_2)) - 2$. Using F430M and F444W, we obtained $\beta_{opt} \approx 0.87$, while for β_{UV} , we found $\beta_{UV} \approx -0.68$ by relying on F115W and F150W. This places *Virgil* within the locus of V-shaped SED galaxies, reinforcing its classification as a LRD. These findings underscore the complexity of LRD selection (Hainline et al. 2024a) and suggest that refining color criteria, potentially incorporating MIRI photometry when available, may be necessary to select *Virgil*-like sources during EoR. Finally, as highlighted in Iani et al. (2024a), we found that *Virgil* satisfies the compactness criterion, showing $c_{F444W} (\equiv F(0.5'')/F(0.25'')) \approx 1.5$.

5. STELLAR PROPERTIES OF *VIRGIL*

5.1. SED fitting

We followed the approach adopted in Iani et al. (2024a) and employed multiple SED-fitting codes to estimate the stellar properties of *Virgil*. While Iani et al. (2024a) present a detailed SED fitting analysis, we focused on deriving key stellar parameters to contextualize our spectral results and investigate the nature of this object. Specifically, we use BAGPIPES (Carnall et al. 2019), CIGALE (Boquien et al. 2019), PROSPECTOR (Johnson et al. 2021), and SYNTHESIZER-AGN (Pérez-González et al. 2003, 2008, 2024a). As demonstrated and largely discussed in Iani et al. (2024a), *Virgil* is well described only when an AGN component is included, except for SYNTHESIZER-AGN, which tends to prefer a two-population solution. With respect to Iani et al. (2024a), we expanded the two-population scenario also to BAGPIPES.

For BAGPIPES, we adopt the same setup as in Rinaldi et al. (2024a) for LRDs, utilizing synthetic templates from Bruzual & Charlot (2003) with a Kroupa IMF, a stellar mass cut-off of $100 M_\odot$, and nebular emission

modeled with CLOUDY (Ferland et al. 2013). We employ a continuity non-parametric SFH model (Leja et al. 2019), defining age bin edges (in look-back time) based on *Virgil*'s spectroscopic redshift, following a logarithmic distribution from $z = 30$ to the cosmic time at that redshift. The same approach is applied to the age parameter.

We let stellar masses range from 10^5 to $10^{13} M_\odot$ (uniform prior in log). We adopt a Calzetti reddening law (Calzetti et al. 2000), allowing A_V to vary between 0 and 6, while metallicity (Z/Z_\odot) spans 0 to 2.5. The ionization parameter is constrained between -4 and 0.001. For the AGN contribution, we follow Carnall et al. (2023) (see their Table 1), adopting broad, flat (uniform) priors for all parameters.

For the two-population scenario, we adopt a delayed SFH with τ ranging from 0.1 to 13 Gyr. Each population follows the same metallicity, age, and dust constraints as the AGN-included run.

For CIGALE, we assume a delayed exponentially declining SFH (delayed- τ model) with two stellar populations. We adopt Bruzual & Charlot (2003) stellar population models with both solar and sub-solar metallicity ($Z = 0.2Z_\odot$) and a Chabrier IMF. Nebular continuum and emission lines are included, assuming solar and sub-solar metallicity, and allowing electron density and ionization parameter values of $n_e = 10, 10^2, 10^3 \text{ cm}^{-3}$ and $\log_{10}(\mathcal{U}) = -3, -2, -1$, respectively. For dust attenuation, we adopt Calzetti et al. (2000), while far-IR emission is modeled with Draine et al. (2014). AGN emission is incorporated using the SKIRTOR models (Stalevski et al. 2012, 2016), following initial parameters from Yang et al. (2023) but allowing for both Type 1 (unobscured) and Type 2 (obscured) AGN.

For SYNTHESIZER-AGN, the SED is modeled as a composite stellar population (Pérez-González et al. 2003, 2008) with AGN emission from the accretion disk and dusty torus (Pérez-González et al. 2024a). Stellar emission consists of a young and an older star formation event, each described by a delayed exponential function with τ between 1 Myr and 1 Gyr, and ages up to the cosmic time at the *Virgil*'s redshift. Each stellar population experiences independent attenuation following Calzetti et al. (2000), with A_V ranging from 0 to 10 mag. The stellar component is modeled with Bruzual & Charlot (2003) templates, assuming a Chabrier IMF with stellar masses between 0.1 and $100 M_\odot$, including nebular emission (Pérez-González et al. 2003). The AGN emission follows a QSO average spectrum (Vanden Berk et al. 2001; Glikman et al. 2006), while its dust component is modeled using self-consistent AGN torus templates from Siebenmorgen et al. (2015).

Finally, for PROSPECTOR, we used a modified version built on the standard implementation, which incorporates the Flexible Stellar Population Synthesis (FSPS; Conroy & Gunn 2010) model for the stellar component. We assumed a Kroupa (2001) initial mass function and a delayed- τ star formation history. Nebular line and continuum emission were included, as pre-configured in FSPS (Byler et al. 2017). We adopted the Calzetti attenuation curve with a flexible slope, following Kriek & Conroy (2013). For galaxy dust emission, given that *Virgil* has $z = 6.64$, we used the empirical IR SED model of Haro 11, a low-metallicity, starbursting dwarf galaxy believed to exhibit typical features of first-generation galaxies in the early Universe (Lyu et al. 2016; De Rossi et al. 2018).

This code employs a set of semi-empirical AGN SED models optimized for AGN identification and characterization (Lyu et al. 2022, 2024). We adopted a model configuration similar to that in Lyu et al. (2024) for the SMILES+JADES AGN identification. The AGN component includes both the AGN-powered continuum from the UV to the far-IR and the narrow and broad emission lines from the UV to the NIR, derived from empirical observations. The continuum shape and line strengths of the AGN SED can be adjusted using a hybrid attenuation model, featuring an SMC-like curve for the typical UV-optical attenuation in Type-1 AGNs and an empirical attenuation law for IR obscuration. We refer the reader to Lyu et al. (2024) for further details.

5.2. Results from SED fitting

We now discuss the results of the SED fitting. Iani et al. (2024a) showed that most SED fitting codes struggle to reproduce the MIRI fluxes unless an AGN component is included, with the exception of SYNTHESIZER-AGN. This is mainly because, by design, SYNTHESIZER-AGN always fits two independent stellar populations—regardless of the inclusion or not of an AGN—providing greater flexibility to account for complex SED shapes.

We first fit *Virgil*'s photometry without including an AGN component, adopting a model with two stellar populations. As shown in Iani et al. (2024a), only SYNTHESIZER-AGN (used here without including an AGN component) was originally capable of such a fit due to its design. Here, we introduced this flexibility in BAGPIPES as well¹³. In both cases, the inferred total M_* is significantly higher than in AGN-inclusive models (see next paragraph), with $\log_{10}(M_*/M_\odot)$ rang-

ing from 9.80 to 10.50. The older population consistently exhibits $A_V \approx 2 - 4$. However, the solutions from BAGPIPES and SYNTHESIZER-AGN differ: the latter yields two very young populations ($t_{\text{age}} \lesssim 50$ Myr) with distinct extinctions ($A_V \approx 3.60$ for the most obscured), consistent with Iani et al. (2024a), while BAGPIPES retrieves two markedly distinct populations—one extremely young ($t_{\text{age}} < 3$ Myr), dust-free, and low-mass ($\log_{10}(M_*/M_\odot) \approx 7.24$), and one older (approaching the age of the Universe at $z \approx 6.64$), massive ($\log_{10}(M_*/M_\odot) \approx 10.48^{14}$), and heavily obscured ($A_V \approx 4$).

When including an AGN component, both SYNTHESIZER-AGN and PROSPECTOR consistently yield $\log_{10}(M_*/M_\odot) \approx 9$, although BAGPIPES retrieves a significantly lower stellar mass by ≈ 1 dex: $\log_{10}(M_*/M_\odot) = 7.92$. Similarly, CIGALE finds $\log_{10}(M_*/M_\odot) = 8.50$. Notably, BAGPIPES predicts a stellar age of $t_{\text{age}} = 400_{-260}^{+260}$ Myr, consistent with both CIGALE and PROSPECTOR within the uncertainties ($t_{\text{age}} \approx 400 - 600$ Myr). However, its mass-weighted age, from BAGPIPES, is only 4_{-3}^{+2} Myr, indicating that a substantial fraction of the stellar mass formed recently, which is consistent with a very recent burst of star formation.

Interestingly, both SYNTHESIZER-AGN and PROSPECTOR, when invoking an AGN, predict $A_V \approx 2 - 4$. In particular, SYNTHESIZER-AGN predicts $A_V \approx 0.74$ mag for the young population ($t_{\text{age}} \approx 10$ Myr), in line with our estimate from NIRSpec/PRISM data, and $A_V \approx 2.40$ for the older population ($t_{\text{age}} \approx 32$ Myr). Similarly, BAGPIPES and CIGALE yield A_V values consistent with those inferred from Balmer lines tracing the young population. Across all fits, the metallicity remains consistent at 10–20%, Z_\odot , in agreement with our spectroscopic constraints.

Overall, all models yield a reduced χ^2 between 6 and 12, with BAGPIPES achieving the best χ^2_ν when including an AGN, while SYNTHESIZER-AGN favors the model of two stellar populations without an AGN. As discussed in Iani et al. (2024a), fitting this object remains challenging, reflecting the well-known difficulty in modeling LRDs in general. Nevertheless, most SED fitting codes used in this work—as it was for Iani et al. (2024a)—favor the (embedded) AGN interpretation. Interestingly, our modified version of PROSPECTOR tailored for obscured AGNs (Lyu et al. 2024) fails to reproduce the observed SED of this object when the AGN component is ex-

¹⁴ Overlapping with the maximum M_* expected from the stellar mass–halo mass relation of Behroozi et al. (2020) at its redshift.

¹³ This flexibility was implemented in BAGPIPES only for the model without the AGN contribution.

cluded. We show the best-fit results in Figure 11 along with other models from the literature (see next section).

6. HIDE AND SEEK: WHAT IS THE NATURE OF VIRGIL?

6.1. Star forming properties

Iani et al. (2024a) introduced *Virgil* as the first LRD with a clearly detected host galaxy and a peculiar rising SED between 4 and 10 μm . At that time, their analysis was limited to photometric data from HST and JWST (NIRCam and MIRI). Leveraging multiple SED-fitting codes, we identified two plausible scenarios for *Virgil*'s nature: either a dusty starburst galaxy or a SFG hosting an obscured AGN. However, in the previous sections, we demonstrated that incorporating spectroscopic data from NIRSpec/PRISM strengthens the interpretation of *Virgil* as a typical SFG during the EoR—or, at the very least, that its AGN nature becomes less clear when the redshift evolution of diagnostic diagrams is taken into account. This is supported by its relatively low M_* , metal-poor nature, and extreme EW_0 for $[\text{O III}]\lambda\lambda 4959, 5007$. Interestingly, *Virgil* shares similarities with GPs and BBs, which are often considered the best low-redshift analogs of high- z galaxies.

In general, when focusing on NIRSpec/PRISM data, we find that *Virgil* appears to be a typical system at $z \approx 6 - 7$ undergoing a bursty star formation episode. At the time of observation, it is either experiencing or fading out of a starburst, while also harboring an older stellar population that dominates its M_* , with formation dating back a few hundred million years, as inferred from BAGPIPES, CIGALE, and PROSPECTOR fits. *Virgil* exhibits extreme emission line ratios, including a high R3 index (≈ 0.8), consistent with other galaxies at similar redshifts (e.g., Cameron et al. 2023; Tang et al. 2023). This is likely driven by intense star formation, with a surface SFR of $\Sigma_{\text{SFR}(\text{H}\alpha)} \approx 5.25 M_\odot \text{yr}^{-1} \text{kpc}^{-2}$ at a moderately low metallicity ($Z \approx 0.1 - 0.2 Z_\odot$). Whether it contains an AGN remains ambiguous if the emission line ratios are interpreted in the context of its redshift and the evolution of these ratios, consistent with trends observed in other LRDs by Rinaldi et al. (2024a). If this interpretation holds, it may also apply to other claimed Type 1 and Type 2 AGN in the literature (e.g., Kokorev et al. 2023; Scholtz et al. 2023).

6.2. *Virgil*'s AGN

However, multiple SED-fitting codes that incorporate wavelengths beyond 5 μm suggest that this galaxy hosts a deeply obscured AGN, a characteristic commonly observed in many LRDs. Notably, *Virgil*'s infrared SED rises even more steeply than those of typical LRDs, mak-

ing it one of the most extreme cases identified to date at $z \approx 6-7$. While *Virgil* may appear exceptional, it has lower-redshift analogs, such as the obscured AGNs identified in the HUDF by Lyu et al. (2024).

Interestingly, Lin et al. (2024) recently identified a subset of GP galaxies that exhibit the V-shaped SED commonly found in high- z LRDs, along with broad emission lines, suggesting a possible evolutionary link between these two populations (see Figure 11).

Further exploring analogies with lower redshift sources provides key insights into the nature of *Virgil*. Iani et al. (2024a) measured a compactness of $c_{F444W} \approx 1.5$ for *Virgil*, consistent with the LRD criterion ($c_{F444W} < 2$; Kokorev et al. 2024). However, this threshold is somewhat arbitrary. If *Virgil* were at $z \approx 3.5$, for instance, the angular scale would be ≈ 7.3 kpc/arcsec instead of 5.4 kpc/arcsec at $z \approx 6.64$, and the 4.44 μm emission would be even more dominated by the obscured AGN, which would make *Virgil* appear even more compact.

Another intriguing analogy is with the very red sources at $z \approx 2$ identified in *Spitzer* observations, commonly known as Dust Obscured Galaxies (DOGs) (e.g., Weedman et al. 2006; Bussmann et al. 2012). The most extreme DOGs exhibit infrared SEDs that rise as steeply as that of *Virgil*, such as SST24 J142648.9+332927 (Bussmann et al. 2012). DOGs are typically classified into two subgroups based on their distinct SEDs: power law (PL) DOGs, indicative of AGN dominance, and “bump” DOGs, which show a flattening near rest-frame 1.6 μm , suggesting a significant contribution from a stellar population (e.g., Dey et al. 2008). Therefore, “bump” DOGs are considered to correspond to galaxies in a star-forming phase (Bussmann et al. 2011), while PL DOGs are associated with galaxies in an AGN phase (e.g., Bussmann et al. 2009). Dey et al. (2008) showed that the fraction of PL DOGs among all DOGs increases with increasing MIR flux density, similar to the luminosity dependence of the AGN fraction in ultraluminous infrared galaxies (ULIRGs; Sanders & Mirabel 1996; Veilleux et al. 1999). Notably, some of these features are commonly observed in LRDs as well (Pérez-González et al. 2024a; Williams et al. 2024).

Hence, *Virgil* is likely experiencing a transition phase at the moment we observe it, allowing us to witness a starburst event with an embedded AGN. As shown in Iani et al. (2024a), the MIRI part of *Virgil*'s SED cannot be solely attributed to star-formation heated dust emission. Otherwise, the required dust temperature would approach the typical sublimation temperature for the dust ($T_{\text{subl}} \approx 1500 - 2000$ K, depending on dust composition; Temple et al. 2021), a scenario that would be

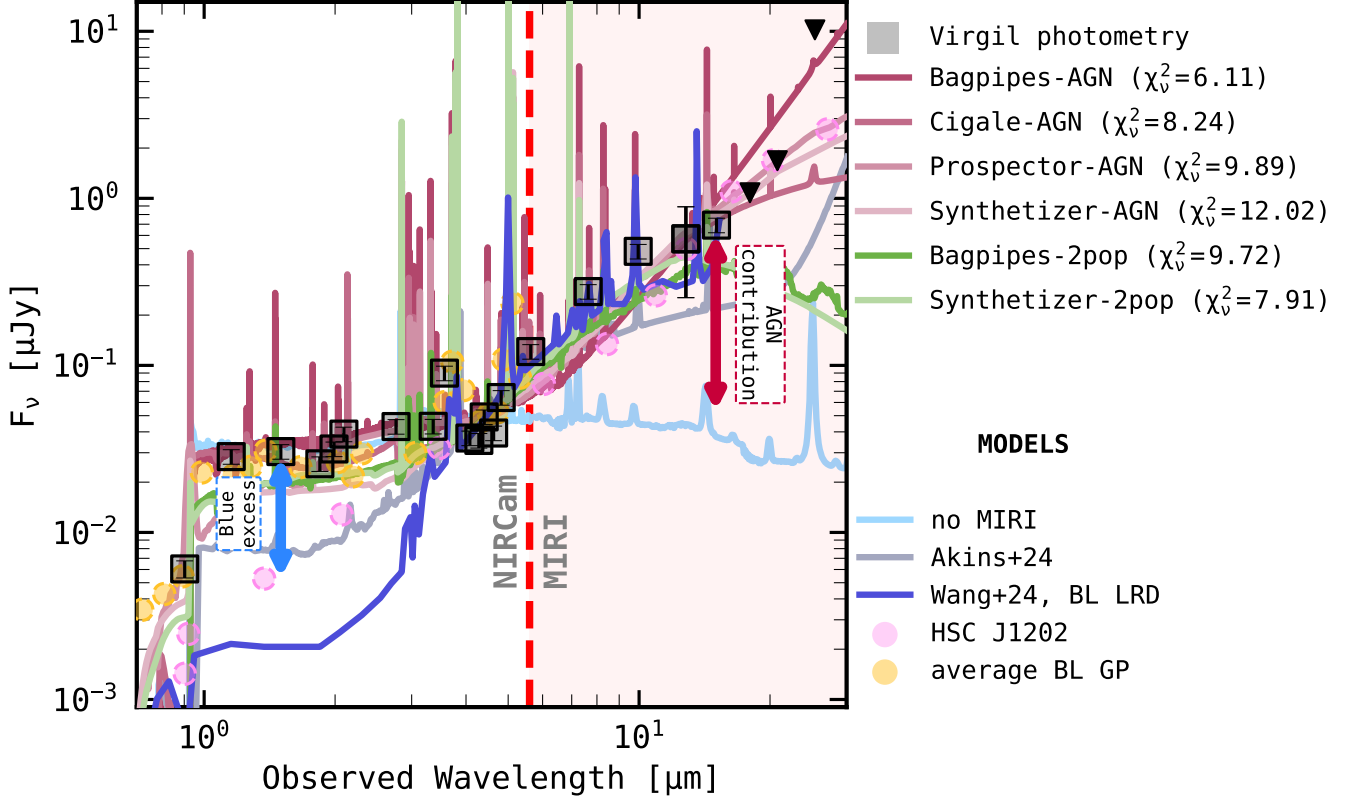


Figure 11. The best-fit results for *Virgil* are shown, with photometric data indicated by black squares and 3σ upper limits by black inverted triangles. The reduced chi-squared values are also reported and computed consistently across the different SED fitting codes to account for their varying treatments of upper limits. The red arrow highlights the IR excess relative to the typical SFG template, which both NIRCcam and NIRSpc data would bias the SED fitting toward. In contrast, the blue arrow indicates the UV excess compared to the average LRD template proposed by Akins et al. (2024). For comparison, we include the LRD model from Akins et al. (2024) and *Virgil*'s SED, excluding the MIRI bands, as derived from BAGPIPES. Additionally, we show the average BL GP SED (green circles) from Lin et al. (2024), considering only sources with M_{\bullet} similar to the estimated value for *Virgil*. Finally, we compare it with the Blue-excess HotDOG (HSC J1202; red circles) from Noboriguchi et al. (2022). RUBIES-BLAGN-1 model from Wang et al. (2024) is shown in blue. The vertical dashed red line marks the transition between the NIRCcam and MIRI domains. All models are normalized to F444W in the *Virgil*'s reference system.

difficult to reconcile with “normal” star formation behavior (e.g., Sommovigo et al. 2020).

However, the DOG family is more diverse. For instance, HotDOGs are among the most luminous objects in the Universe, with bolometric luminosities often exceeding $10^{13-14}L_{\odot}$ (see an example of HotDOG, HSC J1202, in Figure 11). Discovered with the *Wide-field Infrared Survey Explorer* (WISE; Wright 2010), they exhibit extremely red MIR SEDs. Their emission is dominated by hyperluminous, highly obscured AGNs that power their intense mid-to-far infrared radiation (e.g., Eisenhardt et al. 2012). Interestingly, X-ray studies indicate that their obscuration levels are exceptionally high, often reaching or exceeding the Compton-thick limit ($N_H > 1.5 \times 10^{24} \text{ cm}^2$) (e.g., Ricci et al. 2017). Due to this heavy obscuration, the host galaxy could dominate the UV and optical wavelengths, rather than direct AGN emission.

While most HotDOGs exhibit extreme dust obscuration that suppresses UV emission, a subset displays significant excess UV/optical light compared to the average population—these are known as Blue-excess HotDOGs (BHDs; e.g., Assef et al. 2016; Noboriguchi et al. 2022). Assef et al. (2016) proposed several plausible scenarios to explain this excess, including the possibility that a small fraction of AGN light leaks into our line of sight via scattering by dust, gas, or both—a scenario recently studied also by Stepney et al. (2024) in the case of ULASJ2315+0143, a source around Cosmic Noon. In this scenario, the intrinsic emission from the accretion disk and broad-line region is largely absorbed, with only $\lesssim 1\%$ scattered into view on larger spatial scales, where dust grains efficiently reflect shorter-wavelength radiation (Draine 2003).

A similar contrast between the UV and optical colors has been already observed in LRDs (Noboriguchi et al.

2023). While most LRDs exhibit extremely red optical-to-NIR colors ($0.4\text{--}1\ \mu\text{m}$), they show a blue excess in the rest-frame UV ($0.2\text{--}0.4\ \mu\text{m}$), reminiscent of Blue-Excess HotDOGs found at $z \approx 2\text{--}3$. However, LRDs represent a less extreme manifestation of this phenomenon compared to Blue-Excess HotDOGs, as they are found at higher redshifts and exhibit lower M_\bullet and Eddington ratios ($\lambda_{\text{Edd}} \approx 0.1\text{--}1$), suggesting they may be earlier-stage counterparts.

Nonetheless, *Virgil* stands out as an even more extreme case among LRDs, exhibiting both an exceptionally steep SED between F444W and F1500W and an enhanced UV excess. Indeed, *Virgil*'s UV excess is more pronounced compared to the average LRD template proposed by Akins et al. (2024), suggesting a greater contribution from either scattered AGN light or, more likely, a strong star-forming component. At the same time, its SED rises more steeply than seen in most LRDs at wavelengths beyond $0.6\ \mu\text{m}$ (rest-frame), resembling the most obscured DOGs. This dual nature—both an extreme red excess in the MIRI regime and an unusually strong blue excess in the UV—potentially places *Virgil* as a high- z analog of Blue-excess HotDOGs, possibly with a strong contribution at the UV regime from its host.

Noboriguchi et al. (2023) suggested that the connection between LRDs and Blue-excess HotDOGs reflects an evolutionary sequence in which gas-rich mergers trigger dusty starbursts, giving rise to heavily obscured DOGs. Interestingly, when modeling *Virgil* with FORCEPHO, it appears to be composed of two distinct knots in the NIRCам wavelength range, suggesting a possible merger-driven scenario. As AGN feedback disperses the surrounding dust, some of these systems develop a blue excess, akin to what is observed in Blue-excess HotDOGs. In this context, LRDs may represent an even earlier stage in this process, where lower metallicities and dust-to-gas ratios at high redshifts lead to a higher fraction of such objects exhibiting blue excess. Yet, *Virgil* appears even more extreme, with a UV excess likely arising from a combination of AGN activity and star formation, though primarily driven by the host galaxy, while its obscured SMBH shapes an extreme near-IR SED (rest-frame).

As a final analogy with sources at lower redshifts, in Figure 11, we compared *Virgil* to another LRD at a much lower redshift ($z_{\text{spec}} = 3.1$), RUBIES-BLAGN-1, studied by Wang et al. (2024). RUBIES-BLAGN-1 closely follows *Virgil*'s SED at wavelengths beyond $4.4\ \mu\text{m}$. While both objects exhibit a similar trend at IR wavelengths, they diverge significantly in the UV, further emphasizing the striking UV excess observed in *Virgil* compared to

the average LRD population. This divergence highlights once again the peculiar nature of *Virgil*.

7. SUMMARY AND CONCLUSIONS

In this paper, we extend the analysis of *Virgil*, first presented in Iani et al. (2024a), using recent data collected by the MIDIS and PAHSPECS teams for MIRI, and NIRSpec/PRISM data by the OASIS team. *Virgil* is a LAE at $z_{\text{spec}} = 6.6379 \pm 0.003$, detected with VLT/MUSE (Bacon et al. 2023). It shares key photometric properties with the LRD population, including its compactness in F444W ($c_{F444W} \approx 1.5$; Iani et al. 2024a), although it does not strictly meet all their color selection criteria (Kokorev et al. 2024; Rinaldi et al. 2024a).

Our main findings can be summarized as follows:

- *Virgil* exhibits low to moderate dust attenuation based on its Balmer decrement, assuming the SMC reddening law from Gordon et al. (2003). Its metallicity aligns with galaxies of similar M_\star at $z \gtrsim 6$ (Figure 2). By comparing the UV- and H α -based SFRs, we find that *Virgil* may be transitioning into—or fading out of—a bursty phase. Its $f_{\text{esc,LyC}}$ and ξ_{ion} indicate a limited role in Cosmic Reionization, further supported by its moderate $\text{EW}_0(\text{H}\alpha)$ compared to other emitters at similar redshifts (e.g., Rinaldi et al. 2023, 2024b; Simmonds et al. 2024b). Overall, *Virgil*'s spectral properties align with the average galaxy population during the EoR (e.g., Cameron et al. 2023). A full summary of its spectral properties is provided in Table 2.
- The combination of NIRSpec/PRISM data with extensive photometric coverage from HST and JWST, including MIRI detections up to $15\ \mu\text{m}$, offers a unique opportunity to further investigate *Virgil*'s nature. Without an *a priori* assumption that it could host an AGN—as previously suggested by Iani et al. (2024a) and based solely on photometry—we analyze its ISM properties using the R23 vs. O32 and Ne3O2Hd vs. Ne3O2 diagrams (Figure 3). By considering CLOUDY models for SFGs (following the approach outlined in Calabrò et al. 2024a), we find that *Virgil*'s ISM does not significantly deviate from the typical high- z SFGs during the EoR. Interestingly, its properties resemble well-studied GPs and BBs, which are among the best local analogs of high- z galaxies. Notably, despite its moderate $\text{EW}_0(\text{H}\alpha)$, *Virgil* exhibits a huge EW_0 for [O III] $\lambda\lambda 4959, 5007$ ($1514 \pm 20\ \text{\AA}$), comparable to the Extreme Line

Emitters studied by [Boyett et al. \(2024\)](#) at similar redshifts.

- To assess the AGN nature suggested by [Iani et al. \(2024a\)](#), we search for broad Balmer lines (a feature already found in other claimed LRDs), modeling H α with and without a broad component. However, the NIRSpec/PRISM data do not provide a firm conclusion (Figure 4). We note that the source’s position within the slit (Figure 1, right panel)—with the red knot lying near the edge or possibly in the shutter gap—may limit our sensitivity to broad-line emission. Nonetheless, assuming the broadening is real, the inferred M_{\bullet} , L_{Bol} , and Eddington ratio align with expectations for LRDs (Figure 5) and with values already reported in [Iani et al. \(2024a\)](#) by leveraging photometric data only. We examine emission-line diagnostics and find that while *Virgil* lies above the SFG-AGN separation line in the “OHNO” diagram ([Backhaus et al. 2022](#)), it falls below it when accounting for redshift evolution. Similarly, O3Hg-based diagnostics ([Mazzolari et al. 2024](#)) place it among AGNs at high z (e.g., [Nakajima et al. 2023](#); [Scholtz et al. 2023](#)), but when accounting for redshift evolution, its classification becomes ambiguous (Figure 7). Overall, while these high- z diagnostics would classify *Virgil* as an AGN, they do not provide a definitive classification when the redshift evolution is taken into account, instead pointing to a likely mixed nature.
- The newly acquired MIRI data from MIDIS and PAHSPECS, including a clear 15 μm detection of *Virgil*, enabled improved photometry and SED fitting. Using FORCEPHO, we identified two distinct knots, reinforcing evidence of complex UV morphology in LRDs ([Rinaldi et al. 2024a](#)), with one component accounting for the MIRI excess. *Virgil* appears even redder in F444W–F1500W color (≈ 2.84) than typical LRDs and, while it does not meet all standard LRD color criteria ([Kokorev et al. 2024](#)), it satisfies the V-shaped SED selection from [Kocevski et al. \(2024\)](#), suggesting that MIRI bands may be crucial for identifying extreme cases (Figure 9). To contextualize its spectral properties, we applied multiple SED-fitting codes (Figure 11), extending the analysis of [Iani et al. \(2024a\)](#) by incorporating two independent stellar populations in BAGPIPES and utilizing an AGN-optimized version of PROSPECTOR ([Lyu et al. 2024](#)). Interestingly, the tailored version of PROSPECTOR fails to reproduce the observed SED

when an AGN component is not included. While modeling this source remains challenging, our results show that the fits consistently require the presence of a dust-obscured AGN, consistent with the findings of [Iani et al. \(2024a\)](#).

- Combining photometric and spectroscopic data, we find *Virgil* to be among the most extreme LRDs identified to date, with a steeply rising SED beyond 4.44 μm (observed-frame) and a pronounced UV excess. Its SED closely resembles Cosmic Noon objects observed with *Spitzer*, such as SST24 J142648.9+33292, a well-studied DOG, and shares similarities with HotDOGs, whose IR properties align with those of LRDs. [Noboriguchi et al. \(2023\)](#) linked JWST/EROs to DOGs, particularly Blue-Excess HotDOGs, which exhibit extreme IR colors and a flat UV continuum. The UV excess in Blue-Excess HotDOGs has been attributed to AGN light ($< 1\%$; [Assef et al. 2016, 2020](#)) scattered by dust or gas, a scenario that could also contribute to *Virgil*’s properties. A similar finding was also reported for ULASJ2315+014, a Cosmic Noon source, by [Stepney et al. \(2024\)](#). However, *Virgil*’s SED and emission-line features suggest a mix of AGN and star formation activity, with the UV emission likely dominated by the host galaxy. Finally, we compare *Virgil* to RUBIES-BLAGN-1 ($z_{spec} = 3.1$) from [Wang et al. \(2024\)](#), noting that their SEDs diverge at shorter wavelengths, with *Virgil* exhibiting a stronger UV excess.

This study underscores the challenges of studying such systems at high redshift and highlights the necessity of a multi-wavelength approach to identify and characterize extreme sources during Cosmic Reionization. Deep MIRI imaging at $z > 6$ is crucial for uncovering highly dust-obscured AGNs that might otherwise be misclassified as normal SFGs, especially in studies limited to wavelengths below 5 μm . In such cases, both photometric and spectroscopic information can lead to ambiguous classifications, particularly when redshift evolution is taken into account. This reinforces the need to expand MIRI coverage to systematically identify more of these extreme objects and refine our understanding of early black hole growth.

The authors deeply thank Antonello Calabrò for valuable insights on CLOUDY and PYCLOUDY and for publicly sharing their SFG and AGN models. They also express their gratitude to Adam Carnall for their inputs on BAGPIPES and to Camilla Pacifici, Vasily Kokorev, and Cristian Vignali for their insightful discussions.

This work is based on observations made with the NASA/ESA/CSA JWST. The data were obtained from the Mikulski Archive for Space Telescopes (MAST) at the Space Telescope Science Institute, which is operated by the Association of Universities for Research in Astronomy, Inc., under NASA contract NAS 5-03127 for JWST. These observations are associated with JWST programs GTO #1180, GO #1210, GTO#1283, GO #1963, GO #1895, and GO# 3215, and GO#6511.

The authors acknowledge the FRESCO, JEMS, and # 3215 teams led by coPIs P. Oesch, C. C. Williams, M. Maseda, D. Eisenstein, and R. Maiolino for developing their observing program with a zero-exclusive-access period. Processing for the JADES NIRCcam data release was performed on the lux cluster at the University of California, Santa Cruz, funded by NSF MRI grant AST 1828315. Also based on observations made with the NASA/ESA Hubble Space Telescope obtained from the Space Telescope Science Institute, which is operated by the Association of Universities for Research in Astronomy, Inc., under NASA contract NAS 526555. The data presented in this article were obtained from MAST at the Space Telescope Science Institute. The specific observations analyzed can be accessed via DOI: [10.17909/gdyc-7g80](https://doi.org/10.17909/gdyc-7g80), [10.17909/fsc4-dt61](https://doi.org/10.17909/fsc4-dt61), [10.17909/fsc4-dt61](https://doi.org/10.17909/fsc4-dt61), [10.17909/T91019](https://doi.org/10.17909/T91019), [10.17909/1rq3-8048](https://doi.org/10.17909/1rq3-8048), [10.17909/z2gw-mk31](https://doi.org/10.17909/z2gw-mk31).

The authors acknowledge use of the lux supercomputer at UC Santa Cruz, funded by NSF MRI grant AST 1828315.

AJB acknowledge funding from the "FirstGalaxies" Advanced Grant from the European Research Council (ERC) under the European Union's Horizon 2020 research and innovation programme (Grant agreement No. 789056)

PGP-G acknowledges support from grant PID2022-139567NB-I00 funded by Spanish Ministerio de Ciencia e Innovación MCIN/AEI/10.13039/501100011033, FEDER, UE.

BER acknowledges support from the NIRCcam Science Team contract to the University of Arizona, NAS5-02015, and JWST Program 3215.

ST acknowledges support by the Royal Society Research Grant G125142.

The research of CCW is supported by NOIRLab, which is managed by the Association of Universities for Research in Astronomy (AURA) under a cooperative agreement with the National Science Foundation.

JW gratefully acknowledges support from the Cosmic Dawn Center through the DAWN Fellowship. The Cos-

mic Dawn Center (DAWN) is funded by the Danish National Research Foundation under grant No. 140.

YZ, ZJ gratefully acknowledges JWST/NIRCcam contract to the University of Arizona NAS5-02015.

HÜ acknowledges funding by the European Union (ERC APEX, 101164796). Views and opinions expressed are however those of the authors only and do not necessarily reflect those of the European Union or the European Research Council Executive Agency. Neither the European Union nor the granting authority can be held responsible for them.

GCJ acknowledges support by the Science and Technology Facilities Council (STFC), ERC Advanced Grant 695671 "QUENCH".

ACG acknowledges support by JWST contract B0215/JWST-GO-02926.

GO acknowledges support from the Swedish National Space Agency (SNSA)

The Cosmic Dawn Center (DAWN) is funded by the Danish National Research Foundation (DNRF) under grant No. 140.

HI acknowledges support from JSPS KAKENHI grant No. JP21H01129.

MA gratefully acknowledges support from ANID Basal Project FB210003 and ANID MILENIO NCN2024_112.

TDS acknowledges the research project was supported by the Hellenic Foundation for Research and Innovation (HFRI) under the "2nd Call for HFRI Research Projects to support Faculty Members & Researchers" (Project Number: 03382)

RM acknowledges support by the Science and Technology Facilities Council (STFC), by the ERC through Advanced Grant 695671 "QUENCH", and by the UKRI Frontier Research grant RISEandFALL. RM also acknowledges funding from a research professorship from the Royal Society.

IS acknowledges funding Atracción de Talento Grant No.2022-T1/TIC-20472 of the Comunidad de Madrid, Spain and the European Research Council (ERC) under the European Union's Horizon 2020 research and innovation programme (Grant No. 101117541, Distant-Dust).

KIC acknowledges funding from the Dutch Research Council (NWO) through the award of the Vici Grant VI.C.212.036.

Facilities: HST, JWST.

Software: ASTROPY (Astropy Collaboration et al. 2022), BAGPIPES (Carnall et al. 2019), MSAEXP (Brammer 2023) NUMPY (Harris et al. 2020), PANDAS (team 2024) PHOTUTILS (Bradley et al. 2016), TOPCAT (Taylor 2022).

REFERENCES

- Abazajian, K. N., Adelman-McCarthy, J. K., Agüeros, M. A., et al. 2009, *The Astrophysical Journal Supplement Series*, 182, 543, publisher: IOP ADS
Bibcode: 2009ApJS..182..543A.
<https://ui.adsabs.harvard.edu/abs/2009ApJS..182..543A>
- Akhlaghi, M., & Ichikawa, T. 2017, 512, 213, conference Name: Astronomical Data Analysis Software and Systems XXV ADS Bibcode: 2017ASPC..512..213A.
<https://ui.adsabs.harvard.edu/abs/2017ASPC..512..213A>
- Akins, H. B., Casey, C. M., Lambrides, E., et al. 2024, COSMOS-Web: The over-abundance and physical nature of "little red dots"—Implications for early galaxy and SMBH assembly, , publication Title: arXiv e-prints ADS Bibcode: 2024arXiv240610341A, doi:10.48550/arXiv.2406.10341.
<https://ui.adsabs.harvard.edu/abs/2024arXiv240610341A>
- Alberts, S., Lyu, J., Shivaei, I., et al. 2024, SMILES Initial Data Release: Unveiling the Obscured Universe with MIRI Multi-band Imaging, , publication Title: arXiv e-prints ADS Bibcode: 2024arXiv240515972A, doi:10.48550/arXiv.2405.15972.
<https://ui.adsabs.harvard.edu/abs/2024arXiv240515972A>
- Amorín, R., Pérez-Montero, E., Contini, T., et al. 2015, *Astronomy and Astrophysics*, 578, A105, publisher: EDP ADS Bibcode: 2015A&A...578A.105A. <https://ui.adsabs.harvard.edu/abs/2015A&A...578A.105A>
- Anders, P., & Fritze-v. Alvensleben, U. 2003, *Astronomy and Astrophysics*, 401, 1063, aDS Bibcode: 2003A&A...401.1063A.
<https://ui.adsabs.harvard.edu/abs/2003A&A...401.1063A>
- Armah, M., Dors, O. L., Aydar, C. P., et al. 2021, *Monthly Notices of the Royal Astronomical Society*, 508, 371, publisher: OUP ADS Bibcode: 2021MNRAS.508..371A.
<https://ui.adsabs.harvard.edu/abs/2021MNRAS.508..371A>
- Armus, L., Charmandaris, V., & Soifer, B. T. 2020, *Nature Astronomy*, 4, 467, aDS Bibcode: 2020NatAs...4..467A.
<https://ui.adsabs.harvard.edu/abs/2020NatAs...4..467A>
- Arrabal Haro, P., Dickinson, M., Finkelstein, S. L., et al. 2023, *Nature*, 622, 707, aDS Bibcode: 2023Natur.622..707A.
<https://ui.adsabs.harvard.edu/abs/2023Natur.622..707A>
- Asplund, M., Grevesse, N., Sauval, A. J., & Scott, P. 2009, *Annual Review of Astronomy and Astrophysics*, 47, 481, aDS Bibcode: 2009ARA&A..47..481A. <https://ui.adsabs.harvard.edu/abs/2009ARA&A..47..481A>
- Assef, R. J., Walton, D. J., Brightman, M., et al. 2016, *The Astrophysical Journal*, 819, 111, publisher: IOP ADS
Bibcode: 2016ApJ...819..111A.
<https://ui.adsabs.harvard.edu/abs/2016ApJ...819..111A>
- Assef, R. J., Brightman, M., Walton, D. J., et al. 2020, *The Astrophysical Journal*, 897, 112, publisher: IOP ADS
Bibcode: 2020ApJ...897..112A.
<https://ui.adsabs.harvard.edu/abs/2020ApJ...897..112A>
- Astropy Collaboration, Price-Whelan, A. M., Lim, P. L., et al. 2022, *The Astrophysical Journal*, 935, 167, publisher: IOP ADS Bibcode: 2022ApJ...935..167A.
<https://ui.adsabs.harvard.edu/abs/2022ApJ...935..167A>
- Atek, H., Furtak, L. J., Oesch, P., et al. 2022, *Monthly Notices of the Royal Astronomical Society*, 511, 4464, publisher: OUP ADS Bibcode: 2022MNRAS.511.4464A.
<https://ui.adsabs.harvard.edu/abs/2022MNRAS.511.4464A>
- Backhaus, B. E., Trump, J. R., Cleri, N. J., et al. 2022, *The Astrophysical Journal*, 926, 161, publisher: IOP ADS
Bibcode: 2022ApJ...926..161B.
<https://ui.adsabs.harvard.edu/abs/2022ApJ...926..161B>
- Backhaus, B. E., Bridge, J. S., Trump, J. R., et al. 2023, *The Astrophysical Journal*, 943, 37, publisher: IOP ADS
Bibcode: 2023ApJ...943...37B.
<https://ui.adsabs.harvard.edu/abs/2023ApJ...943...37B>
- Backhaus, B. E., Trump, J. R., Pirzkal, N., et al. 2024, *The Astrophysical Journal*, 962, 195, publisher: IOP ADS
Bibcode: 2024ApJ...962..195B.
<https://ui.adsabs.harvard.edu/abs/2024ApJ...962..195B>
- Backhaus, B. E., Cleri, N. J., Trump, J. R., et al. 2025, Emission-Line Diagnostics at $z > 4$: [OIII] $\{\lambda\}$ 4363/H γ , , publication Title: arXiv e-prints ADS Bibcode: 2025arXiv250203519B.
<https://ui.adsabs.harvard.edu/abs/2025arXiv250203519B>
- Bacon, R., Brinchmann, J., Conseil, S., et al. 2023, *Astronomy and Astrophysics*, 670, A4, aDS Bibcode: 2023A&A...670A...4B.
<https://ui.adsabs.harvard.edu/abs/2023A&A...670A...4B>
- Bagley, M. B., Pirzkal, N., Finkelstein, S. L., et al. 2024, *The Astrophysical Journal*, 965, L6, publisher: IOP ADS
Bibcode: 2024ApJ...965L...6B.
<https://ui.adsabs.harvard.edu/abs/2024ApJ...965L...6B>
- Baldwin, J. A., Phillips, M. M., & Terlevich, R. 1981, *Publications of the Astronomical Society of the Pacific*, 93, 5, publisher: IOP ADS Bibcode: 1981PASP...93....5B.
<https://ui.adsabs.harvard.edu/abs/1981PASP...93....5B>

- Barro, G., Pérez-González, P. G., Kocevski, D. D., et al. 2024, *The Astrophysical Journal*, 963, 128, publisher: IOP ADS Bibcode: 2024ApJ...963..128B. <https://ui.adsabs.harvard.edu/abs/2024ApJ...963..128B>
- Behroozi, P., Conroy, C., Wechsler, R. H., et al. 2020, *Monthly Notices of the Royal Astronomical Society*, 499, 5702, publisher: OUP ADS Bibcode: 2020MNRAS.499.5702B. <https://ui.adsabs.harvard.edu/abs/2020MNRAS.499.5702B>
- Berg, D. A., Skillman, E. D., Marble, A. R., et al. 2012, *The Astrophysical Journal*, 754, 98, publisher: IOP ADS Bibcode: 2012ApJ...754...98B. <https://ui.adsabs.harvard.edu/abs/2012ApJ...754...98B>
- Bertin, E., & Arnouts, S. 1996, *Astronomy and Astrophysics Supplement Series*, 117, 393, aDS Bibcode: 1996A&AS..117..393B. <https://ui.adsabs.harvard.edu/abs/1996A&AS..117..393B>
- Bian, F., Kewley, L. J., & Dopita, M. A. 2018, *The Astrophysical Journal*, 859, 175, publisher: IOP ADS Bibcode: 2018ApJ...859..175B. <https://ui.adsabs.harvard.edu/abs/2018ApJ...859..175B>
- Binette, L. 1985, *Astronomy and Astrophysics*, 143, 334, aDS Bibcode: 1985A&A...143..334B. <https://ui.adsabs.harvard.edu/abs/1985A&A...143..334B>
- Binette, L., Dopita, M. A., & Tuohy, I. R. 1985, *The Astrophysical Journal*, 297, 476, publisher: IOP ADS Bibcode: 1985ApJ...297..476B. <https://ui.adsabs.harvard.edu/abs/1985ApJ...297..476B>
- Binette, L., Zovaro, H. R. M., Villar Martín, M., et al. 2024, *Astronomy and Astrophysics*, 684, A53, aDS Bibcode: 2024A&A...684A..53B. <https://ui.adsabs.harvard.edu/abs/2024A&A...684A..53B>
- Blain, A. W., Smail, I., Ivison, R. J., Kneib, J. P., & Frayer, D. T. 2002, *Physics Reports*, 369, 111, aDS Bibcode: 2002PhR...369..111B. <https://ui.adsabs.harvard.edu/abs/2002PhR...369..111B>
- Boquien, M., Burgarella, D., Roehly, Y., et al. 2019, *Astronomy and Astrophysics*, 622, A103, aDS Bibcode: 2019A&A...622A.103B. <https://ui.adsabs.harvard.edu/abs/2019A&A...622A.103B>
- Bouwens, R. J., Illingworth, G. D., Oesch, P. A., et al. 2011, *The Astrophysical Journal*, 737, 90, publisher: IOP ADS Bibcode: 2011ApJ...737...90B. <https://ui.adsabs.harvard.edu/abs/2011ApJ...737...90B>
- Boyett, K., Bunker, A. J., Curtis-Lake, E., et al. 2024, *Monthly Notices of the Royal Astronomical Society*, doi:10.1093/mnras/stae2430, publisher: OUP ADS Bibcode: 2024MNRAS.tmp.2365B. <https://ui.adsabs.harvard.edu/abs/2024MNRAS.tmp.2365B>
- Bradač, M. 2020, *Nature Astronomy*, 4, 478, aDS Bibcode: 2020NatAs...4..478B. <https://ui.adsabs.harvard.edu/abs/2020NatAs...4..478B>
- Bradley, L., Sipocz, B., Robitaille, T., et al. 2016, *Astrophysics Source Code Library*, ascl:1609.011, aDS Bibcode: 2016ascl.soft09011B. <https://ui.adsabs.harvard.edu/abs/2016ascl.soft09011B>
- Bradley, L., Sipocz, B., Robitaille, T., et al. 2022, Zenodo, doi:10.5281/zenodo.6385735, publisher: Zenodo ADS Bibcode: 2022zndo...6385735B. <https://ui.adsabs.harvard.edu/abs/2022zndo...6385735B>
- Brammer, G. 2023, Zenodo, doi:10.5281/zenodo.7299500, publisher: Zenodo ADS Bibcode: 2022zndo...7299500B. <https://ui.adsabs.harvard.edu/abs/2022zndo...7299500B>
- Brinchmann, J. 2023, *Monthly Notices of the Royal Astronomical Society*, 525, 2087, publisher: OUP ADS Bibcode: 2023MNRAS.525.2087B. <https://ui.adsabs.harvard.edu/abs/2023MNRAS.525.2087B>
- Brunker, S. W., Salzer, J. J., Janowiecki, S., Finn, R. A., & Helou, G. 2020, *The Astrophysical Journal*, 898, 68, publisher: IOP ADS Bibcode: 2020ApJ...898...68B. <https://ui.adsabs.harvard.edu/abs/2020ApJ...898...68B>
- Bruzual, G., & Charlot, S. 2003, *Monthly Notices of the Royal Astronomical Society*, 344, 1000, publisher: OUP ADS Bibcode: 2003MNRAS.344.1000B. <https://ui.adsabs.harvard.edu/abs/2003MNRAS.344.1000B>
- Bunker, A. J., NIRSPEC Instrument Science Team, & JAESs Collaboration. 2020, 352, 342, conference Name: Uncovering Early Galaxy Evolution in the ALMA and JWST Era Place: eprint: arXiv:2112.15207 ADS Bibcode: 2020IAUS..352..342B. <https://ui.adsabs.harvard.edu/abs/2020IAUS..352..342B>
- Bunker, A. J., Saxena, A., Cameron, A. J., et al. 2023, *Astronomy and Astrophysics*, 677, A88, publisher: EDP ADS Bibcode: 2023A&A...677A..88B. <https://ui.adsabs.harvard.edu/abs/2023A&A...677A..88B>
- Bunker, A. J., Cameron, A. J., Curtis-Lake, E., et al. 2024, *Astronomy and Astrophysics*, 690, A288, publisher: EDP ADS Bibcode: 2024A&A...690A.288B. <https://ui.adsabs.harvard.edu/abs/2024A&A...690A.288B>
- Bussmann, R. S., Dey, A., Borys, C., et al. 2009, *The Astrophysical Journal*, 705, 184, publisher: IOP ADS Bibcode: 2009ApJ...705..184B. <https://ui.adsabs.harvard.edu/abs/2009ApJ...705..184B>
- Bussmann, R. S., Dey, A., Lotz, J., et al. 2011, *The Astrophysical Journal*, 733, 21, publisher: IOP ADS Bibcode: 2011ApJ...733...21B. <https://ui.adsabs.harvard.edu/abs/2011ApJ...733...21B>

- Bussmann, R. S., Dey, A., Armus, L., et al. 2012, *The Astrophysical Journal*, 744, 150, publisher: IOP ADS Bibcode: 2012ApJ...744..150B. <https://ui.adsabs.harvard.edu/abs/2012ApJ...744..150B>
- Byler, N., Dalcanton, J. J., Conroy, C., & Johnson, B. D. 2017, *The Astrophysical Journal*, 840, 44, publisher: IOP ADS Bibcode: 2017ApJ...840...44B. <https://ui.adsabs.harvard.edu/abs/2017ApJ...840...44B>
- Calabrò, A., Pentericci, L., Feltre, A., et al. 2023, *Astronomy and Astrophysics*, 679, A80, publisher: EDP ADS Bibcode: 2023A&A...679A..80C. <https://ui.adsabs.harvard.edu/abs/2023A&A...679A..80C>
- Calabrò, A., Castellano, M., Zavala, J. A., et al. 2024a, *The Astrophysical Journal*, 975, 245, publisher: IOP ADS Bibcode: 2024ApJ...975..245C. <https://ui.adsabs.harvard.edu/abs/2024ApJ...975..245C>
- Calabrò, A., Pentericci, L., Santini, P., et al. 2024b, *Astronomy and Astrophysics*, 690, A290, publisher: EDP ADS Bibcode: 2024A&A...690A.290C. <https://ui.adsabs.harvard.edu/abs/2024A&A...690A.290C>
- Calzetti, D., Armus, L., Bohlin, R. C., et al. 2000, *The Astrophysical Journal*, 533, 682, publisher: IOP ADS Bibcode: 2000ApJ...533..682C. <https://ui.adsabs.harvard.edu/abs/2000ApJ...533..682C>
- Cameron, A. J., Saxena, A., Bunker, A. J., et al. 2023, *Astronomy and Astrophysics*, 677, A115, publisher: EDP ADS Bibcode: 2023A&A...677A.115C. <https://ui.adsabs.harvard.edu/abs/2023A&A...677A.115C>
- Caputi, K. I., Deshmukh, S., Ashby, M. L. N., et al. 2017, *The Astrophysical Journal*, 849, 45, publisher: IOP ADS Bibcode: 2017ApJ...849...45C. <https://ui.adsabs.harvard.edu/abs/2017ApJ...849...45C>
- Caputi, K. I., Caminha, G. B., Fujimoto, S., et al. 2021, *The Astrophysical Journal*, 908, 146, publisher: IOP ADS Bibcode: 2021ApJ...908..146C. <https://ui.adsabs.harvard.edu/abs/2021ApJ...908..146C>
- Cardamone, C. N., Schawinski, K., Sarzi, M., et al. 2009, *Monthly Notices of the Royal Astronomical Society*, 399, 1191, arXiv:0907.4155 [astro-ph]. <http://arxiv.org/abs/0907.4155>
- Carnall, A. C., McLure, R. J., Dunlop, J. S., et al. 2019, *Monthly Notices of the Royal Astronomical Society*, 490, 417, publisher: OUP ADS Bibcode: 2019MNRAS.490..417C. <https://ui.adsabs.harvard.edu/abs/2019MNRAS.490..417C>
- . 2023, *Nature*, 619, 716, aDS Bibcode: 2023Natur.619..716C. <https://ui.adsabs.harvard.edu/abs/2023Natur.619..716C>
- Carniani, S., Hainline, K., D'Eugenio, F., et al. 2024a, *A shining cosmic dawn: spectroscopic confirmation of two luminous galaxies at $z \sim 14$* , , , publication Title: arXiv e-prints ADS Bibcode: 2024arXiv240518485C, doi:10.48550/arXiv.2405.18485. <https://ui.adsabs.harvard.edu/abs/2024arXiv240518485C>
- . 2024b, *Nature*, 633, 318, aDS Bibcode: 2024Natur.633..318C. <https://ui.adsabs.harvard.edu/abs/2024Natur.633..318C>
- Chisholm, J., Saldana-Lopez, A., Flury, S., et al. 2022, *Monthly Notices of the Royal Astronomical Society*, 517, 5104, publisher: OUP ADS Bibcode: 2022MNRAS.517.5104C. <https://ui.adsabs.harvard.edu/abs/2022MNRAS.517.5104C>
- Cleri, N. J., Olivier, G. M., Hutchison, T. A., et al. 2023, *The Astrophysical Journal*, 953, 10, publisher: IOP ADS Bibcode: 2023ApJ...953...10C. <https://ui.adsabs.harvard.edu/abs/2023ApJ...953...10C>
- Colina, L., Crespo Gómez, A., Álvarez Márquez, J., et al. 2023, *Astronomy and Astrophysics*, 673, L6, publisher: EDP ADS Bibcode: 2023A&A...673L...6C. <https://ui.adsabs.harvard.edu/abs/2023A&A...673L...6C>
- Conroy, C., & Gunn, J. E. 2010, *Astrophysics Source Code Library*, ascl:1010.043, aDS Bibcode: 2010ascl.soft10043C. <https://ui.adsabs.harvard.edu/abs/2010ascl.soft10043C>
- Curti, M., Cresci, G., Mannucci, F., et al. 2017, *Monthly Notices of the Royal Astronomical Society*, 465, 1384, publisher: OUP ADS Bibcode: 2017MNRAS.465.1384C. <https://ui.adsabs.harvard.edu/abs/2017MNRAS.465.1384C>
- Curti, M., Mannucci, F., Cresci, G., & Maiolino, R. 2020, *Monthly Notices of the Royal Astronomical Society*, 491, 944, publisher: OUP ADS Bibcode: 2020MNRAS.491..944C. <https://ui.adsabs.harvard.edu/abs/2020MNRAS.491..944C>
- Curti, M., D'Eugenio, F., Carniani, S., et al. 2023, *Monthly Notices of the Royal Astronomical Society*, 518, 425, publisher: OUP ADS Bibcode: 2023MNRAS.518..425C. <https://ui.adsabs.harvard.edu/abs/2023MNRAS.518..425C>
- Curti, M., Maiolino, R., Curtis-Lake, E., et al. 2024, *Astronomy and Astrophysics*, 684, A75, publisher: EDP ADS Bibcode: 2024A&A...684A..75C. <https://ui.adsabs.harvard.edu/abs/2024A&A...684A..75C>
- Curtis-Lake, E., Carniani, S., Cameron, A., et al. 2023, *Nature Astronomy*, 7, 622, aDS Bibcode: 2023NatAs...7..622C. <https://ui.adsabs.harvard.edu/abs/2023NatAs...7..622C>

- de Graaff, A., Rix, H.-W., Carniani, S., et al. 2024, *Astronomy and Astrophysics*, 684, A87, publisher: EDP
ADS Bibcode: 2024A&A...684A..87D.
<https://ui.adsabs.harvard.edu/abs/2024A&A...684A..87D>
- De Rossi, M. E., Rieke, G. H., Shivaeei, I., Bromm, V., & Lyu, J. 2018, *The Astrophysical Journal*, 869, 4, publisher: IOP ADS Bibcode: 2018ApJ...869....4D.
<https://ui.adsabs.harvard.edu/abs/2018ApJ...869....4D>
- D'Eugenio, F., Cameron, A. J., Scholtz, J., et al. 2024, JADES Data Release 3 – NIRSpec/MSA spectroscopy for 4,000 galaxies in the GOODS fields, , , publication Title: arXiv e-prints ADS Bibcode: 2024arXiv240406531D, doi:10.48550/arXiv.2404.06531.
<https://ui.adsabs.harvard.edu/abs/2024arXiv240406531D>
- Dey, A., Soifer, B. T., Desai, V., et al. 2008, *The Astrophysical Journal*, 677, 943, publisher: IOP ADS Bibcode: 2008ApJ...677..943D.
<https://ui.adsabs.harvard.edu/abs/2008ApJ...677..943D>
- Dickinson, M., Giavalisco, M., & GOODS Team. 2003, *The Great Observatories Origins Deep Survey* (eprint: arXiv:astro-ph/0204213), conference Name: The Mass of Galaxies at Low and High Redshift Pages: 324 ADS Bibcode: 2003mgjh.conf..324D, doi:10.1007/10899892_78.
<https://ui.adsabs.harvard.edu/abs/2003mgjh.conf..324D>
- Dors, O. L., Maiolino, R., Cardaci, M. V., et al. 2020, *Monthly Notices of the Royal Astronomical Society*, 496, 3209, publisher: OUP ADS Bibcode: 2020MNRAS.496.3209D. <https://ui.adsabs.harvard.edu/abs/2020MNRAS.496.3209D>
- Draine, B. T. 2003, *The Astrophysical Journal*, 598, 1017, publisher: IOP ADS Bibcode: 2003ApJ...598.1017D.
<https://ui.adsabs.harvard.edu/abs/2003ApJ...598.1017D>
- Draine, B. T., Aniano, G., Krause, O., et al. 2014, *The Astrophysical Journal*, 780, 172, publisher: IOP ADS Bibcode: 2014ApJ...780..172D.
<https://ui.adsabs.harvard.edu/abs/2014ApJ...780..172D>
- Eisenhardt, P. R. M., Wu, J., Tsai, C.-W., et al. 2012, *The Astrophysical Journal*, 755, 173, publisher: IOP ADS Bibcode: 2012ApJ...755..173E.
<https://ui.adsabs.harvard.edu/abs/2012ApJ...755..173E>
- Eisenstein, D. J., Johnson, B. D., Robertson, B., et al. 2023a, *The JADES Origins Field: A New JWST Deep Field in the JADES Second NIRCAM Data Release*, , , publication Title: arXiv e-prints ADS Bibcode: 2023arXiv231012340E, doi:10.48550/arXiv.2310.12340.
<https://ui.adsabs.harvard.edu/abs/2023arXiv231012340E>
- Eisenstein, D. J., Willott, C., Alberts, S., et al. 2023b, *Overview of the JWST Advanced Deep Extragalactic Survey (JADES)*, , , publication Title: arXiv e-prints ADS Bibcode: 2023arXiv230602465E, doi:10.48550/arXiv.2306.02465.
<https://ui.adsabs.harvard.edu/abs/2023arXiv230602465E>
- Eldridge, J. J., Stanway, E. R., Xiao, L., et al. 2017, *Publications of the Astronomical Society of Australia*, 34, e058, aDS Bibcode: 2017PASA...34...58E.
<https://ui.adsabs.harvard.edu/abs/2017PASA...34...58E>
- Elston, R., Rieke, G. H., & Rieke, M. J. 1988, *The Astrophysical Journal*, 331, L77, publisher: IOP ADS Bibcode: 1988ApJ...331L..77E.
<https://ui.adsabs.harvard.edu/abs/1988ApJ...331L..77E>
- Elston, R., Rieke, M. J., & Rieke, G. H. 1989, *The Astrophysical Journal*, 341, 80, publisher: IOP ADS Bibcode: 1989ApJ...341...80E.
<https://ui.adsabs.harvard.edu/abs/1989ApJ...341...80E>
- Faisst, A. L., Capak, P. L., Emami, N., Tacchella, S., & Larson, K. L. 2019, *The Astrophysical Journal*, 884, 133, publisher: IOP ADS Bibcode: 2019ApJ...884..133F.
<https://ui.adsabs.harvard.edu/abs/2019ApJ...884..133F>
- Fazio, G. G., Hora, J. L., Allen, L. E., et al. 2004, *The Astrophysical Journal Supplement Series*, 154, 10, publisher: IOP ADS Bibcode: 2004ApJS..154...10F.
<https://ui.adsabs.harvard.edu/abs/2004ApJS..154...10F>
- Feltre, A., Charlot, S., & Gutkin, J. 2016, *Monthly Notices of the Royal Astronomical Society*, 456, 3354, publisher: OUP ADS Bibcode: 2016MNRAS.456.3354F. <https://ui.adsabs.harvard.edu/abs/2016MNRAS.456.3354F>
- Ferland, G. J., Porter, R. L., van Hoof, P. A. M., et al. 2013, *Revista Mexicana de Astronomía y Astrofísica*, 49, 137, aDS Bibcode: 2013RMxAA..49..137F. <https://ui.adsabs.harvard.edu/abs/2013RMxAA..49..137F>
- Ferland, G. J., Chatzikos, M., Guzmán, F., et al. 2017, *Revista Mexicana de Astronomía y Astrofísica*, 53, 385, aDS Bibcode: 2017RMxAA..53..385F. <https://ui.adsabs.harvard.edu/abs/2017RMxAA..53..385F>
- Ferruit, P., Jakobsen, P., Giardino, G., et al. 2022, *Astronomy and Astrophysics*, 661, A81, publisher: EDP ADS Bibcode: 2022A&A...661A..81F.
<https://ui.adsabs.harvard.edu/abs/2022A&A...661A..81F>
- Feuillet, L. M., Meléndez, M., Kraemer, S., et al. 2024, *The Astrophysical Journal*, 962, 104, publisher: IOP ADS Bibcode: 2024ApJ...962..104F.
<https://ui.adsabs.harvard.edu/abs/2024ApJ...962..104F>
- Furtak, L. J., Zitrin, A., Plat, A., et al. 2023, *The Astrophysical Journal*, 952, 142, publisher: IOP ADS Bibcode: 2023ApJ...952..142F.
<https://ui.adsabs.harvard.edu/abs/2023ApJ...952..142F>

- Gardner, J. P., Mather, J. C., Abbott, R., et al. 2023, Publications of the Astronomical Society of the Pacific, 135, 068001, publisher: IOP ADS Bibcode: 2023PASP..135f8001G. <https://ui.adsabs.harvard.edu/abs/2023PASP..135f8001G>
- Gehrz, R. D., Roellig, T. L., Werner, M. W., et al. 2007, Review of Scientific Instruments, 78, 011302, publisher: AIP ADS Bibcode: 2007RScl...78a1302G. <https://ui.adsabs.harvard.edu/abs/2007RScl...78a1302G>
- Giavalisco, M., Ferguson, H. C., Koekemoer, A. M., et al. 2004, The Astrophysical Journal, 600, L93, publisher: IOP ADS Bibcode: 2004ApJ...600L..93G. <https://ui.adsabs.harvard.edu/abs/2004ApJ...600L..93G>
- Gillman, S., Pye, J. P., Alonso-Herrero, A., et al. 2025, MIDIS: Quantifying the AGN component of X-ray-detected galaxies, , publication Title: arXiv e-prints ADS Bibcode: 2025arXiv250111491G, doi:10.48550/arXiv.2501.11491. <https://ui.adsabs.harvard.edu/abs/2025arXiv250111491G>
- Glikman, E., Djorgovski, S. G., Stern, D., Bogosavljević, M., & Mahabal, A. 2007, The Astrophysical Journal, 663, L73, publisher: IOP ADS Bibcode: 2007ApJ...663L..73G. <https://ui.adsabs.harvard.edu/abs/2007ApJ...663L..73G>
- Glikman, E., Helfand, D. J., & White, R. L. 2006, The Astrophysical Journal, 640, 579, publisher: IOP ADS Bibcode: 2006ApJ...640..579G. <https://ui.adsabs.harvard.edu/abs/2006ApJ...640..579G>
- Gordon, K. D., Clayton, G. C., Misselt, K. A., Landolt, A. U., & Wolff, M. J. 2003, The Astrophysical Journal, 594, 279, publisher: IOP ADS Bibcode: 2003ApJ...594..279G. <https://ui.adsabs.harvard.edu/abs/2003ApJ...594..279G>
- Greene, J. E., Seth, A., Kim, M., et al. 2016, The Astrophysical Journal, 826, L32, publisher: IOP ADS Bibcode: 2016ApJ...826L..32G. <https://ui.adsabs.harvard.edu/abs/2016ApJ...826L..32G>
- Greene, J. E., Labbe, I., Goulding, A. D., et al. 2024, The Astrophysical Journal, 964, 39, publisher: IOP ADS Bibcode: 2024ApJ...964...39G. <https://ui.adsabs.harvard.edu/abs/2024ApJ...964...39G>
- Groves, B. A., Dopita, M. A., & Sutherland, R. S. 2004, The Astrophysical Journal Supplement Series, 153, 75, publisher: IOP ADS Bibcode: 2004ApJS..153...75G. <https://ui.adsabs.harvard.edu/abs/2004ApJS..153...75G>
- Hainline, K. N., Maiolino, R., Juodzbališ, I., et al. 2024a, An Investigation Into The Selection and Colors of Little Red Dots and Active Galactic Nuclei, , publication Title: arXiv e-prints ADS Bibcode: 2024arXiv241000100H, doi:10.48550/arXiv.2410.00100. <https://ui.adsabs.harvard.edu/abs/2024arXiv241000100H>
- Hainline, K. N., Johnson, B. D., Robertson, B., et al. 2024b, The Astrophysical Journal, 964, 71, publisher: IOP ADS Bibcode: 2024ApJ...964...71H. <https://ui.adsabs.harvard.edu/abs/2024ApJ...964...71H>
- Harikane, Y., Zhang, Y., Nakajima, K., et al. 2023, The Astrophysical Journal, 959, 39, publisher: IOP ADS Bibcode: 2023ApJ...959...39H. <https://ui.adsabs.harvard.edu/abs/2023ApJ...959...39H>
- Harris, C. R., Millman, K. J., van der Walt, S. J., et al. 2020, Nature, 585, 357, aDS Bibcode: 2020Natur.585..357H. <https://ui.adsabs.harvard.edu/abs/2020Natur.585..357H>
- Heintz, K. E., Brammer, G. B., Watson, D., et al. 2025, Astronomy and Astrophysics, 693, A60, publisher: EDP ADS Bibcode: 2025A&A...693A..60H. <https://ui.adsabs.harvard.edu/abs/2025A&A...693A..60H>
- Helou, G., & Kessler, M. F. 1995, 73, 659, conference Name: From Gas to Stars to Dust ADS Bibcode: 1995ASPC...73..659H. <https://ui.adsabs.harvard.edu/abs/1995ASPC...73..659H>
- Henry, A., Scarlata, C., Martin, C. L., & Erb, D. 2015, The Astrophysical Journal, 809, 19, publisher: IOP ADS Bibcode: 2015ApJ...809...19H. <https://ui.adsabs.harvard.edu/abs/2015ApJ...809...19H>
- Hirschmann, M., Charlot, S., Feltre, A., et al. 2023, Monthly Notices of the Royal Astronomical Society, 526, 3610, publisher: OUP ADS Bibcode: 2023MNRAS.526.3610H. <https://ui.adsabs.harvard.edu/abs/2023MNRAS.526.3610H>
- Hopkins, P. F., Strauss, M. A., Hall, P. B., et al. 2004, The Astronomical Journal, 128, 1112, publisher: IOP ADS Bibcode: 2004AJ....128.1112H. <https://ui.adsabs.harvard.edu/abs/2004AJ....128.1112H>
- Huang, K.-H., Bradač, M., Lemaux, B. C., et al. 2016, The Astrophysical Journal, 817, 11, publisher: IOP ADS Bibcode: 2016ApJ...817...11H. <https://ui.adsabs.harvard.edu/abs/2016ApJ...817...11H>
- Iani, E., Rinaldi, P., Caputi, K. I., et al. 2024a, MIDIS: MIRI uncovers Virgil, an extended source at $z \sim 6.6$ with the photometric properties of Little Red Dots, , publication Title: arXiv e-prints ADS Bibcode: 2024arXiv240618207I, doi:10.48550/arXiv.2406.18207. <https://ui.adsabs.harvard.edu/abs/2024arXiv240618207I>
- Iani, E., Caputi, K. I., Rinaldi, P., et al. 2024b, The Astrophysical Journal, 963, 97, publisher: IOP ADS Bibcode: 2024ApJ...963...97I. <https://ui.adsabs.harvard.edu/abs/2024ApJ...963...97I>

- Isobe, Y., Ouchi, M., Nakajima, K., et al. 2023, *The Astrophysical Journal*, 956, 139, publisher: IOP ADS Bibcode: 2023ApJ...956..139I. <https://ui.adsabs.harvard.edu/abs/2023ApJ...956..139I>
- Izotov, Y. I., Schaerer, D., Thuan, T. X., et al. 2016, *Monthly Notices of the Royal Astronomical Society*, 461, 3683, publisher: OUP ADS Bibcode: 2016MNRAS.461.3683I. <https://ui.adsabs.harvard.edu/abs/2016MNRAS.461.3683I>
- Izotov, Y. I., Stasińska, G., Meynet, G., Guseva, N. G., & Thuan, T. X. 2006, *Astronomy and Astrophysics*, 448, 955, aDS Bibcode: 2006A&A...448..955I. <https://ui.adsabs.harvard.edu/abs/2006A&A...448..955I>
- Izotov, Y. I., Thuan, T. X., Guseva, N. G., & Liss, S. E. 2018, *Monthly Notices of the Royal Astronomical Society*, 473, 1956, publisher: OUP ADS Bibcode: 2018MNRAS.473.1956I. <https://ui.adsabs.harvard.edu/abs/2018MNRAS.473.1956I>
- Jakobsen, P., Ferruit, P., Alves de Oliveira, C., et al. 2022, *Astronomy and Astrophysics*, 661, A80, aDS Bibcode: 2022A&A...661A..80J. <https://ui.adsabs.harvard.edu/abs/2022A&A...661A..80J>
- Jaskot, A. E., & Oey, M. S. 2013, *The Astrophysical Journal*, 766, 91, publisher: IOP ADS Bibcode: 2013ApJ...766...91J. <https://ui.adsabs.harvard.edu/abs/2013ApJ...766...91J>
- Johnson, B. D., Leja, J., Conroy, C., & Speagle, J. S. 2021, *The Astrophysical Journal Supplement Series*, 254, 22, publisher: IOP ADS Bibcode: 2021ApJS..254...22J. <https://ui.adsabs.harvard.edu/abs/2021ApJS..254...22J>
- Juodžbalis, I., Maiolino, R., Baker, W. M., et al. 2024, A dormant, overmassive black hole in the early Universe, , , publication Title: arXiv e-prints ADS Bibcode: 2024arXiv240303872J, doi:10.48550/arXiv.2403.03872. <https://ui.adsabs.harvard.edu/abs/2024arXiv240303872J>
- Kauffmann, G., Heckman, T. M., White, S. D. M., et al. 2003, *Monthly Notices of the Royal Astronomical Society*, 341, 33, publisher: OUP ADS Bibcode: 2003MNRAS.341...33K. <https://ui.adsabs.harvard.edu/abs/2003MNRAS.341...33K>
- Kennicutt, R. C., & Evans, N. J. 2012, *Annual Review of Astronomy and Astrophysics*, 50, 531, aDS Bibcode: 2012ARA&A..50..531K. <https://ui.adsabs.harvard.edu/abs/2012ARA&A..50..531K>
- Kewley, L. J., Nicholls, D. C., Sutherland, R., et al. 2019, *The Astrophysical Journal*, 880, 16, publisher: IOP ADS Bibcode: 2019ApJ...880...16K. <https://ui.adsabs.harvard.edu/abs/2019ApJ...880...16K>
- Killi, M., Watson, D., Brammer, G., et al. 2023, Deciphering the JWST spectrum of a 'little red dot' at $z \sim 4.53$: An obscured AGN and its star-forming host, , , publication Title: arXiv e-prints ADS Bibcode: 2023arXiv231203065K, doi:10.48550/arXiv.2312.03065. <https://ui.adsabs.harvard.edu/abs/2023arXiv231203065K>
- Kocevski, D. D., Onoue, M., Inayoshi, K., et al. 2023, *The Astrophysical Journal*, 954, L4, publisher: IOP ADS Bibcode: 2023ApJ...954L...4K. <https://ui.adsabs.harvard.edu/abs/2023ApJ...954L...4K>
- Kocevski, D. D., Finkelstein, S. L., Barro, G., et al. 2024, The Rise of Faint, Red AGN at $z > 4$: A Sample of Little Red Dots in the JWST Extragalactic Legacy Fields, , , publication Title: arXiv e-prints ADS Bibcode: 2024arXiv240403576K, doi:10.48550/arXiv.2404.03576. <https://ui.adsabs.harvard.edu/abs/2024arXiv240403576K>
- Kokorev, V., Fujimoto, S., Labbe, I., et al. 2023, *The Astrophysical Journal*, 957, L7, publisher: IOP ADS Bibcode: 2023ApJ...957L...7K. <https://ui.adsabs.harvard.edu/abs/2023ApJ...957L...7K>
- Kokorev, V., Caputi, K. I., Greene, J. E., et al. 2024, *The Astrophysical Journal*, 968, 38, publisher: IOP ADS Bibcode: 2024ApJ...968...38K. <https://ui.adsabs.harvard.edu/abs/2024ApJ...968...38K>
- Koyama, Y., Shimakawa, R., Yamamura, I., Kodama, T., & Hayashi, M. 2019, *Publications of the Astronomical Society of Japan*, 71, 8, publisher: OUP ADS Bibcode: 2019PASJ...71....8K. <https://ui.adsabs.harvard.edu/abs/2019PASJ...71....8K>
- Kriek, M., & Conroy, C. 2013, *The Astrophysical Journal*, 775, L16, publisher: IOP ADS Bibcode: 2013ApJ...775L..16K. <https://ui.adsabs.harvard.edu/abs/2013ApJ...775L..16K>
- Kron, R. G. 1980, *The Astrophysical Journal Supplement Series*, 43, 305, publisher: IOP ADS Bibcode: 1980ApJS...43..305K. <https://ui.adsabs.harvard.edu/abs/1980ApJS...43..305K>
- Kroupa, P. 2001, *Monthly Notices of the Royal Astronomical Society*, 322, 231, publisher: OUP ADS Bibcode: 2001MNRAS.322..231K. <https://ui.adsabs.harvard.edu/abs/2001MNRAS.322..231K>
- Kuruvanthodi, A., Schaerer, D., Marques-Chaves, R., et al. 2024, *Astronomy and Astrophysics*, 691, A310, publisher: EDP ADS Bibcode: 2024A&A...691A.310K. <https://ui.adsabs.harvard.edu/abs/2024A&A...691A.310K>
- Labbé, I., van Dokkum, P., Nelson, E., et al. 2023, *Nature*, 616, 266, aDS Bibcode: 2023Natur.616..266L. <https://ui.adsabs.harvard.edu/abs/2023Natur.616..266L>

- Lacy, M., & Sajina, A. 2020, *Nature Astronomy*, 4, 352, aDS Bibcode: 2020NatAs...4..352L
<https://ui.adsabs.harvard.edu/abs/2020NatAs...4..352L>
- Lam, D., Bouwens, R. J., Coe, D., et al. 2019, Detection of a Lensed $z \approx 11$ Galaxy in the Rest-Optical with Spitzer/IRAC and the Inferred SFR, Stellar Mass, and Physical Size, , , publication Title: arXiv e-prints ADS Bibcode: 2019arXiv190308177L, doi:10.48550/arXiv.1903.08177.
<https://ui.adsabs.harvard.edu/abs/2019arXiv190308177L>
- Langan, I., Ceverino, D., & Finlator, K. 2020, *Monthly Notices of the Royal Astronomical Society*, 494, 1988, publisher: OUP ADS Bibcode: 2020MNRAS.494.1988L.
<https://ui.adsabs.harvard.edu/abs/2020MNRAS.494.1988L>
- Langeroodi, D., & Hjorth, J. 2024a, Genesis-Metallicity: Universal Non-Parametric Gas-Phase Metallicity Estimation, , , publication Title: arXiv e-prints ADS Bibcode: 2024arXiv240907455L, doi:10.48550/arXiv.2409.07455.
<https://ui.adsabs.harvard.edu/abs/2024arXiv240907455L>
- . 2024b, NIRSPEC View of the Appearance and Evolution of Balmer Breaks and the Transition from Bursty to Smooth Star Formation Histories from Deep Within the Epoch of Reionization to Cosmic Noon, , , publication Title: arXiv e-prints ADS Bibcode: 2024arXiv240413045L, doi:10.48550/arXiv.2404.13045.
<https://ui.adsabs.harvard.edu/abs/2024arXiv240413045L>
- Langeroodi, D., Hjorth, J., Ferrara, A., & Gall, C. 2024, Rapid Dust Formation in the Early Universe, , , publication Title: arXiv e-prints ADS Bibcode: 2024arXiv241014671L, doi:10.48550/arXiv.2410.14671.
<https://ui.adsabs.harvard.edu/abs/2024arXiv241014671L>
- Langeroodi, D., Hjorth, J., Chen, W., et al. 2023, *The Astrophysical Journal*, 957, 39, publisher: IOP ADS Bibcode: 2023ApJ...957...39L.
<https://ui.adsabs.harvard.edu/abs/2023ApJ...957...39L>
- Larson, R. L., Finkelstein, S. L., Kocevski, D. D., et al. 2023, *The Astrophysical Journal*, 953, L29, publisher: IOP ADS Bibcode: 2023ApJ...953L..29L.
<https://ui.adsabs.harvard.edu/abs/2023ApJ...953L..29L>
- Leja, J., Carnall, A. C., Johnson, B. D., Conroy, C., & Speagle, J. S. 2019, *The Astrophysical Journal*, 876, 3, publisher: IOP ADS Bibcode: 2019ApJ...876....3L.
<https://ui.adsabs.harvard.edu/abs/2019ApJ...876....3L>
- Li, M., Cai, Z., Bian, F., et al. 2023, *The Astrophysical Journal*, 955, L18, publisher: IOP ADS Bibcode: 2023ApJ...955L..18L.
<https://ui.adsabs.harvard.edu/abs/2023ApJ...955L..18L>
- Libralato, M., Argyriou, I., Dicken, D., et al. 2024, *Publications of the Astronomical Society of the Pacific*, 136, 034502, publisher: IOP ADS Bibcode: 2024PASP..136c4502L.
<https://ui.adsabs.harvard.edu/abs/2024PASP..136c4502L>
- Liddle, A. R. 2007, *Monthly Notices of the Royal Astronomical Society*, 377, L74, publisher: OUP ADS Bibcode: 2007MNRAS.377L..74L. <https://ui.adsabs.harvard.edu/abs/2007MNRAS.377L..74L>
- Lin, R., Zheng, Z.-Y., Jiang, C., et al. 2024, Discovery of Local Analogs to JWST's Little Red Dots, , , publication Title: arXiv e-prints ADS Bibcode: 2024arXiv241208396L, doi:10.48550/arXiv.2412.08396.
<https://ui.adsabs.harvard.edu/abs/2024arXiv241208396L>
- Lovell, C. C., Vijayan, A. P., Thomas, P. A., et al. 2021, *Monthly Notices of the Royal Astronomical Society*, 500, 2127, publisher: OUP ADS Bibcode: 2021MNRAS.500.2127L. <https://ui.adsabs.harvard.edu/abs/2021MNRAS.500.2127L>
- Luo, B., Brandt, W. N., Xue, Y. Q., et al. 2017, *The Astrophysical Journal Supplement Series*, 228, 2, publisher: IOP ADS Bibcode: 2017ApJS..228....2L.
<https://ui.adsabs.harvard.edu/abs/2017ApJS..228....2L>
- Luridiana, V., Morisset, C., & Shaw, R. A. 2015, *Astronomy and Astrophysics*, 573, A42, aDS Bibcode: 2015A&A...573A..42L.
<https://ui.adsabs.harvard.edu/abs/2015A&A...573A..42L>
- Lyu, J., Alberts, S., Rieke, G. H., & Rujopakarn, W. 2022, *The Astrophysical Journal*, 941, 191, publisher: IOP ADS Bibcode: 2022ApJ...941..191L.
<https://ui.adsabs.harvard.edu/abs/2022ApJ...941..191L>
- Lyu, J., Rieke, G. H., & Alberts, S. 2016, *The Astrophysical Journal*, 816, 85, publisher: IOP ADS Bibcode: 2016ApJ...816...85L.
<https://ui.adsabs.harvard.edu/abs/2016ApJ...816...85L>
- Lyu, J., Alberts, S., Rieke, G. H., et al. 2024, *The Astrophysical Journal*, 966, 229, publisher: IOP ADS Bibcode: 2024ApJ...966..229L.
<https://ui.adsabs.harvard.edu/abs/2024ApJ...966..229L>
- Maiolino, R., Scholtz, J., Witstok, J., et al. 2024, *Nature*, 627, 59, aDS Bibcode: 2024Natur.627...59M.
<https://ui.adsabs.harvard.edu/abs/2024Natur.627...59M>
- Mascia, S., Pentericci, L., Calabrò, A., et al. 2023, *Astronomy and Astrophysics*, 672, A155, publisher: EDP ADS Bibcode: 2023A&A...672A.155M. <https://ui.adsabs.harvard.edu/abs/2023A&A...672A.155M>
- Matsuoka, Y., Onoue, M., Kashikawa, N., et al. 2019, *The Astrophysical Journal*, 872, L2, publisher: IOP ADS Bibcode: 2019ApJ...872L..2M.
<https://ui.adsabs.harvard.edu/abs/2019ApJ...872L..2M>

- Matthee, J., Sobral, D., Best, P., et al. 2017, *Monthly Notices of the Royal Astronomical Society*, 465, 3637, publisher: OUP ADS Bibcode: 2017MNRAS.465.3637M. <https://ui.adsabs.harvard.edu/abs/2017MNRAS.465.3637M>
- Matthee, J., Feltre, A., Maseda, M., et al. 2022, *Astronomy and Astrophysics*, 660, A10, aDS Bibcode: 2022A&A...660A..10M. <https://ui.adsabs.harvard.edu/abs/2022A&A...660A..10M>
- Matthee, J., Naidu, R. P., Brammer, G., et al. 2024, *The Astrophysical Journal*, 963, 129, publisher: IOP ADS Bibcode: 2024ApJ...963..129M. <https://ui.adsabs.harvard.edu/abs/2024ApJ...963..129M>
- Mazzolari, G., Übler, H., Maiolino, R., et al. 2024, *New AGN diagnostic diagrams based on the [OIII] λ 4363 auroral line*, , publication Title: arXiv e-prints ADS Bibcode: 2024arXiv240410811M, doi:10.48550/arXiv.2404.10811. <https://ui.adsabs.harvard.edu/abs/2024arXiv240410811M>
- McClymont, W., Tacchella, S., D'Eugenio, F., et al. 2024, *The density-bounded twilight of starbursts in the early Universe*, , publication Title: arXiv e-prints ADS Bibcode: 2024arXiv240515859M, doi:10.48550/arXiv.2405.15859. <https://ui.adsabs.harvard.edu/abs/2024arXiv240515859M>
- Mingozzi, M., James, B. L., Arellano-Córdova, K. Z., et al. 2022, *The Astrophysical Journal*, 939, 110, publisher: IOP ADS Bibcode: 2022ApJ...939..110M. <https://ui.adsabs.harvard.edu/abs/2022ApJ...939..110M>
- Mobasher, B., Dickinson, M., Ferguson, H. C., et al. 2005, *The Astrophysical Journal*, 635, 832, publisher: IOP ADS Bibcode: 2005ApJ...635..832M. <https://ui.adsabs.harvard.edu/abs/2005ApJ...635..832M>
- Nagao, T., Murayama, T., & Taniguchi, Y. 2001, *The Astrophysical Journal*, 549, 155, publisher: IOP ADS Bibcode: 2001ApJ...549..155N. <https://ui.adsabs.harvard.edu/abs/2001ApJ...549..155N>
- Nakajima, K., & Maiolino, R. 2022, *Monthly Notices of the Royal Astronomical Society*, 513, 5134, publisher: OUP ADS Bibcode: 2022MNRAS.513.5134N. <https://ui.adsabs.harvard.edu/abs/2022MNRAS.513.5134N>
- Nakajima, K., Ouchi, M., Isobe, Y., et al. 2023, *The Astrophysical Journal Supplement Series*, 269, 33, publisher: IOP ADS Bibcode: 2023ApJS..269...33N. <https://ui.adsabs.harvard.edu/abs/2023ApJS..269...33N>
- Navarro-Carrera, R., Rinaldi, P., Caputi, K. I., et al. 2024, *Burstiness in low stellar-mass Ha emitters at $z \sim 2$ and $z \sim 4-6$ from JWST medium band photometry in GOODS-S*, , publication Title: arXiv e-prints ADS Bibcode: 2024arXiv241023249N, doi:10.48550/arXiv.2410.23249. <https://ui.adsabs.harvard.edu/abs/2024arXiv241023249N>
- Nelson, D., Pillepich, A., Springel, V., et al. 2019, *Monthly Notices of the Royal Astronomical Society*, 490, 3234, publisher: OUP ADS Bibcode: 2019MNRAS.490.3234N. <https://ui.adsabs.harvard.edu/abs/2019MNRAS.490.3234N>
- Netzer, H. 2009, *Monthly Notices of the Royal Astronomical Society*, 399, 1907, publisher: OUP ADS Bibcode: 2009MNRAS.399.1907N. <https://ui.adsabs.harvard.edu/abs/2009MNRAS.399.1907N>
- Neugebauer, G., Habing, H. J., van Duinen, R., et al. 1984, *The Astrophysical Journal*, 278, L1, publisher: IOP ADS Bibcode: 1984ApJ...278L...1N. <https://ui.adsabs.harvard.edu/abs/1984ApJ...278L...1N>
- Noboriguchi, A., Inoue, A. K., Nagao, T., Toba, Y., & Misawa, T. 2023, *The Astrophysical Journal*, 959, L14, publisher: IOP ADS Bibcode: 2023ApJ...959L..14N. <https://ui.adsabs.harvard.edu/abs/2023ApJ...959L..14N>
- Noboriguchi, A., Nagao, T., Toba, Y., et al. 2022, *The Astrophysical Journal*, 941, 195, publisher: IOP ADS Bibcode: 2022ApJ...941..195N. <https://ui.adsabs.harvard.edu/abs/2022ApJ...941..195N>
- Oesch, P. A., Bouwens, R. J., Illingworth, G. D., et al. 2014, *The Astrophysical Journal*, 786, 108, publisher: IOP ADS Bibcode: 2014ApJ...786..108O. <https://ui.adsabs.harvard.edu/abs/2014ApJ...786..108O>
- Oesch, P. A., Brammer, G., van Dokkum, P. G., et al. 2016, *The Astrophysical Journal*, 819, 129, publisher: IOP ADS Bibcode: 2016ApJ...819..129O. <https://ui.adsabs.harvard.edu/abs/2016ApJ...819..129O>
- Oesch, P. A., Brammer, G., Naidu, R. P., et al. 2023, *Monthly Notices of the Royal Astronomical Society*, 525, 2864, publisher: OUP ADS Bibcode: 2023MNRAS.525.2864O. <https://ui.adsabs.harvard.edu/abs/2023MNRAS.525.2864O>
- Oke, J. B., & Gunn, J. E. 1983, *The Astrophysical Journal*, 266, 713, publisher: IOP ADS Bibcode: 1983ApJ...266..713O. <https://ui.adsabs.harvard.edu/abs/1983ApJ...266..713O>
- Osterbrock, D. E., & Ferland, G. J. 2006, *Astrophysics of gaseous nebulae and active galactic nuclei*, publication Title: *Astrophysics of gaseous nebulae and active galactic nuclei* ADS Bibcode: 2006agna.book.....O. <https://ui.adsabs.harvard.edu/abs/2006agna.book.....O>

- Pacucci, F., Nguyen, B., Carniani, S., Maiolino, R., & Fan, X. 2023, *The Astrophysical Journal*, 957, L3, publisher: IOP ADS Bibcode: 2023ApJ...957L...3P
<https://ui.adsabs.harvard.edu/abs/2023ApJ...957L...3P>
- Papovich, C., Moustakas, L. A., Dickinson, M., et al. 2006, *The Astrophysical Journal*, 640, 92, publisher: IOP ADS Bibcode: 2006ApJ...640...92P
<https://ui.adsabs.harvard.edu/abs/2006ApJ...640...92P>
- Papovich, C., Simons, R. C., Estrada-Carpenter, V., et al. 2022, *The Astrophysical Journal*, 937, 22, publisher: IOP ADS Bibcode: 2022ApJ...937...22P
<https://ui.adsabs.harvard.edu/abs/2022ApJ...937...22P>
- Perna, M., Lanzuisi, G., Brusa, M., Cresci, G., & Mignoli, M. 2017, *Astronomy and Astrophysics*, 606, A96, aDS Bibcode: 2017A&A...606A..96P
<https://ui.adsabs.harvard.edu/abs/2017A&A...606A..96P>
- Pilbratt, G. L., Riedinger, J. R., Passvogel, T., et al. 2010, *Astronomy and Astrophysics*, 518, L1, aDS Bibcode: 2010A&A...518L...1P
<https://ui.adsabs.harvard.edu/abs/2010A&A...518L...1P>
- Pustilnik, S. A., Egorova, E. S., Kniazev, A. Y., et al. 2021, *Monthly Notices of the Royal Astronomical Society*, 507, 944, publisher: OUP ADS Bibcode: 2021MNRAS.507..944P <https://ui.adsabs.harvard.edu/abs/2021MNRAS.507..944P>
- Pérez-González, P. G., Gil de Paz, A., Zamorano, J., et al. 2003, *Monthly Notices of the Royal Astronomical Society*, 338, 508, publisher: OUP ADS Bibcode: 2003MNRAS.338..508P <https://ui.adsabs.harvard.edu/abs/2003MNRAS.338..508P>
- Pérez-González, P. G., Rieke, G. H., Villar, V., et al. 2008, *The Astrophysical Journal*, 675, 234, publisher: IOP ADS Bibcode: 2008ApJ...675..234P
<https://ui.adsabs.harvard.edu/abs/2008ApJ...675..234P>
- Pérez-González, P. G., Costantin, L., Langeroodi, D., et al. 2023, *The Astrophysical Journal*, 951, L1, publisher: IOP ADS Bibcode: 2023ApJ...951L...1P
<https://ui.adsabs.harvard.edu/abs/2023ApJ...951L...1P>
- Pérez-González, P. G., Barro, G., Rieke, G. H., et al. 2024a, *The Astrophysical Journal*, 968, 4, publisher: IOP ADS Bibcode: 2024ApJ...968...4P
<https://ui.adsabs.harvard.edu/abs/2024ApJ...968...4P>
- Pérez-González, P. G., Rinaldi, P., Caputi, K. I., et al. 2024b, *The Astrophysical Journal*, 969, L10, publisher: IOP ADS Bibcode: 2024ApJ...969L..10P
<https://ui.adsabs.harvard.edu/abs/2024ApJ...969L..10P>
- Ranalli, P., Comastri, A., Vignali, C., et al. 2013, *Astronomy and Astrophysics*, 555, A42, publisher: EDP ADS Bibcode: 2013A&A...555A..42R
<https://ui.adsabs.harvard.edu/abs/2013A&A...555A..42R>
- Reddy, N. A., Shapley, A. E., Sanders, R. L., et al. 2018, *The Astrophysical Journal*, 869, 92, publisher: IOP ADS Bibcode: 2018ApJ...869...92R
<https://ui.adsabs.harvard.edu/abs/2018ApJ...869...92R>
- Reines, A. E., Greene, J. E., & Geha, M. 2013, *The Astrophysical Journal*, 775, 116, publisher: IOP ADS Bibcode: 2013ApJ...775..116R
<https://ui.adsabs.harvard.edu/abs/2013ApJ...775..116R>
- Reines, A. E., & Volonteri, M. 2015, *The Astrophysical Journal*, 813, 82, publisher: IOP ADS Bibcode: 2015ApJ...813...82R
<https://ui.adsabs.harvard.edu/abs/2015ApJ...813...82R>
- Rhoads, J. E., Wold, I. G. B., Harish, S., et al. 2023, *The Astrophysical Journal*, 942, L14, publisher: IOP ADS Bibcode: 2023ApJ...942L..14R
<https://ui.adsabs.harvard.edu/abs/2023ApJ...942L..14R>
- Ricci, C., Bauer, F. E., Treister, E., et al. 2017, *Monthly Notices of the Royal Astronomical Society*, 468, 1273, publisher: OUP ADS Bibcode: 2017MNRAS.468.1273R
<https://ui.adsabs.harvard.edu/abs/2017MNRAS.468.1273R>
- Rieke, G. H. 2006, *The Last of the Great Observatories: Spitzer and the Era of Faster, Better, Cheaper at NASA*, 3rd edn. (Tucson: University of Arizona Press)
- Rieke, G. H., Alberts, S., Shivaee, I., et al. 2024, *The Astrophysical Journal*, 975, 83, publisher: IOP ADS Bibcode: 2024ApJ...975...83R
<https://ui.adsabs.harvard.edu/abs/2024ApJ...975...83R>
- Rieke, G. H., Young, E. T., Engelbracht, C. W., et al. 2004, *The Astrophysical Journal Supplement Series*, 154, 25, publisher: IOP ADS Bibcode: 2004ApJS..154...25R
<https://ui.adsabs.harvard.edu/abs/2004ApJS..154...25R>
- Rieke, M. J., Kelly, D. M., Misselt, K., et al. 2023a, *Publications of the Astronomical Society of the Pacific*, 135, 028001, publisher: IOP ADS Bibcode: 2023PASP..135b8001R <https://ui.adsabs.harvard.edu/abs/2023PASP..135b8001R>
- Rieke, M. J., Robertson, B., Tacchella, S., et al. 2023b, *The Astrophysical Journal Supplement Series*, 269, 16, publisher: IOP ADS Bibcode: 2023ApJS..269...16R
<https://ui.adsabs.harvard.edu/abs/2023ApJS..269...16R>
- Rinaldi, P., Caputi, K. I., van Mierlo, S. E., et al. 2022, *The Astrophysical Journal*, 930, 128, publisher: IOP ADS Bibcode: 2022ApJ...930..128R
<https://ui.adsabs.harvard.edu/abs/2022ApJ...930..128R>
- Rinaldi, P., Caputi, K. I., Costantin, L., et al. 2023, *The Astrophysical Journal*, 952, 143, publisher: IOP ADS Bibcode: 2023ApJ...952..143R
<https://ui.adsabs.harvard.edu/abs/2023ApJ...952..143R>

- Rinaldi, P., Bonaventura, N., Rieke, G. H., et al. 2024a, Not Just a Dot: the complex UV morphology and underlying properties of Little Red Dots, , , publication Title: arXiv e-prints ADS Bibcode: 2024arXiv241114383R, doi:10.48550/arXiv.2411.14383. <https://ui.adsabs.harvard.edu/abs/2024arXiv241114383R>
- Rinaldi, P., Caputi, K. I., Iani, E., et al. 2024b, The Astrophysical Journal, 969, 12, publisher: IOP ADS Bibcode: 2024ApJ...969...12R. <https://ui.adsabs.harvard.edu/abs/2024ApJ...969...12R>
- Rinaldi, P., Navarro-Carrera, R., Caputi, K. I., et al. 2024c, The emergence of the Star Formation Main Sequence with redshift unfolded by JWST, , , publication Title: arXiv e-prints ADS Bibcode: 2024arXiv240613554R, doi:10.48550/arXiv.2406.13554. <https://ui.adsabs.harvard.edu/abs/2024arXiv240613554R>
- Roberts-Borsani, G., Treu, T., Shapley, A., et al. 2024, The Astrophysical Journal, 976, 193, publisher: IOP ADS Bibcode: 2024ApJ...976..193R. <https://ui.adsabs.harvard.edu/abs/2024ApJ...976..193R>
- Robertson, B. E., Furlanetto, S. R., Schneider, E., et al. 2013, The Astrophysical Journal, 768, 71. <https://ui.adsabs.harvard.edu/abs/2013ApJ...768...71R/abstract>
- Sanders, D. B., & Mirabel, I. F. 1996, Annual Review of Astronomy and Astrophysics, 34, 749, aDS Bibcode: 1996ARA&A..34..749S. <https://ui.adsabs.harvard.edu/abs/1996ARA&A..34..749S>
- Sanders, R. L., Shapley, A. E., Topping, M. W., Reddy, N. A., & Brammer, G. B. 2024, The Astrophysical Journal, 962, 24, publisher: IOP ADS Bibcode: 2024ApJ...962...24S. <https://ui.adsabs.harvard.edu/abs/2024ApJ...962...24S>
- Sanders, R. L., Shapley, A. E., Jones, T., et al. 2021, The Astrophysical Journal, 914, 19, publisher: IOP ADS Bibcode: 2021ApJ...914...19S. <https://ui.adsabs.harvard.edu/abs/2021ApJ...914...19S>
- Sandles, L., D'Eugenio, F., Maiolino, R., et al. 2024, Astronomy and Astrophysics, 691, A305, publisher: EDP ADS Bibcode: 2024A&A...691A.305S. <https://ui.adsabs.harvard.edu/abs/2024A&A...691A.305S>
- Scarlata, C., Hayes, M., Panagia, N., et al. 2024, On the universal validity of Case B recombination theory, , , publication Title: arXiv e-prints ADS Bibcode: 2024arXiv240409015S, doi:10.48550/arXiv.2404.09015. <https://ui.adsabs.harvard.edu/abs/2024arXiv240409015S>
- Scholtz, J., Maiolino, R., D'Eugenio, F., et al. 2023, JADES: A large population of obscured, narrow line AGN at high redshift, , , publication Title: arXiv e-prints ADS Bibcode: 2023arXiv231118731S, doi:10.48550/arXiv.2311.18731. <https://ui.adsabs.harvard.edu/abs/2023arXiv231118731S>
- Seyfert, C. K. 1943, The Astrophysical Journal, 97, 28, publisher: IOP ADS Bibcode: 1943ApJ....97...28S. <https://ui.adsabs.harvard.edu/abs/1943ApJ....97...28S>
- Shapley, A. E., Sanders, R. L., Topping, M. W., et al. 2024, The AURORA Survey: A New Era of Emission-line Diagrams with JWST/NIRSpec, , , publication Title: arXiv e-prints ADS Bibcode: 2024arXiv240700157S, doi:10.48550/arXiv.2407.00157. <https://ui.adsabs.harvard.edu/abs/2024arXiv240700157S>
- Shivaei, I., Reddy, N., Rieke, G., et al. 2020, The Astrophysical Journal, 899, 117, publisher: IOP ADS Bibcode: 2020ApJ...899..117S. <https://ui.adsabs.harvard.edu/abs/2020ApJ...899..117S>
- Siebenmorgen, R., Heymann, F., & Efstathiou, A. 2015, Astronomy and Astrophysics, 583, A120, aDS Bibcode: 2015A&A...583A.120S. <https://ui.adsabs.harvard.edu/abs/2015A&A...583A.120S>
- Simmonds, C., Tacchella, S., Hainline, K., et al. 2024a, Ionising properties of galaxies in JADES for a stellar mass complete sample: resolving the cosmic ionising photon budget crisis at the Epoch of Reionisation, , , publication Title: arXiv e-prints ADS Bibcode: 2024arXiv240901286S, doi:10.48550/arXiv.2409.01286. <https://ui.adsabs.harvard.edu/abs/2024arXiv240901286S>
- . 2024b, Monthly Notices of the Royal Astronomical Society, 527, 6139, publisher: OUP ADS Bibcode: 2024MNRAS.527.6139S. <https://ui.adsabs.harvard.edu/abs/2024MNRAS.527.6139S>
- Simons, R. C., Papovich, C., Momcheva, I. G., et al. 2023, The Astrophysical Journal Supplement Series, 266, 13, publisher: IOP ADS Bibcode: 2023ApJS..266...13S. <https://ui.adsabs.harvard.edu/abs/2023ApJS..266...13S>
- Skillman, E. D., Salzer, J. J., Berg, D. A., et al. 2013, The Astronomical Journal, 146, 3, publisher: IOP ADS Bibcode: 2013AJ....146....3S. <https://ui.adsabs.harvard.edu/abs/2013AJ....146....3S>
- Sommovigo, L., Ferrara, A., Pallottini, A., et al. 2020, Monthly Notices of the Royal Astronomical Society, 497, 956, publisher: OUP ADS Bibcode: 2020MNRAS.497..956S. <https://ui.adsabs.harvard.edu/abs/2020MNRAS.497..956S>

- Stalevski, M., Fritz, J., Baes, M., Nakos, T., & Popović, L. ?. 2012, *Monthly Notices of the Royal Astronomical Society*, 420, 2756, publisher: OUP ADS Bibcode: 2012MNRAS.420.2756S. <https://ui.adsabs.harvard.edu/abs/2012MNRAS.420.2756S>
- Stalevski, M., Ricci, C., Ueda, Y., et al. 2016, *Monthly Notices of the Royal Astronomical Society*, 458, 2288, publisher: OUP ADS Bibcode: 2016MNRAS.458.2288S. <https://ui.adsabs.harvard.edu/abs/2016MNRAS.458.2288S>
- Steidel, C. C., Giavalisco, M., Dickinson, M., & Adelberger, K. L. 1996, *The Astronomical Journal*, 112, 352, publisher: IOP ADS Bibcode: 1996AJ....112..352S. <https://ui.adsabs.harvard.edu/abs/1996AJ....112..352S>
- Stepney, M., Banerji, M., Tang, S., et al. 2024, *Monthly Notices of the Royal Astronomical Society*, 533, 2948, publisher: OUP ADS Bibcode: 2024MNRAS.533.2948S. <https://ui.adsabs.harvard.edu/abs/2024MNRAS.533.2948S>
- Stern, D., Chary, R.-R., Eisenhardt, P. R. M., & Moustakas, L. A. 2006, *The Astronomical Journal*, 132, 1405, publisher: IOP ADS Bibcode: 2006AJ....132.1405S. <https://ui.adsabs.harvard.edu/abs/2006AJ....132.1405S>
- Stern, J., & Laor, A. 2012, *Monthly Notices of the Royal Astronomical Society*, 423, 600, publisher: OUP ADS Bibcode: 2012MNRAS.423..600S. <https://ui.adsabs.harvard.edu/abs/2012MNRAS.423..600S>
- Strait, V., Bradač, M., Coe, D., et al. 2020, *The Astrophysical Journal*, 888, 124, publisher: IOP ADS Bibcode: 2020ApJ...888..124S. <https://ui.adsabs.harvard.edu/abs/2020ApJ...888..124S>
- Sérsic, J. L. 1968, *Atlas de Galaxias Australes*, publication Title: Cordoba ADS Bibcode: 1968adga.book.....S. <https://ui.adsabs.harvard.edu/abs/1968adga.book.....S>
- Tang, M., Stark, D. P., Chen, Z., et al. 2023, *Monthly Notices of the Royal Astronomical Society*, 526, 1657, publisher: OUP ADS Bibcode: 2023MNRAS.526.1657T. <https://ui.adsabs.harvard.edu/abs/2023MNRAS.526.1657T>
- Taylor, M. 2022, 532, 3, conference Name: Astronomical Data Analysis Software and Systems XXX ADS Bibcode: 2022ASPC..532....3T. <https://ui.adsabs.harvard.edu/abs/2022ASPC..532....3T>
- team, T. p. d. 2024, pandas-dev/pandas: Pandas, Zenodo, doi:10.5281/zenodo.13819579. <https://zenodo.org/records/13819579>
- Temple, M. J., Banerji, M., Hewett, P. C., Rankine, A. L., & Richards, G. T. 2021, *Monthly Notices of the Royal Astronomical Society*, 501, 3061, publisher: OUP ADS Bibcode: 2021MNRAS.501.3061T. <https://ui.adsabs.harvard.edu/abs/2021MNRAS.501.3061T>
- Theios, R. L., Steidel, C. C., Strom, A. L., et al. 2019, *The Astrophysical Journal*, 871, 128, publisher: IOP ADS Bibcode: 2019ApJ...871..128T. <https://ui.adsabs.harvard.edu/abs/2019ApJ...871..128T>
- Topping, M. W., Stark, D. P., Senchyna, P., et al. 2024, *Monthly Notices of the Royal Astronomical Society*, 529, 3301, publisher: OUP ADS Bibcode: 2024MNRAS.529.3301T. <https://ui.adsabs.harvard.edu/abs/2024MNRAS.529.3301T>
- Topping, M. W., Sanders, R. L., Shapley, A. E., et al. 2025, *The AURORA Survey: The Evolution of Multi-phase Electron Densities at High Redshift*, , publication Title: arXiv e-prints ADS Bibcode: 2025arXiv250208712T. <https://ui.adsabs.harvard.edu/abs/2025arXiv250208712T>
- Tripodi, R., D'Eugenio, F., Maiolino, R., et al. 2024, *Spatially resolved emission lines in galaxies at $4 \leq z < 10$ from the JADES survey: evidence for enhanced central star formation*, , publication Title: arXiv e-prints ADS Bibcode: 2024arXiv240308431T, doi:10.48550/arXiv.2403.08431. <https://ui.adsabs.harvard.edu/abs/2024arXiv240308431T>
- Trouille, L., Barger, A., & Tremonti, C. 2011, 217, 326.03, conference Name: American Astronomical Society Meeting Abstracts #217 ADS Bibcode: 2011AAS...21732603T. <https://ui.adsabs.harvard.edu/abs/2011AAS...21732603T>
- Trump, J. R., Arrabal Haro, P., Simons, R. C., et al. 2023, *The Astrophysical Journal*, 945, 35, publisher: IOP ADS Bibcode: 2023ApJ...945...35T. <https://ui.adsabs.harvard.edu/abs/2023ApJ...945...35T>
- Ucci, G., Dayal, P., Hutter, A., et al. 2023, *Monthly Notices of the Royal Astronomical Society*, 518, 3557, publisher: OUP ADS Bibcode: 2023MNRAS.518.3557U. <https://ui.adsabs.harvard.edu/abs/2023MNRAS.518.3557U>
- Vanden Berk, D. E., Richards, G. T., Bauer, A., et al. 2001, *The Astronomical Journal*, 122, 549, publisher: IOP ADS Bibcode: 2001AJ....122..549V. <https://ui.adsabs.harvard.edu/abs/2001AJ....122..549V>
- Veilleux, S., Kim, D. C., & Sanders, D. B. 1999, *The Astrophysical Journal*, 522, 113, publisher: IOP ADS Bibcode: 1999ApJ...522..113V. <https://ui.adsabs.harvard.edu/abs/1999ApJ...522..113V>

- Wang, B., Fujimoto, S., Labbé, I., et al. 2023, *The Astrophysical Journal*, 957, L34, publisher: IOP ADS
Bibcode: 2023ApJ...957L..34W.
<https://ui.adsabs.harvard.edu/abs/2023ApJ...957L..34W>
- Wang, B., de Graaff, A., Davies, R. L., et al. 2024, RUBIES: JWST/NIRSpec Confirmation of an Infrared-luminous, Broad-line Little Red Dot with an Ionized Outflow, , , publication Title: arXiv e-prints ADS
Bibcode: 2024arXiv240302304W,
doi:10.48550/arXiv.2403.02304. <https://ui.adsabs.harvard.edu/abs/2024arXiv240302304W>
- Weedman, D. W., Soifer, B. T., Hao, L., et al. 2006, *The Astrophysical Journal*, 651, 101, publisher: IOP ADS
Bibcode: 2006ApJ...651..101W.
<https://ui.adsabs.harvard.edu/abs/2006ApJ...651..101W>
- Whitaker, K. E., Ashas, M., Illingworth, G., et al. 2019, *The Astrophysical Journal Supplement Series*, 244, 16, publisher: IOP ADS
Bibcode: 2019ApJS..244..16W.
<https://ui.adsabs.harvard.edu/abs/2019ApJS..244..16W>
- Williams, C. C., Tacchella, S., Maseda, M. V., et al. 2023, *The Astrophysical Journal Supplement Series*, 268, 64, publisher: IOP ADS
Bibcode: 2023ApJS..268..64W.
<https://ui.adsabs.harvard.edu/abs/2023ApJS..268..64W>
- Williams, C. C., Alberts, S., Ji, Z., et al. 2024, *The Astrophysical Journal*, 968, 34, publisher: IOP ADS
Bibcode: 2024ApJ...968...34W.
<https://ui.adsabs.harvard.edu/abs/2024ApJ...968...34W>
- Wilson, G., Huang, J. S., Pérez-González, P. G., et al. 2004, *The Astrophysical Journal Supplement Series*, 154, 107, publisher: IOP ADS
Bibcode: 2004ApJS..154..107W.
<https://ui.adsabs.harvard.edu/abs/2004ApJS..154..107W>
- Wilson, G., Huang, J. S., Fazio, G. G., et al. 2007, *The Astrophysical Journal*, 660, L59, publisher: IOP ADS
Bibcode: 2007ApJ...660L..59W.
<https://ui.adsabs.harvard.edu/abs/2007ApJ...660L..59W>
- Witstok, J., Smit, R., Maiolino, R., et al. 2021, *Monthly Notices of the Royal Astronomical Society*, 508, 1686, publisher: OUP ADS
Bibcode: 2021MNRAS.508.1686W.
<https://ui.adsabs.harvard.edu/abs/2021MNRAS.508.1686W>
- Wright, E. L. 2010, 216, 104.01, conference Name: American Astronomical Society Meeting Abstracts #216
ADS Bibcode: 2010AAS...21610401W. <https://ui.adsabs.harvard.edu/abs/2010AAS...21610401W>
- Wright, G. S., Rieke, G. H., Glasse, A., et al. 2023, *Publications of the Astronomical Society of the Pacific*, 135, 048003, publisher: IOP ADS
Bibcode: 2023PASP..135d8003W. <https://ui.adsabs.harvard.edu/abs/2023PASP..135d8003W>
- Yan, H., Dickinson, M., Giavalisco, M., et al. 2006, *The Astrophysical Journal*, 651, 24, publisher: IOP ADS
Bibcode: 2006ApJ...651...24Y.
<https://ui.adsabs.harvard.edu/abs/2006ApJ...651...24Y>
- Yan, H., Dickinson, M., Eisenhardt, P. R. M., et al. 2004, *The Astrophysical Journal*, 616, 63, publisher: IOP ADS
Bibcode: 2004ApJ...616...63Y.
<https://ui.adsabs.harvard.edu/abs/2004ApJ...616...63Y>
- Yang, G., Caputi, K. I., Papovich, C., et al. 2023, *The Astrophysical Journal*, 950, L5, publisher: IOP ADS
Bibcode: 2023ApJ...950L...5Y.
<https://ui.adsabs.harvard.edu/abs/2023ApJ...950L...5Y>
- Yang, H., Malhotra, S., Rhoads, J. E., & Wang, J. 2017a, *The Astrophysical Journal*, 847, 38, publisher: IOP ADS
Bibcode: 2017ApJ...847...38Y.
<https://ui.adsabs.harvard.edu/abs/2017ApJ...847...38Y>
- Yang, H., Malhotra, S., Gronke, M., et al. 2017b, *The Astrophysical Journal*, 844, 171, publisher: IOP ADS
Bibcode: 2017ApJ...844..171Y.
<https://ui.adsabs.harvard.edu/abs/2017ApJ...844..171Y>
- York, D. G., Adelman, J., Anderson, Jr., J. E., et al. 2000, *The Astronomical Journal*, 120, 1579, publisher: IOP ADS
Bibcode: 2000AJ....120.1579Y.
<https://ui.adsabs.harvard.edu/abs/2000AJ....120.1579Y>
- Zavala, J. A., Castellano, M., Akins, H. B., et al. 2025, *Nature Astronomy*, 9, 155, aDS
Bibcode: 2025NatAs...9..155Z.
<https://ui.adsabs.harvard.edu/abs/2025NatAs...9..155Z>
- Zeimann, G. R., Ciardullo, R., Gebhardt, H., et al. 2015, *The Astrophysical Journal*, 798, 29, publisher: IOP ADS
Bibcode: 2015ApJ...798...29Z.
<https://ui.adsabs.harvard.edu/abs/2015ApJ...798...29Z>
- Zhang, X. 2024, *The Astrophysical Journal*, 960, 108, publisher: IOP ADS
Bibcode: 2024ApJ...960..108Z.
<https://ui.adsabs.harvard.edu/abs/2024ApJ...960..108Z>
- Östlin, G., Pérez-González, P. G., Melinder, J., et al. 2024, MIRI Deep Imaging Survey (MIDIS) of the Hubble Ultra Deep Field, , , publication Title: arXiv e-prints ADS
Bibcode: 2024arXiv241119686O,
doi:10.48550/arXiv.2411.19686. <https://ui.adsabs.harvard.edu/abs/2024arXiv241119686O>
- Übler, H., Maiolino, R., Curtis-Lake, E., et al. 2023, *Astronomy and Astrophysics*, 677, A145. <https://ui.adsabs.harvard.edu/abs/2023A&A...677A.145U/abstract>
- Übler, H., D'Eugenio, F., Perna, M., et al. 2024a, *Monthly Notices of the Royal Astronomical Society*, 533, 4287, publisher: OUP ADS
Bibcode: 2024MNRAS.533.4287U.
<https://ui.adsabs.harvard.edu/abs/2024MNRAS.533.4287U>

Übler, H., Maiolino, R., Pérez-González, P. G., et al. 2024b,
Monthly Notices of the Royal Astronomical Society, 531,
355, publisher: OUP ADS Bibcode:
2024MNRAS.531..355U. [https:
//ui.adsabs.harvard.edu/abs/2024MNRAS.531..355U](https://ui.adsabs.harvard.edu/abs/2024MNRAS.531..355U)